University of Alberta

Structural Behaviour of Syncrude's Aurora II Crusher

by

Cara Leigh Denkhaus 

A thesis submitted to the Faculty of Graduate Studies and Research

in partial fulfillment of the

requirements for the degree of Master of Science

in

Structural Engineering

Department of *Civil and Environmental Engineering*

Edmonton, Alberta

Fall 2004

Your file Votre référence
ISBN: 0-612-95734-9
Our file Notre référence
ISBN: 0-612-95734-9

ACKNOWLEDGEMENTS

I would like to acknowledge the financial support provided by the Natural Science and Engineering Research Council of Canada, Syncrude Canada Ltd., and ISIS Canada.

Silvia Gonzalez, Khaled Obaia and Mal Carroll of Syncrude Canada helped with instrumentation and training for Syncrude site work. Ved Sharma of the University of Alberta also assisted with instrumentation and some data reduction, specifically the temperature data. Krupp Canada supplied the structural drawings and numerical model. Their assistance is greatly appreciated.

The support and guidance of my supervisor Dr. J.J.R. Cheng was invaluable through my program.

I would also like to thank my mom, Shirley Denkhaus for helping edit my thesis as well as my family for their support throughout my schooling.

TABLE OF CONTENTS

LIST OF TABLES

LIST OF FIGURES

LIST OF SYMBOLS AND ABBREVIATIONS

CIM	Canadian Institute of Mining, Metallurgy and Petroleum
DRC6	Double Roll Crusher 6, North Mine
DRC7	Double Roll Crusher 7, North Mine
LVDTs	Linear Variable Differential Transducers
STAAD	Structural Analysis and Design Computer Program
Hz	hertz
kg/m^3	kilogram per cubic meter
kN/m	kilonewton per meter
mm	millimeter
MPa	megapascals
t/hr	ton per hour
$\mu\varepsilon/°C$	microstrain per degree Celsius
V/g	volt/acceleration due to gravity
%	percent

1. Introduction

1.1. Background

Syncrude Canada uses trucks and shovels to mine oil sand at their mine outside of Fort McMurray, Alberta. In order to use their slurry transport system the oil sand must be smaller than a maximum size of 400 mm. To ensure this standard is met Syncrude uses Double Roll Crusher to break large lumps of oil sand. The double roll crusher consists of two rotating rolls with metal teeth. For maximum efficiency the oil sand must be dropped from a height and then passed through these rolls. The crusher structure was designed by Krupp Canada to allow for the trucks to dump the oil sand into a hopper and the oil sand then travels on an apron feeder and drops onto the crusher rolls. Designing the crusher with a diamond shape allows two trucks to dump oil sand into the hopper simultaneously. In order to support the mechanical and structural components of the crusher and hopper, a supporting structure consisting of columns and a pontoon was built.

1.2. Scope and Objectives

Syncrude approached the University of Alberta's civil engineering program to institute a Structural Health Monitoring Program for the crusher, to be a part of its Structural Reliability Program for its equipment. Syncrude wanted to gain further knowledge on the crusher because the precise loading is unknown and they would like to improve the design of the crusher so that they can design a fully-mobile crusher in the future. They also wanted to decrease downtime as it is expensive and costs them production losses. This research program is the first phase of a program initiated by Syncrude and the University of Alberta to create a monitoring program for the crusher. This phase will determine the global structural behaviour of the crusher. The information learned in this phase will allow for the creation of a monitoring program to manage the crusher efficiently and proactively.

The main objective of this research program is to characterize the structural behaviour of Syncrude's Aurora II Crusher in order to provide information to the vendor to refine the design and to further research for the development of a structural health monitoring

program for the crusher. The design model supplied by Krupp will be calibrated with test data to verify boundary conditions and stress patterns. The relationship between temperature and strain will be determined to provide a basis for boundary condition changes. Column stress distribution will be determined for known events to create an event signature. Impact factor will be calculated during normal operation to provide information on how this value changes with location and stress range.

1.3. Thesis Layout

This research examines the structural behaviour of Syncrude's Aurora II Crusher to supplement the implementation of a Structural Health Monitoring Program for the crusher. Chapter 2 summarizes the design elements of the crusher and previous testing done on the crusher at Syncrude through a literature review. Chapter 3 describes the numerical model used in this research program. Chapter 4 describes the experimental program of testing. Test results are summarized in Chapter 5. Chapter 6 discusses the structural behaviour of the crusher by examining thermal strains, event characterization, impact factor, and the comparison to the design model.

2. Literature Review

2.1. Crusher Selection and Design

Syncrude conducted an expansion study in 1987/1988 and determined the average required feeder capacity was 4650 t/hr, which was beyond the existing feeder breaker capabilities. After a literature search and mine visits, field tests were completed to determine the best alternative to the current feeder breakers. The double roll crusher performed well in field tests and was able to perform with high throughputs (Quapp and Maciejewski 1991). Therefore, the double roll crusher was chosen and a detailed design of a semi-mobile crusher was completed.

The maximum rock size a double roll crusher can handle depends on the roll diameter and the roll width (Quapp and Maciejewski 1991). Gravity assists the flow of loose material as a feeder brings the material to a height above the rollers. The concept of crushing used in the double roll crusher utilizes the kinetic energy of the high speed, high inertia rolls to create the required breaking forces, suitable for high compressive strength materials (Quapp and Maciejewski 1991). Although a double roll crusher is often used as a secondary crusher, it is ideal to handle sticky material and hard rock (www.krupp.ca/syncrude%20crusher.htm).

In order to maximize the crusher throughput, Quapp and Maciejewski (1991) suggest that the bin geometry for the feeder portion (i.e. hopper) of the crusher needs to be optimized. The double roll crushers at Syncrude have been improved as the loads from the trucks are becoming larger. The first double roll crusher was designed to receive material from a single 240 tonne truck. An improvement was made possible by designing the hopper geometry as a diamond shape allowing for two trucks to dump at the same time. Two crushers at the North Mine were designed and constructed that accepted two 320 ton trucks at once. The hopper at Aurora was designed to receive material from two 400 ton trucks simultaneously (www.krupp.ca/syncrude%20crusher.htm).

The structural design of the crusher was performed by Krupp using a STAAD (Structural Analysis and Design) Model. Various load combinations were performed for both normal and upset loading conditions. The finite element model then indicated areas of high stress in the pontoon and the hopper. (www.krupp.ca/syncrude%20crusher.htm)

2.2. Past Problems

The double roll crusher was chosen by Syncrude to investigate because of problems encountered with similar structures in the past. In September and October of 1999, a study to investigate the displacement of crushers at the North Mine, DRC6 and DRC7, was done due to concerns about excessive displacement at DRC7. The investigation was documented in a Syncrude Progress Report (Fowler and Gonzalez 1999) and is summarized here. Displacement measurements were taken by attaching LVDTs (Linear Variable Differential Transducers) to the columns and recording movements with respect to the retaining wall. These measurements were taken at the top of the columns and therefore include both the rigid body motion of the structure and the bending of the structure. Measurements were taken for various loading cases by changing the level of material in the hopper. Only one side of the hopper was instrumented so the loads also varied whether the load impacted the instrumented side or the non-instrumented side of the hopper. With a high quality ore and an empty hopper the displacement varied between 24.4 and 36.4 mm. The back columns (Gridline 2) experienced ten more millimetres of displacement than the middle column (Gridline 3). See Figure 2-1 for the locations of the gridlines. The rich ore resulted in the truck load exiting in one mass, creating a larger load. For mid-grade ore the displacement varied between 9.5 and 12.2 mm. Again the back column experienced more displacement than the middle column, but much less than for the rich ore, only 0.6 to 2.6 mm. The practice of dumping into a hopper with existing material proves to help limit the displacement.

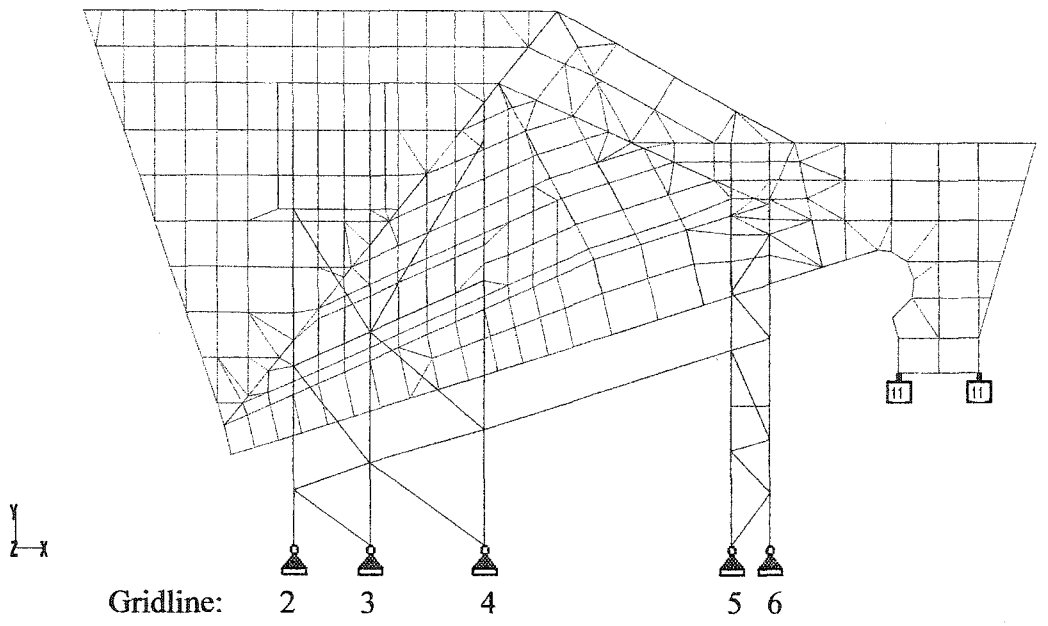

Figure 2-1: Side view of crusher

The testing done at DRC6 measured the same displacements. Only rich ore was available to use during the testing. The largest displacement value was 17.8 mm. This was observed at the back column when dumping into an empty hopper with rich ore. A number of dumps recorded negligible displacement, unlike at DRC7. When the hopper was at the setpoint, half-full, or fuller, the displacements were all less than 10 mm.

See Table 2-1 for the values supplied by Krupp for expected displacement in millimetres. The values depend on the assumption of a rigid base or an allowance for support rotation.

Table 2-1: Summary of Krupp Displacement Data

Hopper Level	Support Rotation		Rigid Base	
	Middle (mm)	Back (mm)	Middle (mm)	Back (mm)
Empty	40.9	54.2	1.8	10.7
Setpoint	47.7	55.3	8.6	11.8

The results of these tests showed that the displacement for DRC7 is significantly larger than for DRC6. The difference ranged from 1.5 times for the hopper at setpoint and 2 times for dumping into an empty hopper. This study also showed that dumping into a

partially full hopper and dumping mid-grade ore which allows for the load to exit slowly reduce the displacements of the columns.

After completing this study, the authors raised some areas for further investigation. The report suggests that factors contributing to structural displacement need to be further investigated because the model predicts larger displacement when dumping into a full hopper, not an empty one as is observed. The report also suggests that the degree of support displacement should be investigated to determine the extent of the displacement due to support rotation.

Following the original investigation summarized above, Syncrude carried out another study to investigate the support displacement at DRC7, Syncrude Progress Report 29 (5) (Fowler and Gonzalez 2000). The study involved repeating the tests done in the fall of 1999 in March 2000 on DRC7. The values could then be compared to see how much of the displacement of the columns was due to support rotation as the ground was frozen and assumed to be rigid. The maximum displacements ranged between 16.5mm and 36.4mm. These were 45 percent of the displacements found in the fall. Therefore, over half of the observed displacement was likely due to support rotation and the displacements are within acceptable values.

Following the above investigation, Syncrude again researched the displacements of the crushers. In Syncrude Progress Report 30 (09), Obaia and Gonzalez (2001) summarized the results of their study of the support displacement. This study involved observing the displacement of the concrete pile cap and the base of the steel column. The purpose of the investigation was to determine whether movement of the concrete pile cap, or the steel column base, was causing the excessive rotation and therefore the excessive displacement at the column top. LVDTs were used to measure the vertical displacement of the column, and the pile cap as well as one horizontal direction (the z-direction). Testing involved control data sampled during normal operation and control testing. The control testing involved two high grade oil sand (13.4%) dumps and two low grade oil sand (8.6%) dumps, always dumping into an empty hopper. These tests were completed

in March 2001 with frozen ground conditions, and in July 2001 with summer conditions. The summer tests did not contain data for low grade ore as it was not available. The maximum observed displacement in winter of 0.61 mm occurred with high grade oil sand. The vertical displacements were larger than the horizontal displacement, 0.61mm compared to 0.39mm. The vertical displacement is the same for dumping on both sides of the hopper indicating that the support movement is lateral and not rotational. The displacements observed were larger at the steel column base than the concrete pile cap. The displacement was characterized by a dynamic portion as well as a static portion. The summer tests resulted in the same observation; however, the displacement was larger than observed in the winter, a maximum of 0.95 mm. The displacements were quite small as compared to the observed displacement at the top of the columns and Obaia suggests that support movement should not be thought of as the reason for the difference between the displacement values of DRC6 and DRC7. The authors also caution that the values for displacement are within the error of the LVDTs and should be thought of as trends rather than actual values.

In summary, DRC6 and DRC7 displacements were investigated thoroughly because of "excessive" vibration observed by the operators of DRC7 in order to determine if this displacement was within acceptable levels and why there was a difference between DRC6 and DRC7 even though they were designed identically. Although no conclusions were drawn in these reports, it has provided a background to the behaviour of the double roll crushers. The crushers experience static and dynamic loading. The dynamic effect is larger when the truck load is dumped into an empty hopper. The overall effect is larger when the oil sand is of higher grade because the truck load tends to discharge all in one lump instead of gradually. These investigations also allowed for an indication of the range of displacements seen on the crushers, less than 1mm at the base and approximately 55 mm at the top of the columns. These past problems also gave Syncrude the desire to have a better understanding of the crusher's behaviour, which has lead to the investigation of the Aurora II Crusher.

2.3. Monitoring Programs at Syncrude

In the past, Syncrude has used monitoring programs to improve equipment reliability and operating conditions. Carroll presented two of these monitoring programs in a paper at the 1997 CIM Conference.

He summarized a study on the track roller of a hydraulic shovel. The track rollers were failing prematurely and the monitoring system was used to provide a better understanding of the actual loads imposed on the rollers. Strain gauges were installed on the inside of the roller and stresses were calculated assuming the strains were in the linear elastic range. A finite element analysis program was used to translate stresses in the interior of the roller to forces acting at the exterior of the roller. The strain gauge information was used to calibrate the finite element model. The loads found in this monitoring program were used to redesign a new roller with an improved operating life.

Carroll also summarized a monitoring program on the dragline boom. The dragline experiences highly cyclical loading which causes fatigue failure. If the stress range the boom experiences could be reduced, the fatigue life would be increased. Syncrude implemented a program whereby the boom stresses were monitored. The hoisting and swinging of the boom most affected the loading on the boom. The magnitudes of these cycles are highly operator dependent. The boom monitoring program provided the operator with a signal indicating boom loading. Because the operators were aware of how their actions affected boom stress and could practice better operating techniques, the high stress on the dragline booms was reduced; therefore, the lifecycle of the booms was increased.

These monitoring programs show that equipment monitoring can be used to improve operating conditions. More information on loading can be used to improve design for future equipment. Carroll suggests that "future dynamic load monitoring on crusher systems" could be implemented (1997).

3. Numerical Model

3.1 Description of Crusher

The crusher consists of six main components: the pontoon, the columns, the apron feeder, the hopper, the crusher rolls and the tower. The tower holds the hydraulic house and the electronic house and is structurally and vibrationally separate from the rest of the components; therefore, it is not considered. The mechanical parts are the apron feeder and the crusher rolls. The apron feeder acts as the bottom of the hopper and transports the oil sand from the hopper to the inlet chute above the crusher rolls. Because the apron feeder and crusher rolls are mechanical components, they have not been considered in this research.

3.2 Model Description

The numerical model of the crusher was provided for the project by Krupp. Their model was used during design and consisted of two separate models: the pontoon and the hopper with the columns. All of the components of both models are steel with properties outlined in Table 3-1.

Table 3-1: Model Steel Properties

Modulus of Elasticity, E	205 000 MPa
Poission's ratio, ν	0.30
Density, ρ	7851.81 kg/m^3

3.2.1 Pontoon

The pontoon was modelled entirely as steel plates and is shown in Figure 3-1. The boundary conditions for the pontoon varied at each corner.

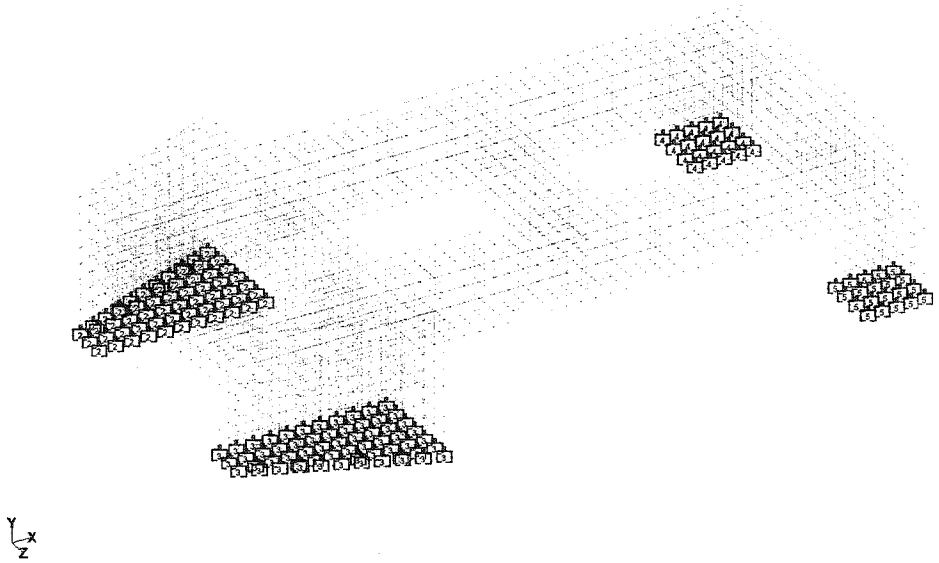

Figure 3-1: Krupp Pontoon Model

The boundary conditions of the top left corner (Figure 3-1), are pinned in the horizontal directions (x & z), and spring supported with a spring constant of 30 500 kN/m in the vertical (y) direction. The top right corner is free to rotate in all directions and move in the horizontal directions and spring supported with a spring constant of 30 000 kN/m in the vertical direction. The bottom left corner is free to rotate in all directions and move in the horizontal directions and spring supported with a spring constant of 30 500 kN/m in the vertical direction. The bottom right corner is free to rotate in all directions and free to move in the z-direction, fixed in the x-direction and spring supported in the vertical direction with a spring constant of 30 000 kN/m. The vertical spring support represents the geotechnical conditions of the piles supporting the pontoon.

The pontoon was modeled with fourteen load cases, nine individual load cases and five combination load cases. The individual load cases include: self-weight, equipment load (apron feeder and drives), superimposed dead load (apron feeder and encrustation of material), live load (material at hopper), live load (hopper, apron feeder and platform), and four impact load cases. The impact factor used in all cases was 1.4. The combination loads use a dead load factor of 1.25 and a live load factor of 1.5. The

pontoon load cases were taken by transmitting loads from the hopper through the columns.

3.2.2 Hopper

The hopper was modelled using steel plates for the hopper walls and some bracing elements in the columns and beam elements for the columns and stiffeners supporting the hopper as seen in Figure 3-2.

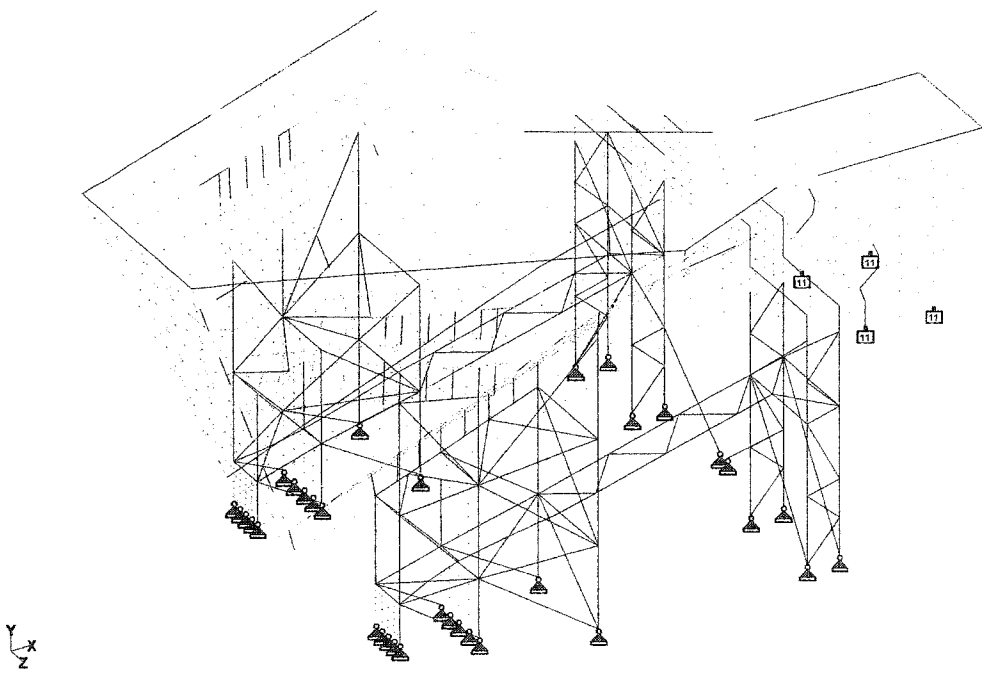

Figure 3-2: Krupp Hopper Model

The hopper columns are assumed pinned where they connect to the pontoon. The base of the inlet chute of the hopper is assumed to be spring supported with spring constants of 343 kN/m in the horizontal directions (x & z), 16 700 kN/m in the y-direction. The values of these spring constants come from the vibration isolator at this location.

The hopper had approximately sixty load cases. The fundamental load cases are: dead load, including self-weight and superimposed dead load, material load based on active earth pressures; and inlet chute becoming plugged with an impact load of 1000 kN. There are ten combination load cases.

3.3 Preliminary Model Analysis

In order to decide on the instrumentation locations the model was analyzed. The analysis provided information on expected ranges for displacement, and high stress locations.

3.3.1 Pontoon

The pontoon model was analyzed and combined load cases were used to determine maximum displacements and stresses. The maximum rotations and displacements are summarized in Table 3-2. The maximum displacement experienced was 34.7mm due to a large vertical defection at the center of the pontoon. See Figure 3-3.

Table 3-2: Pontoon Model Displacements

x-displacement	9.6	mm
y-displacement	34.5	mm
z-displacement	13.7	mm
x- rotation	0.6	Degrees
y-rotation	0.3	Degrees
z-rotation	0.5	Degrees

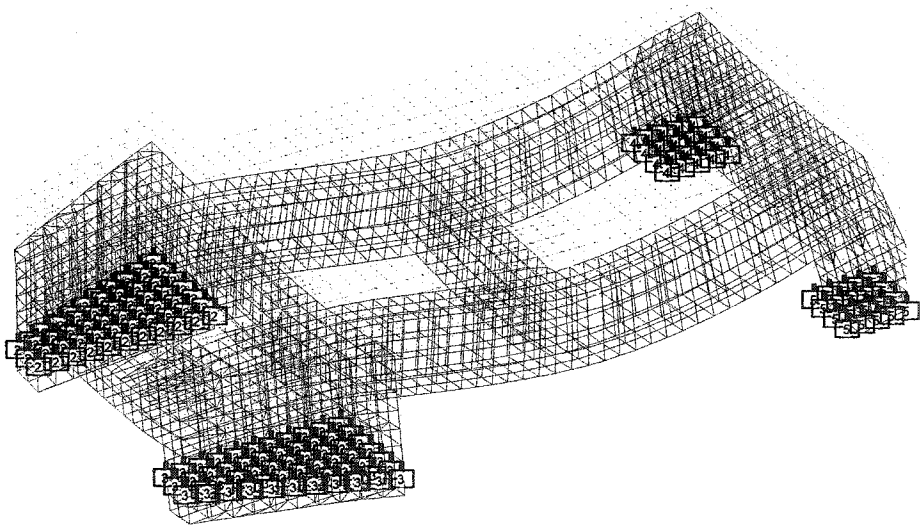

Figure 3-3: Pontoon Displacements

The pontoon was also analyzed for maximum stresses. A contour plot of the stresses in the pontoon is shown in Figure 3-4. The maximum stresses occurred in the corner below the main dumping area for the hopper. The maximum stress obtained from the model

was 432 MPa which is over the design yield strength of the steel, 350 MPa. Because this was observed in a localized area and under fully factored loading conditions, this high stress was not a concern. Also, the pontoon is made of large steel plates which have an ability to redistribute stress.

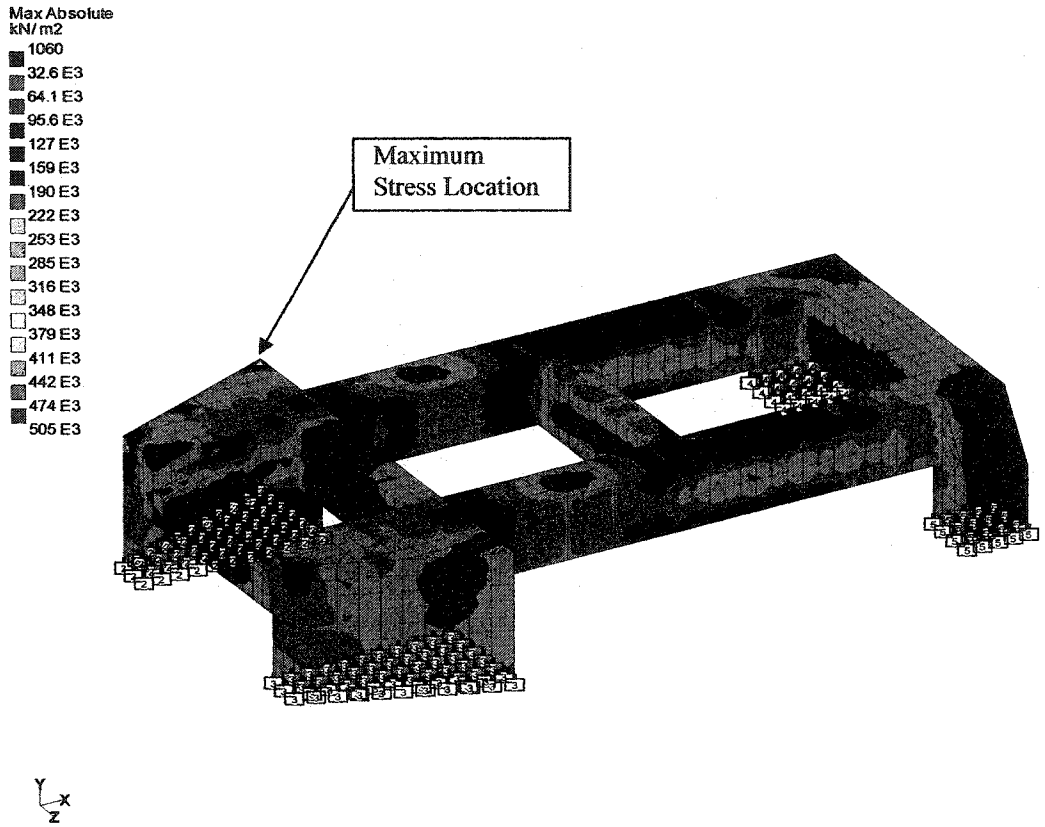

Figure 3-4: Pontoon Maximum Stresses

3.3.2 Hopper

The hopper model was analyzed with combined loads to determine high stress locations and maximum displacements. When the actual data is collected, it will need to be compared with only live load model analysis. This analysis gives and indication of hot spots amd maximum ranges required for LVDTs. The maximum displacements are summarized in Table 3-3. The maximum displacement occurred along the bottom of the hopper walls.

Table 3-3: Hopper Maximum Displacements

x-displacement	22.7	mm
y-displacement	32.0	mm
z-displacement	49.7	mm
x- rotation	1.1	Degrees
y-rotation	0.7	Degrees
z-rotation	0.4	Degrees

The stresses in the hopper walls were low even under fully factored loading conditions. The maximum stress in the hopper walls was 240 MPa, which is below the yield stress of 350 MPa. The maximum stress occurred at the back columns of the hopper at the connection between the columns and the hopper walls. The contours of the hopper plate stresses are shown in Figure 3-5.

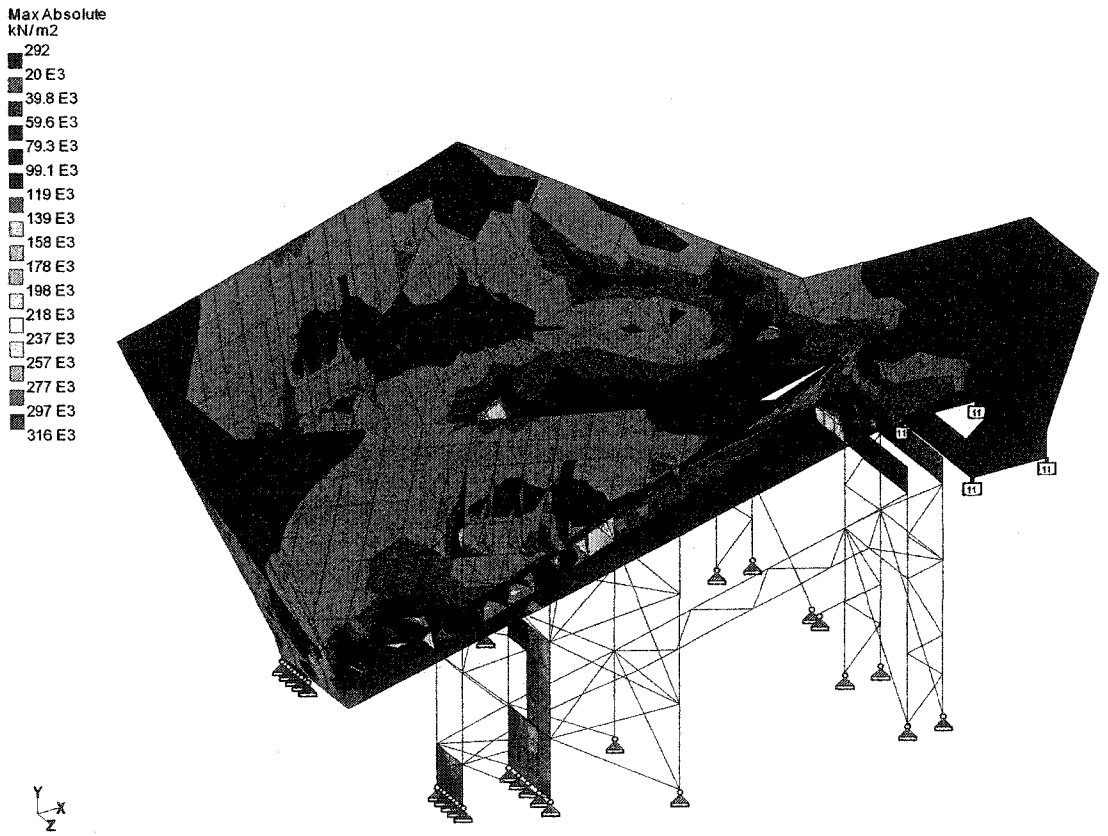

Figure 3-5: Hopper Plate Stresses

Although the hopper plate stresses were low, there were beams in the hopper model that indicated very high stress areas. A maximum stress of 1416 MPa was shown in the

model analysis and twenty-three beams showed a stress level over the yield strength of 350 MPa under fully factored dead and live load. This stress occurred at a location of discontinuity at the end of a beam on the extreme corner. The average stress in the beam at the location was calculated by averaging the four corner stresses and it was only 136 MPa. The beams in the actual hopper would never experience this high of a stress because their stress cannot exceed the ultimate strength of the steel, 450 MPa. This was not a major concern because the model was a design tool and the section could have been increased before construction to reduce these stresses and the loading is a once in a lifetime event. The model showed that there were areas of high stress near the top of the hopper columns.

3.4 Summary

The preliminary analysis of the model provided information about maximum stresses and displacements of the crusher which allowed for the creation of the instrumentation and experimental program as described in Chapter 4. The preliminary analysis was done using fully factored combination loading conditions. These conditions can not be compared to the data collected as the strain and displacement measurements will only be measuring the service live loads. A load will be created in the STAAD model to represent a dump event. The stress and displacements calculated in the model will be compared to the data collected in Section 6.4.1.

4. Experimental Program

4.1. Instrumentation

In order to achieve the objectives of this research, a combination of strain gauges, LVDTs, accelerometers and thermocouples were installed on the crusher over a six week period. A National Instruments Data Acquisition System and Lab View Software were used due to Syncrude's and the University of Alberta's compatibility and familiarity with both. The system allows for ninety-six input channels including sixty-four strain gauge channels, twenty-four analog input channels and one spare module of eight channels for future use. The analog channels are a combination of input from accelerometers, LVDTs, and thermocouples.

4.1.1. Strain Gauges

Weldable strain gauges were used on this project because they will be operating for a long period of time and in a harsh climate. Having a more durable method of application, weldable strain gauges have a higher fatigue life than glueable strain gauges. Sixty strain gauges were installed on the crusher. Thirty-six gauges were installed on the columns near their base to gain an understanding of the axial stresses in the columns and therefore the loads transmitted to the pontoon. The gauges were installed midway between the braces in the bottom section of the column. This location should eliminate the bending strain measured. Although the amount of bending in the column would have been useful information, the amount of channels required to measure this accurately was not available. These gauges were installed in pairs with one on each flange of the column so that the strain could be averaged to gain the axial stress in the column. To gain an understanding of the distribution of axial stress in the column, four gauges were installed on the columns near the top of the column. This distribution gives an indication of the bending moment distribution in the column. They were installed in two locations with one gauge on each flange of the column. See Figure 4-1 for the exact locations of the column gauges, labelled C1 through C40.

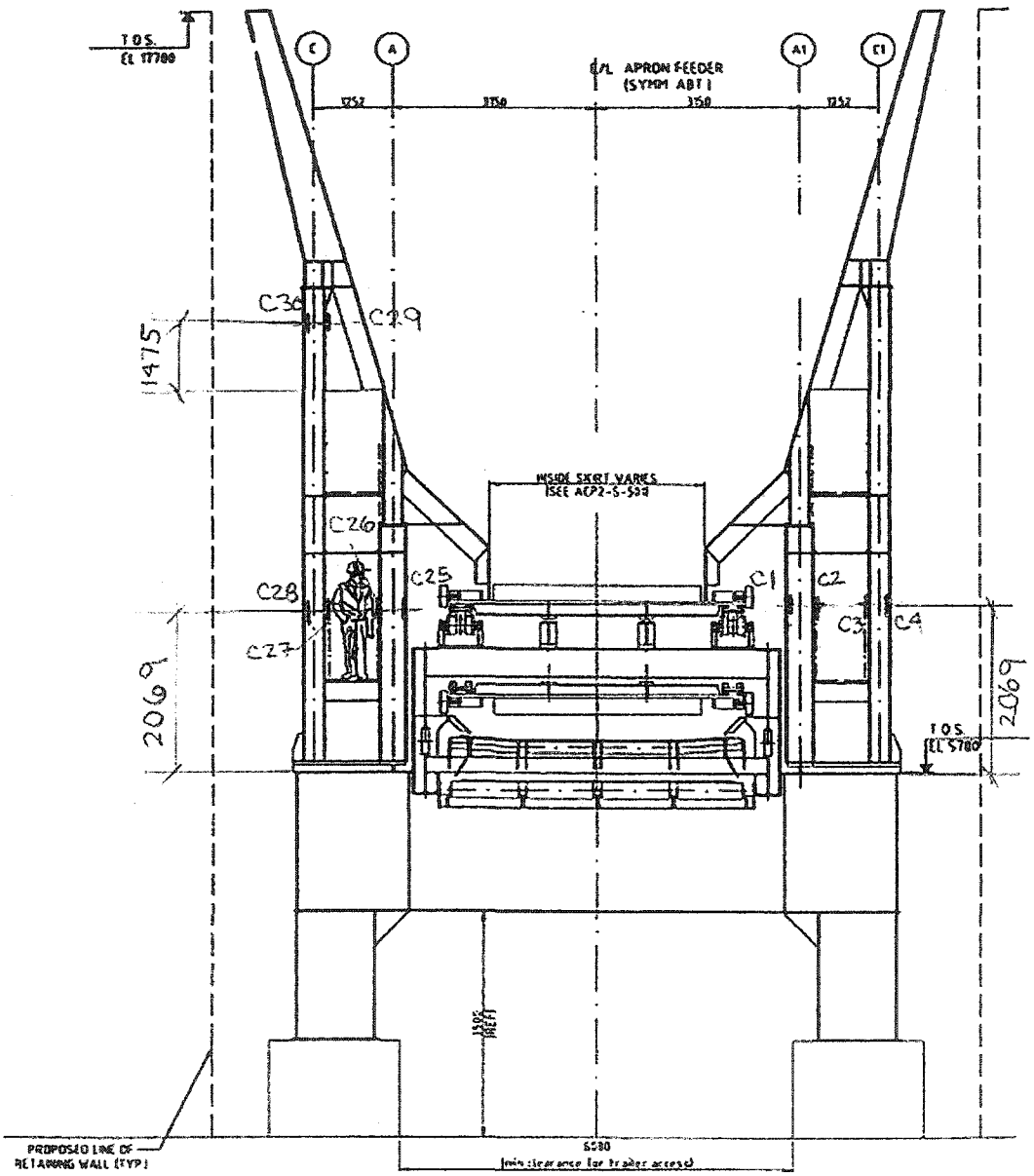

a) Gridline 2

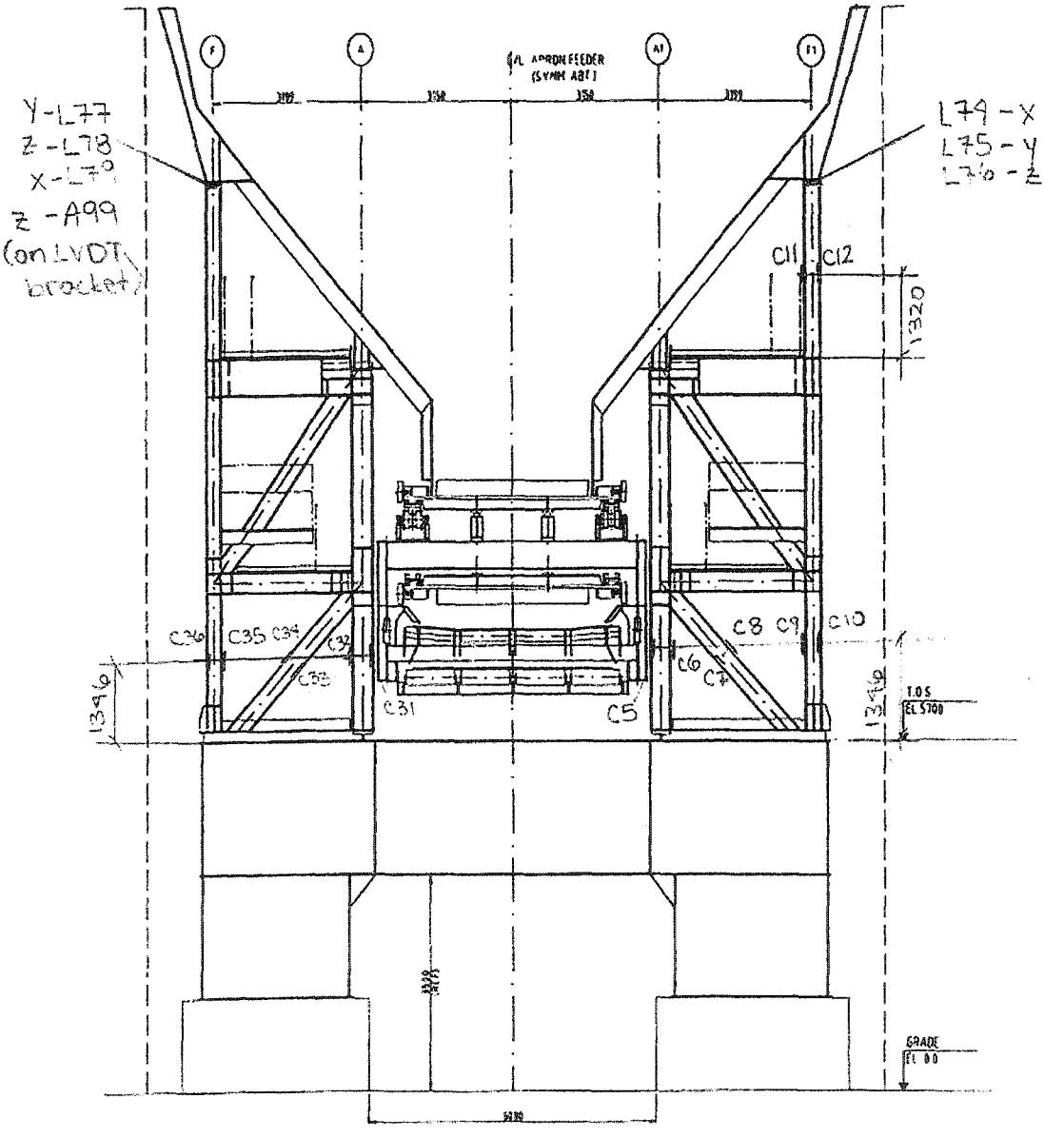

b) Gridline 4

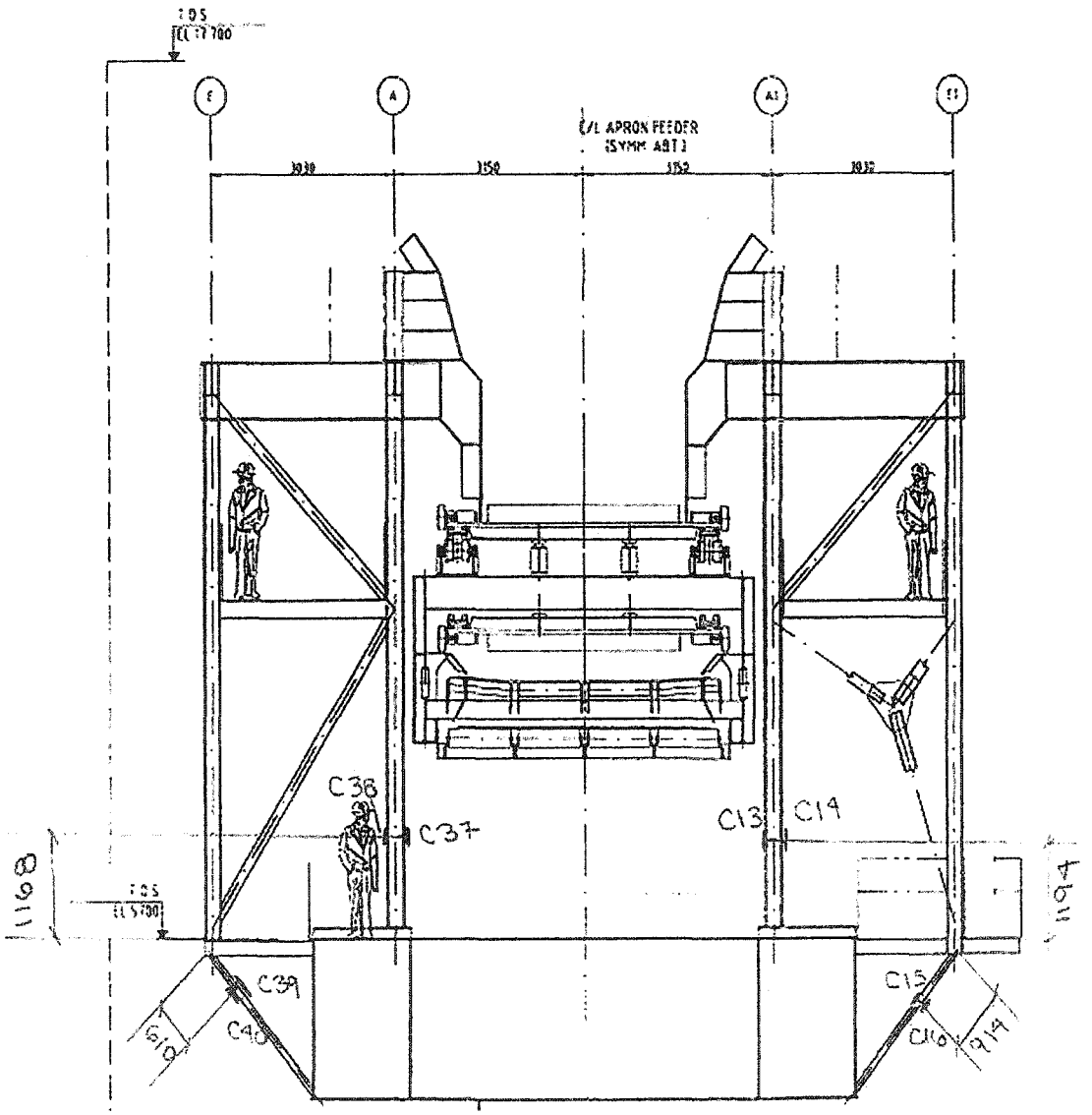

c) Gridline 5

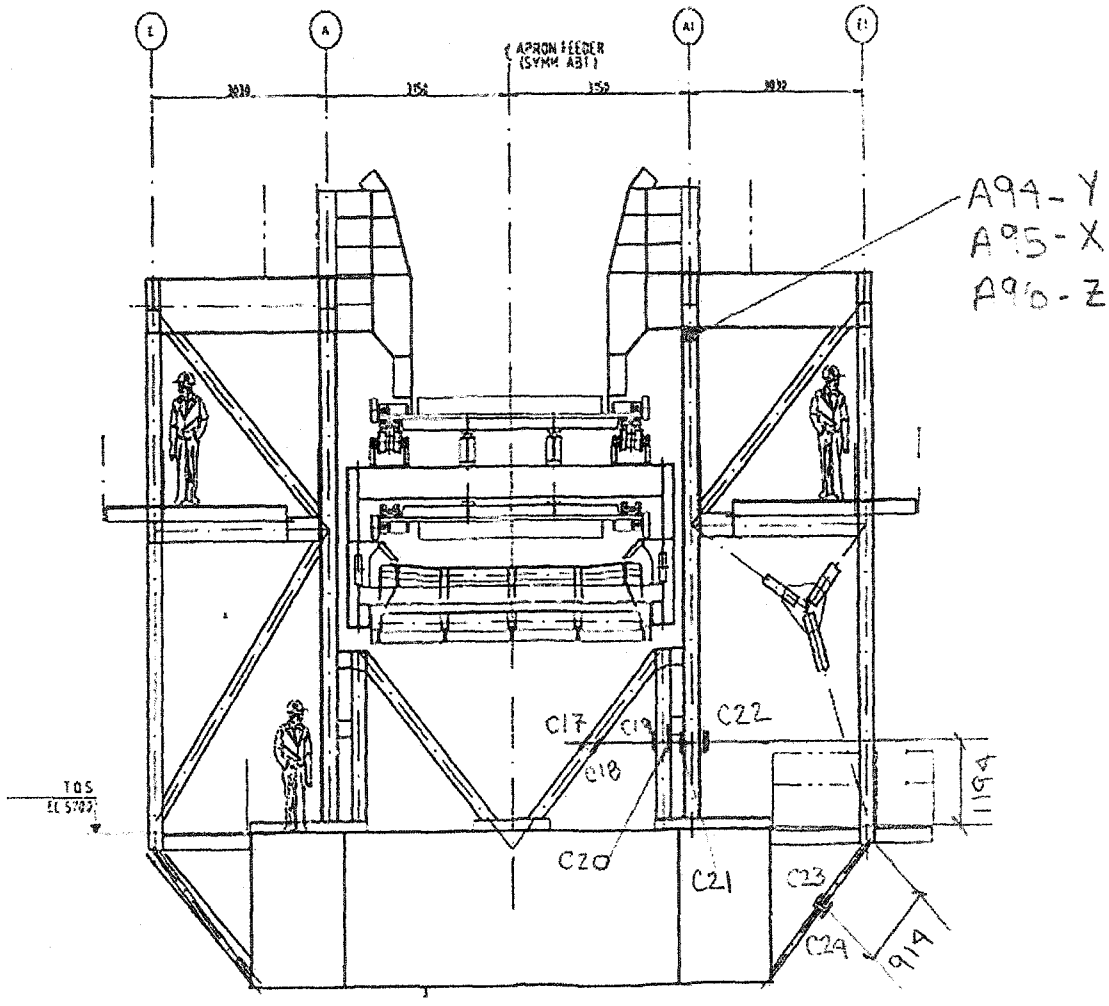

d) Gridline 6

Figure 4-1: Column Instrument Locations

The pontoon was instrumented with ten strain gauges to gain information on the bending moment profile. Gauges were installed at five locations with one gauge near the top of the pontoon and one gauge near the bottom. Originally the strain gauges were to be installed on the bottom and top of the pontoon in the middle of one side of the box girders. These locations were deemed unsuitable because of foot traffic and the non-slip surface installed on the top of the pontoon. The locations were then chosen on the web of the pontoon. All of the bottom gauges are 154.2 mm from the bottom of the flange. The top gauges were installed as high as possible. P45, P47 and P49 were installed 154.2 mm from the top of the flange. Because access was restricted to the top of the pontoon for the

other locations, P51 was installed 355.6 mm from the top of the flange and P53 was installed 1285.6 mm from the top of the flange. See Figure 4-2 for exact locations of the pontoon gauges.

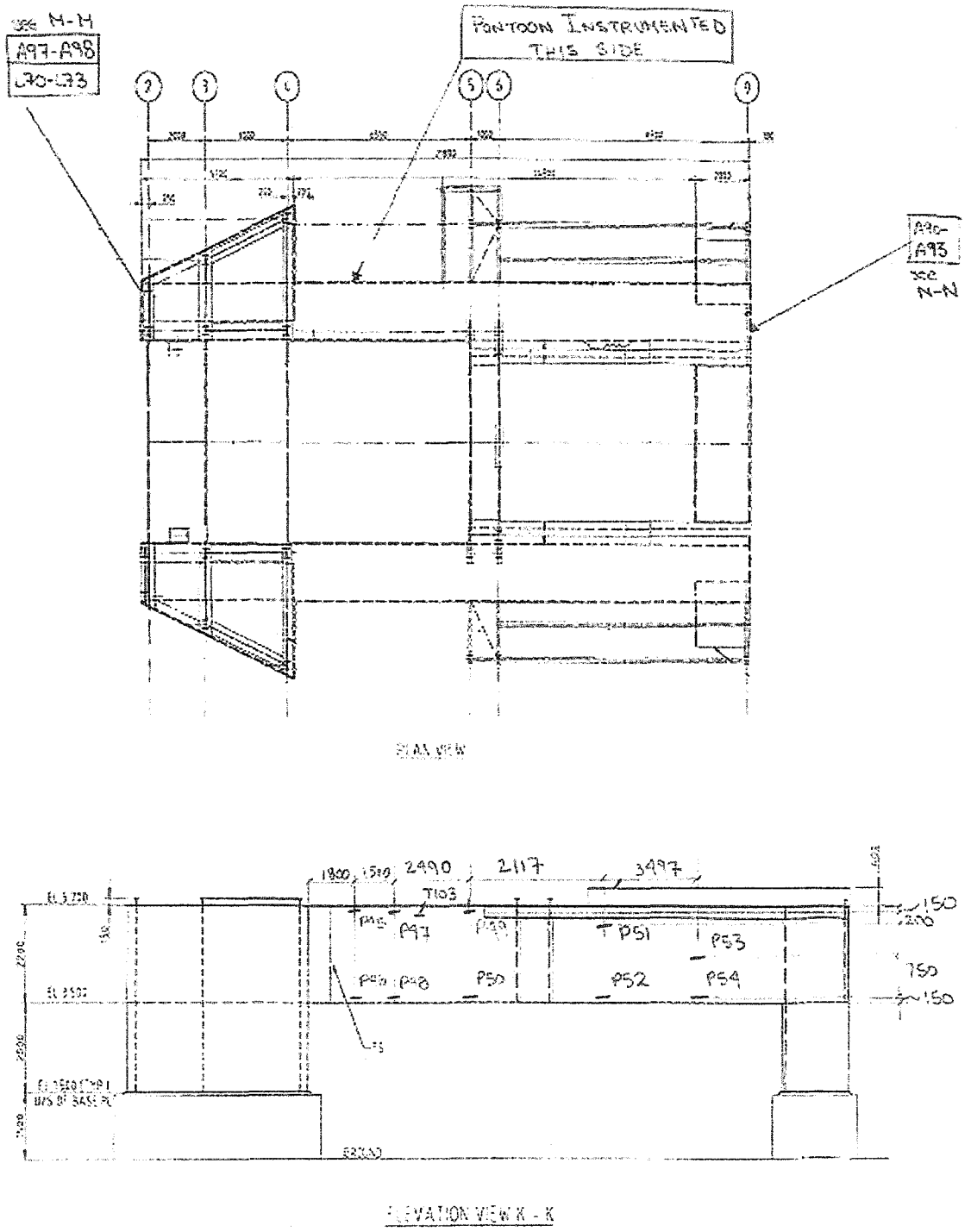

Figure 4-2: Pontoon Strain Gauge Locations

Ten strain gauges were installed on the hopper to determine the stress profile in the hopper. Due to the complexity of the hopper, only one panel was instrumented. The panel between Gridlines 3 and 4 was chosen because it would likely see the most impact. See Figure 4-3 for exact locations of the hopper gauges. Six strain gauges were arranged in a cluster with two gauges on the horizontal stiffeners, two gauges on the vertical stiffeners and two gauges on the hopper wall. See Figure 4-4. This cluster was installed to gain a detailed stress picture at this location. Three gauges were installed one row below the cluster at the junction of the vertical and horizontal stiffeners. At the midpoint between the vertical stiffeners, one additional gauge was installed on a horizontal stiffener at the same level as the bottom row of the cluster.

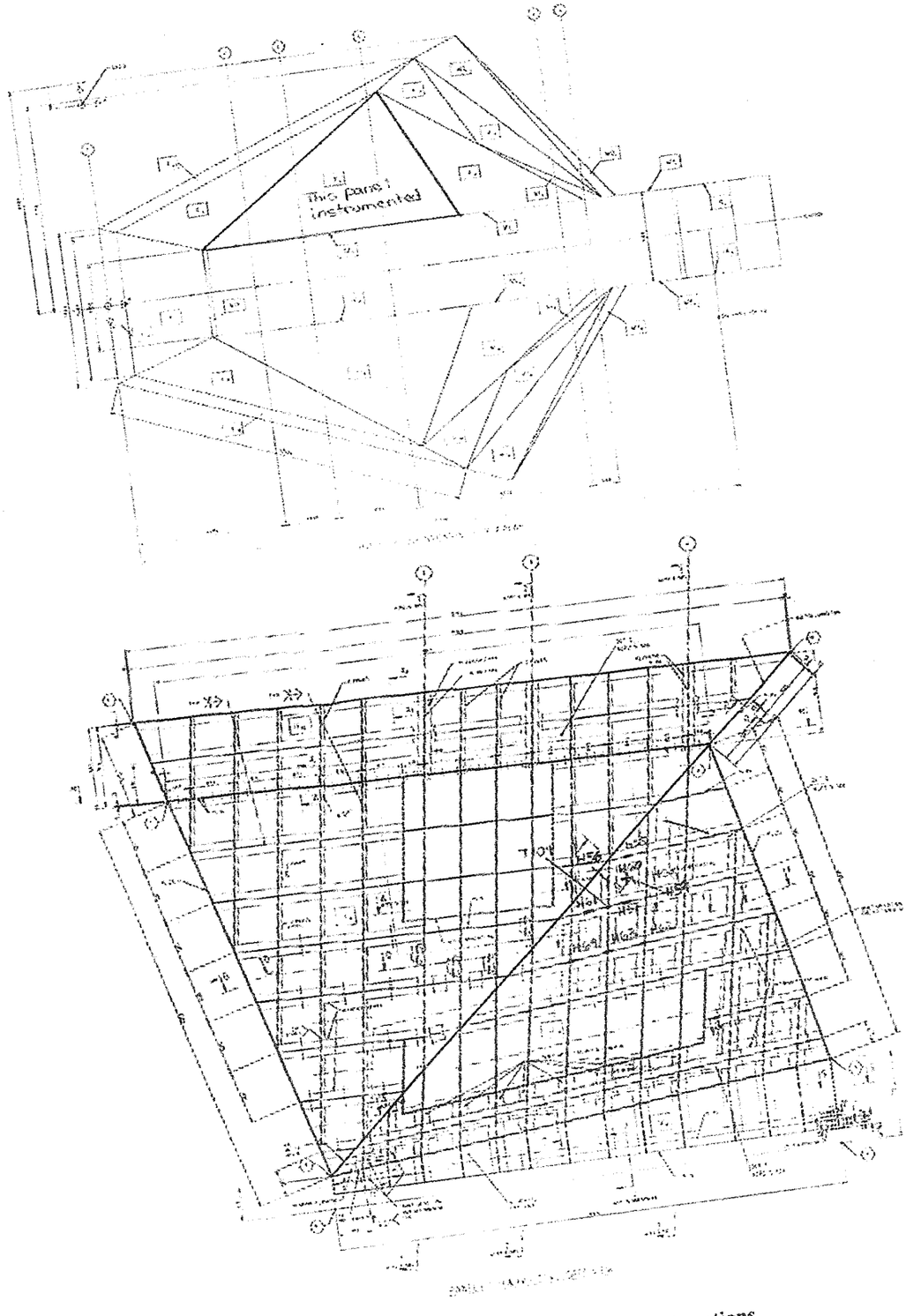

Figure 4-3: Hopper Strain Gauge Locations

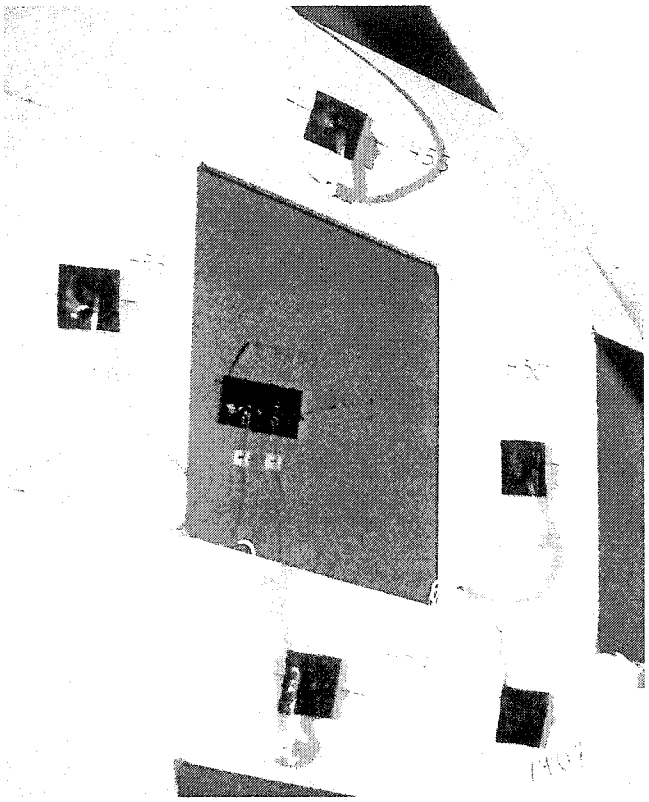

Figure 4-4: Hopper Cluster

In order to install the strain gauges, exact locations were marked with chalk. The surface was prepared by grinding to remove the paint and buffing with two successively finer buffing pads as seen in Figure 4-5. To avoid creating a short circuit in the gauge, the locations were cleaned using a degreaser and Windex to remove residue. The gauges were installed using a weldable strain gauge unit (Figure 4-6). Once installed, the gauge was checked by ensuring the resistance through the gauge was still 350 ohms. That the gauge was not shorted with respect to the surface was also assessed.

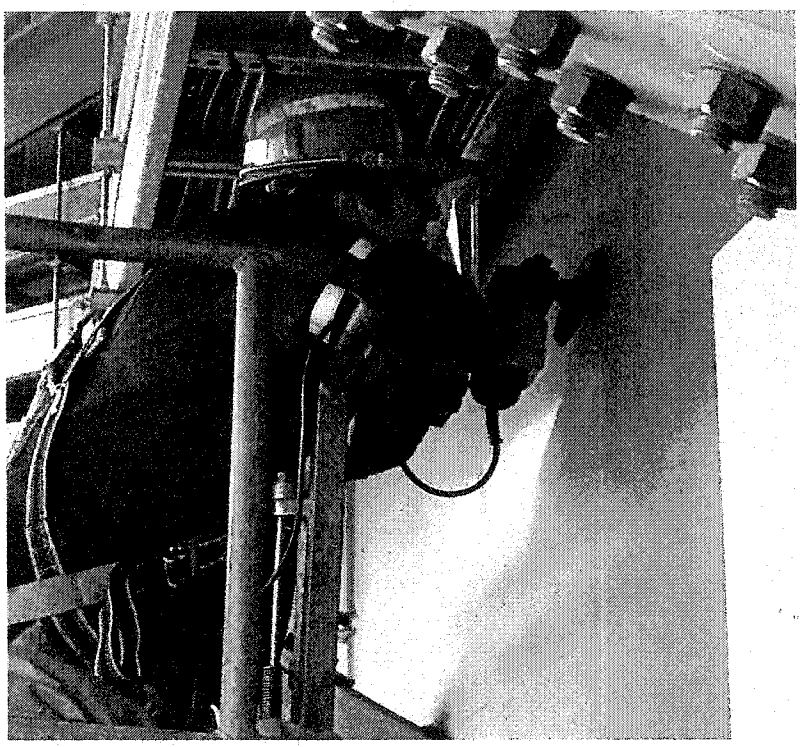

Figure 4-5: Surface Preparation, Grinding and Buffing

Figure 4-6: Welding Strain Gauge

After the gauge was installed and checked, an Air Drying Nitrile Rubber Coating was applied to seal the gauge, followed by a Teflon Tape and neoprene rubber pads underneath the lead wires and overtop the entire gauge, to protect the wires if direct pressure was applied. An aluminium insulating tape covered the Teflon tape and rubber

pads. A Butyl Rubber Sealant Coating covered the entire assembly. Electricians pulled 22 gauge 4 conductor overall foil shielded cables to all of the gauge locations. The cables were soldered to the lead wires and the gauge was checked again to ensure it was still intact. Another sheet of the Butyl Rubber Sealant Coating was applied to seal the entire assembly, as seen in Figure 4-7.

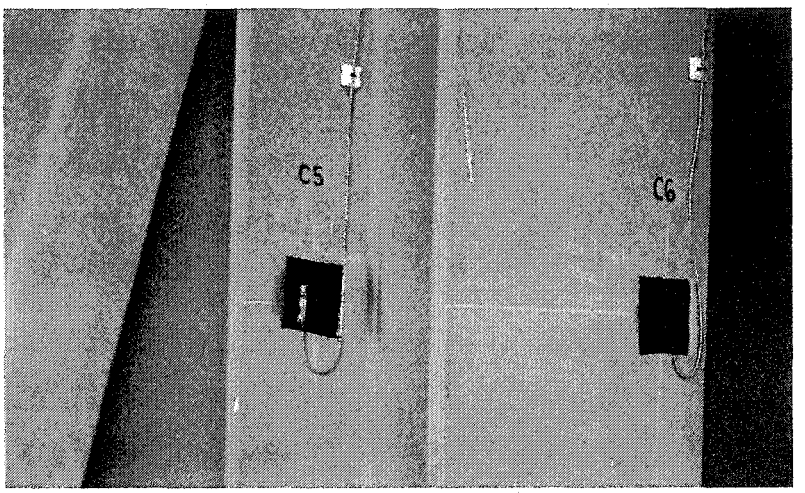

Figure 4-7: Gauges completed protected with rubber pad

4.1.2. LVDTs and Accelerometers

LVDTs and accelerometers were installed to measure the displacement of the pontoon and hopper. The LVDTs measured the displacement of the pontoon and hopper with respect to the retaining wall. Small angle brackets were used to mount the LVDTs to the columns or the pontoon with a magnet. In order to obtain horizontal and vertical measurements, brackets were installed on the retaining wall to create a perpendicular surface for measurement. See Figure 4-8 and Figure 4-9.

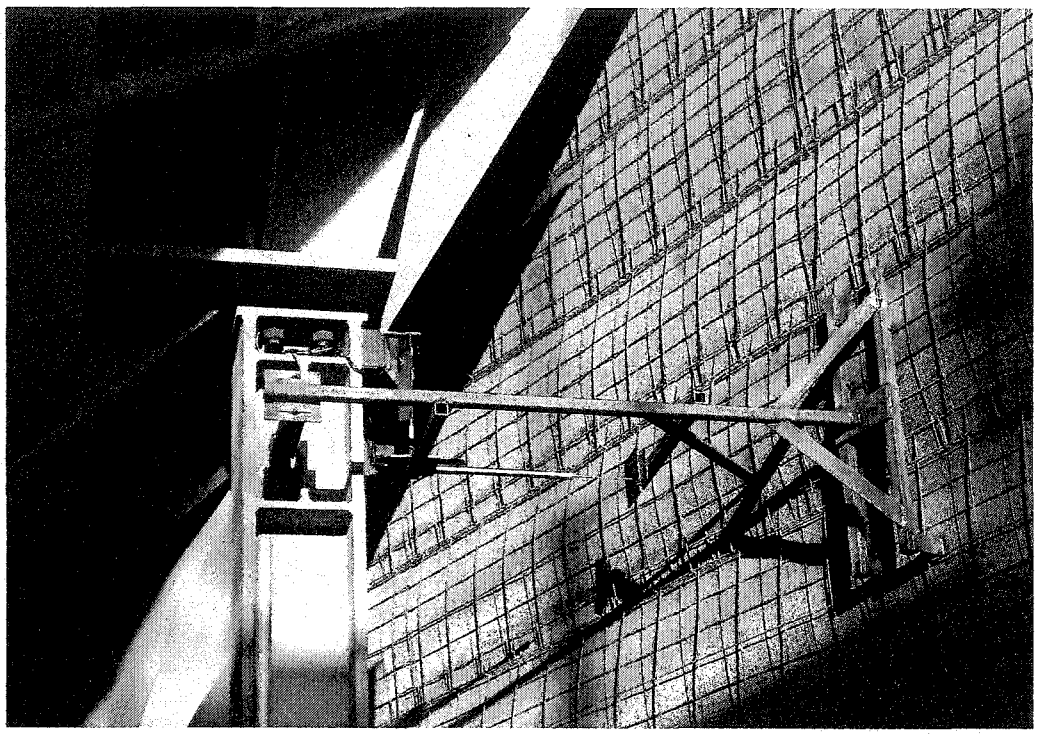

Figure 4-8: Upper LVDT Bracket Assembly

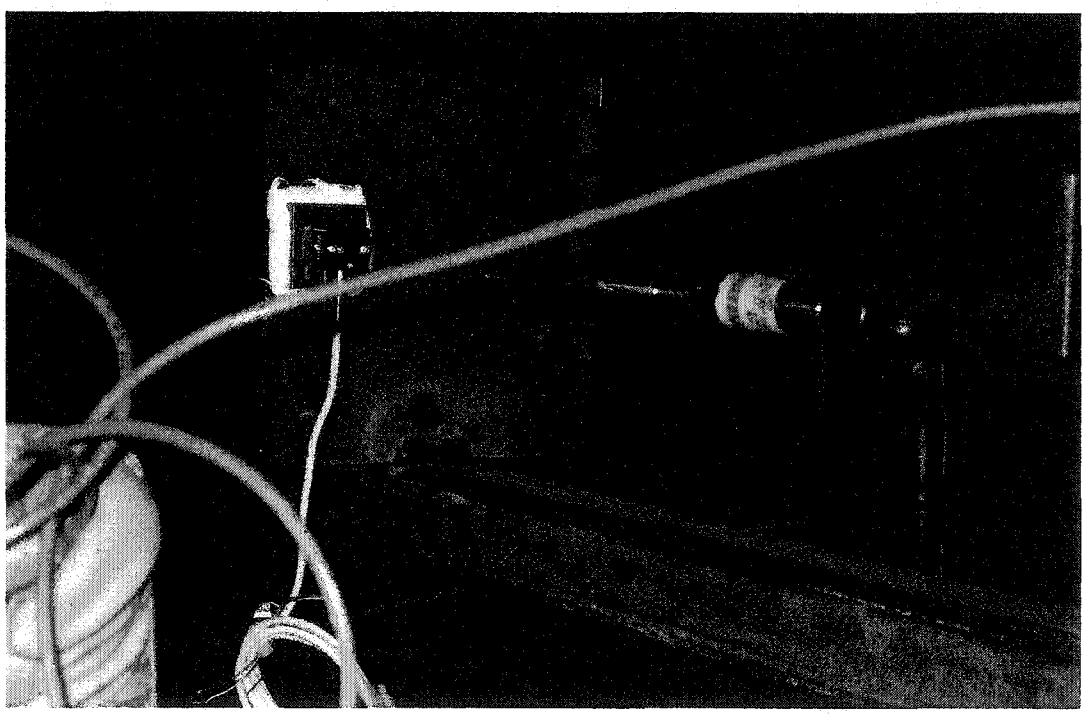

Figure 4-9: Lower LVDT Assembly

Because the LVDTs experience large vibrations while the crusher is in operation, captive guided spring return LVDTs were used for all horizontal measurements. The pontoon

was expected to experience very small displacements, approximately 1mm; therefore LVDTs with the range of ±12.5 mm (0.5 inches) were chosen for y and z-displacements of the pontoon. X, y, and z-displacements were measured at the top of the columns at Gridline 4. The x-displacements were measured with ±50 mm (2 inches); the z-displacements were measured with ±150mm (6 inches). Due to a shortage of captive guided spring return LVDTs, the y-displacements were measure using captive guided LVDTs with a range of ±50mm (2 inches). All of the LVDTs have an output of ±5 volts and an error of ±0.25% of their full range.

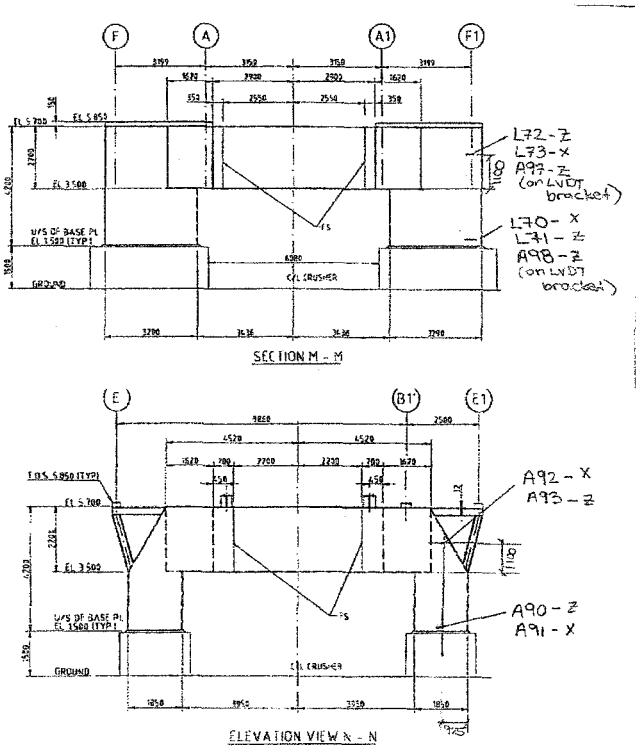

Figure 4-10: Pontoon LVDT & Accelerometer Locations

Because the retaining wall was too far away, LVDTs could not be used; therefore, accelerometers were used at the other end of the crusher. Four accelerometers were installed on the pontoon at the far end from the LVDTs to measure indirectly the identical displacements as the LVDTs at the other end. See Figure 4-1 and Figure 4-10 for LVDT and accelerometer locations. Accelerometers were also installed at the top of the columns at Gridline 6 to measure all three displacements. The accelerometers were

installed with magnets and then sealed around the edge of the bracket with silicon to ensure there was no movement of the bracket due to the vibration of the crusher. See Figure 4-11 for the accelerometers installed at Gridline 6. Three accelerometers were installed on the brackets for the LVDTs to gain information on how much the retaining wall movement is contributing to the displacement measurements. The accelerometers were installed to measure the z-displacement. The accelerometers have an output of ±5 volts, and a calibration of 2.5 V/g. With the LVDTs and accelerometers the rigid body motion of the hopper can be interpreted and the displacement of the pontoon.

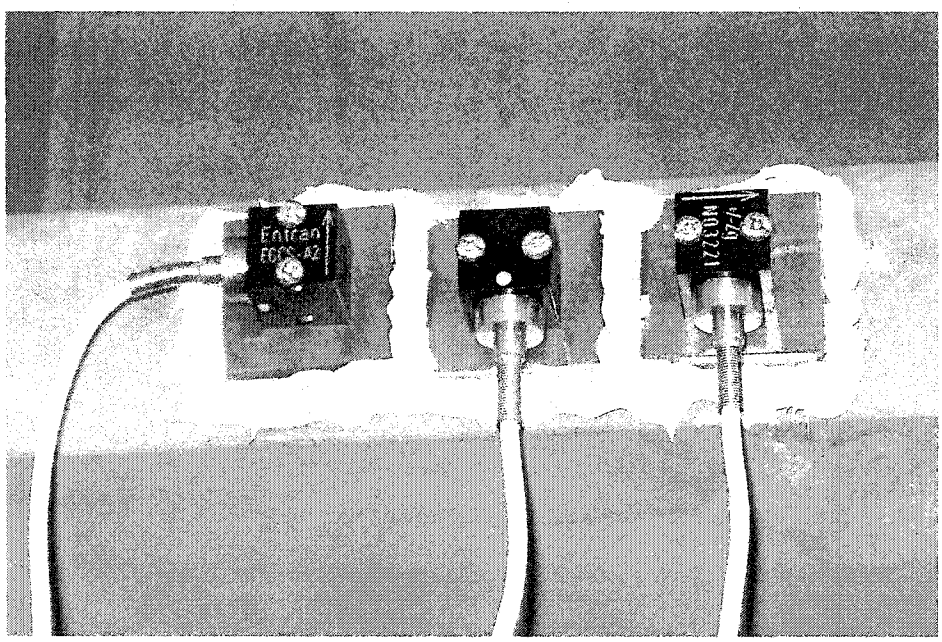

Figure 4-11: Installed Accelerometers, A94, A95, & A96

4.1.3. Thermocouples

Type T thermocouples were installed at four locations on the crusher in order to determine the temperature of the crusher at the location of the gauges. The thermocouples were installed by sticking them to the surface of the crusher at a location near the gauge. A Butyl Rubber Sealant Coating was applied over the thermocouple to protect it. Only enough thermocouple wire was available to run to two gauges: one on the pontoon near gauge P47 and one on the hopper near gauge H57. The wire was soldered to the lead wires of the thermocouple and the entire assembly was covered by a sheet of the Butyl Rubber Sealant Coating.

4.2. Test Program

4.2.1. Thermal Strains

In order to determine how much of an affect the temperature has on the strain in the crusher, data was collected for a 24 hour period before the crusher had begun operation. This data gives the relationship between strain and temperature. A value for each gauge will be calculated with Microsoft Excel's Linear Regression capabilities to determine the amount of strain experienced for each degree Celsius. The Data Acquisition System is taking readings at a frequency of 100 Hz which is too frequent for the temperature data. It was found that a ten minute average of temperature data is adequate; therefore, all temperature data will be averaged at ten minute intervals.

4.2.2. Load Testing

The Aurora II Crusher was new when it was instrumented. The first set of data collected was during a twelve hour period when the production train was tested on October 18, 2003. The data was collected at a rate of 100 Hz. A second data set was collected during normal operation of the crusher on April 14, and April 15, 2004. Data was sampled at 100 Hz; seven minutes of data was collected on April 14 and a half an hour of data was collected on April 15. In order to have a better understanding of the data, a video camera was used to provide visual observations of the loading.

4.2.3. Control Testing

Due to production constraints, controlled testing was conducted over a forty-five minute period on April 15, 2004. All of the testing done in the controlled testing was conducted with the hopper completely empty. The following characteristics were known during each controlled dump: weight of the load in the dump truck, grade of oil sand dumped, location (side) of dumping, and truck number. During control testing, digital video was recorded to supplement the data with visual observations. The control tests will allow for the characterization of events and the creation of a dump event to be used in the numerical model. Rich oil sand tends to discharge quickly in one large lump, where as the lean oil sand discharges slowly. Table 4-1 contains the details of the controlled dumping.

Table 4-1: Control Test Details

Time	Dump Weight (tonnes)	Oil sand Grade	Dump Location	Truck Number	Data File	Event time in Data File (seconds)
13:48	364	Rich	North	507	15.April(testplan)_1	114
13:52	520	Lean	South	504	15.April(testplan)_2	335
13:56	362 382	Rich Lean	North South	525 503	15.April(testplan)_3	610

5. Test Results

5.1. Thermal Data Results

The thermal data was collected at 100 Hz as was all the data in the first stage. This was too high of a sampling rate for the thermal results. The data was averaged at intervals of one minute, five minutes, ten minutes and twenty minutes, forty minutes and eighty minutes. The standard deviation of the average was determined for each interval. The standard deviation of the standard deviation was also calculated and was lowest for intervals of ten and twenty minutes. In the other ranges the standard deviation of temperature increased significantly; therefore the temperature data and the strain gauge data collected during the 24 hour period before loading began was averaged in ten minute intervals and then analyzed.

5.1.1. Columns

In order to calculate the variation of strain with temperature for each gauge the ten minute averaged data was plotted with microstrain on the vertical axis and temperature on the horizontal axis. The temperature data used for the column gauges was averaged not only on ten minute intervals but both thermocouple data was averaged. Using gauge C10 as an example the initial plot includes all the data points, see Figure 5-1.

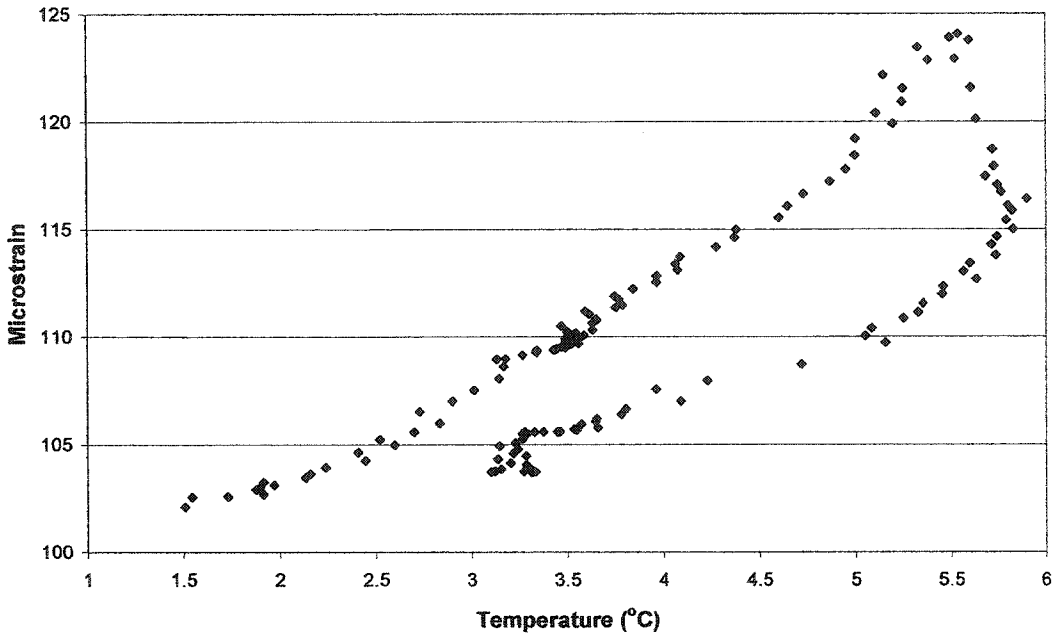

Figure 5-1: Strain C10 Entire Data Thermal Plot

The data is quite scattered as the temperature stops increasing and begins cooling off. This pattern is observed in most of the gauges and therefore the data was refined to include only the linear increasing temperature portion. Once this refined data was plotted, linear regression in Microsoft Excel could be used to fit a straight line to the data points and a value for the change in strain with temperature could be calculated, see Figure 5-2 .

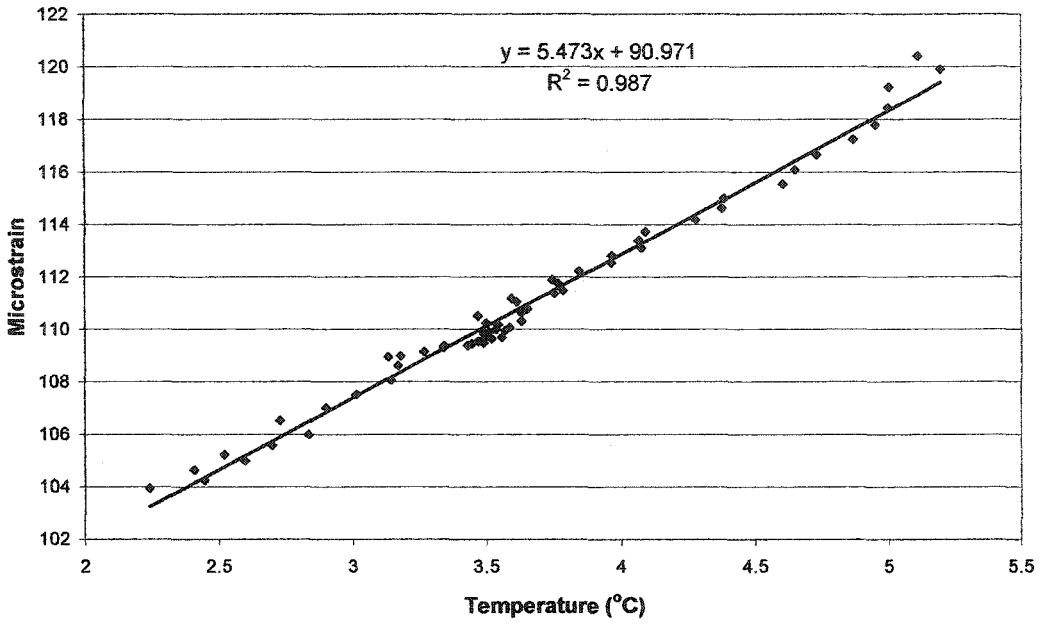

Figure 5-2: Strain C10 Refined Data Thermal Plot

This process was done for all of the column gauges and a summary of the values for their strain variation with temperature is provided in Table 5-1.

Gauges C25, C26, C30, C31, C39 and C40 did not have a linear response to the temperature change and therefore are not included in the table. The remaining gauges showed a good fit to a linear response as the fit is greater than eighty-five percent and generally greater than ninety-five percent.

Table 5-1: Column Thermal Results

Gauge	slope(με/°C)	R^2	Gauge	slope(με/°C)	R^2
C1	2.95	0.955	C18	4.04	0.971
C2	4.37	0.982	C19	4.37	0.956
C3	4.53	0.989	C20	4.66	0.960
C4	4.58	0.988	C21	5.36	0.978
C5	3.96	0.966	C22	5.11	0.952
C6	4.44	0.963	C23	3.43	0.888
C7	4.00	0.983	C24	3.50	0.912
C8	4.89	0.988	C27	4.30	0.945

C9	4.25	0.975	C28	1.65	0.957
C10	5.47	0.987	C29	2.34	0.958
C11	4.99	0.969	C32	1.82	0.847
C12	4.63	0.973	C33	4.65	0.978
C13	3.69	0.967	C34	4.68	0.969
C14	4.20	0.939	C35	5.21	0.948
C15	4.14	0.932	C37	1.31	0.891
C16	4.30	0.916	C38	1.73	0.877
C17	4.55	0.988			

5.1.2. Pontoon

The same process as described in the columns section was performed for the pontoon gauges; however, only one thermocouple was used. The temperature was average on ten minute intervals but T104 was used as the temperature data because it was located directly on the pontoon. Table 5-2 shows the thermal coefficients for each pontoon gauge.

Table 5-2: Pontoon Thermal Results

Gauge	slope(με/°C)	R^2	Gauge	slope(με/°C)	R^2
P45	3.61	0.963	P50	2.80	0.900
P46	2.43	0.887	P51	3.44	0.975
P47	4.23	0.966	P52	2.45	0.916
P48	2.81	0.916	P53	2.73	0.937
P49	4.26	0.971	P54	2.75	0.959

5.1.3. Hopper

Thermal coefficients were also calculated for all working gauges in the hopper. Gauge H59 was faulty after installation. The thermocouple used for thermal data in the hopper was gauge T103 as it was located on the hopper between gauges H57 and H61.

Table 5-3 summarizes the relationship between the temperature and thermal strain in the hopper.

Table 5-3: Hopper Thermal Results

Gauge	slope(με/°C)	R^2	Gauge	slope(με/°C)	R^2
H55	6.43	0.951	H61	5.99	0.928
H56	5.69	0.973	H62	5.28	0.951
H57	6.42	0.940	H63	5.22	0.940
H58	5.70	0.958	H64	5.48	0.945
H60	5.08	0.961			

5.2. *Hopper Results*

5.2.1. Stress Distribution

Ten strain gauges on the hopper collected data at 100 Hz. Events were identified by calculating the range of microstrain in each data file. If the difference between the maximum and minimum strain over the file (approximately ten minutes) was greater than ten microstrain the file would be examined. Sixteen of sixty files from the October testing and nine of the fifteen files from the April Testing had events. For each file with an event present the strain versus time was plotted. An event was identified by a drastic change in strain over a short period. An example of an event identified by the plot is shown in Figure 5-3. At first, this was done for all gauges; however, after the first few files only selected gauges were plotted as they provided the general event start and end times.

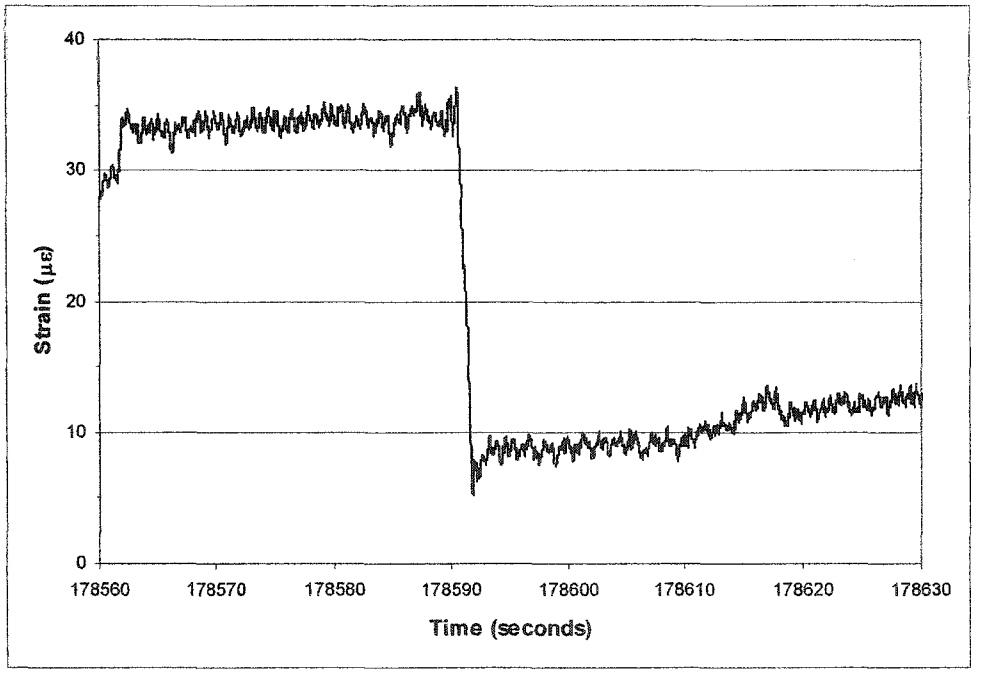

Figure 5-3: Event in Hopper Gauge H62

From the strain versus time plot the beginning and ending of the event were identified visually. A one minute average of the strain was taken at these points; designated the strain before and strain after the event. The difference in these strains was the static strain change observed for the event. Assuming linear elastic behaviour this strain change was converted into a stress change by multiplying by the modulus of elasticity, E,

which was taken as 205 000 MPa from the STAAD model of the Aurora II Crusher. Because this was an existing structure, no auxiliary material tests could be conducted to determine the actual modulus of elasticity. The model value was used for ease of comparison because the model's only output is stress. Gauge H59 was damaged and therefore no results from this gauge were obtained. Gauge H60 which was the other gauge on the hopper plate consistently showed little to no change; therefore, this gauge was also not used during analysis. Twenty-five events were identified from the October testing, summarized in Figure 5-4, Figure 5-5 and Figure 5-6. Seven events were identified during the normal operating data collected in April; results are shown in Figure 5-7. Control testing was conducted in April. Three loading scenarios were conducted, explained in Section 4.2.3. The results from the Control Tests are shown in Figure 5-8.

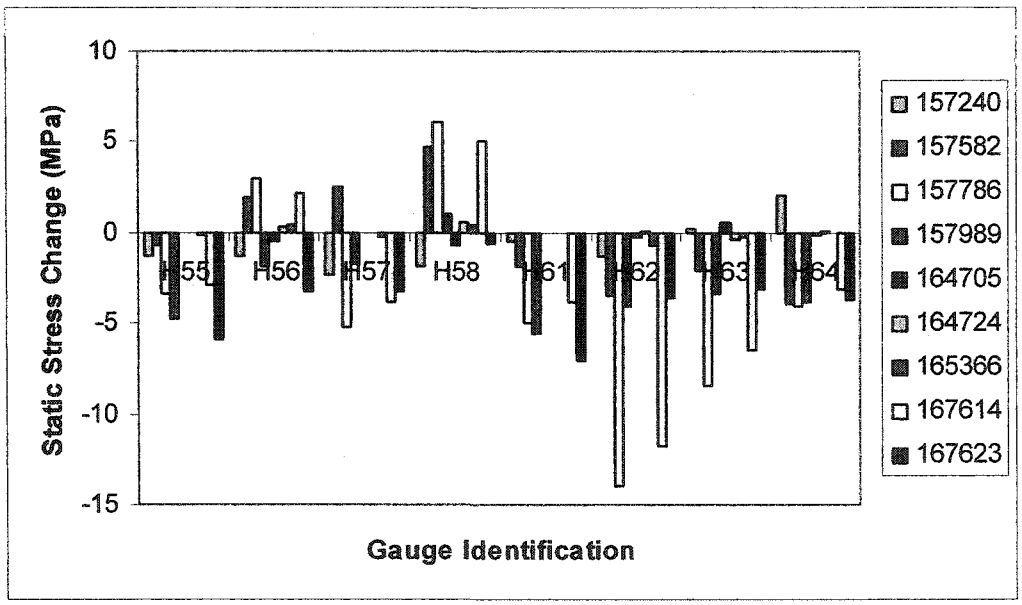

Figure 5-4: Hopper Stress Distribution October Events 1-9

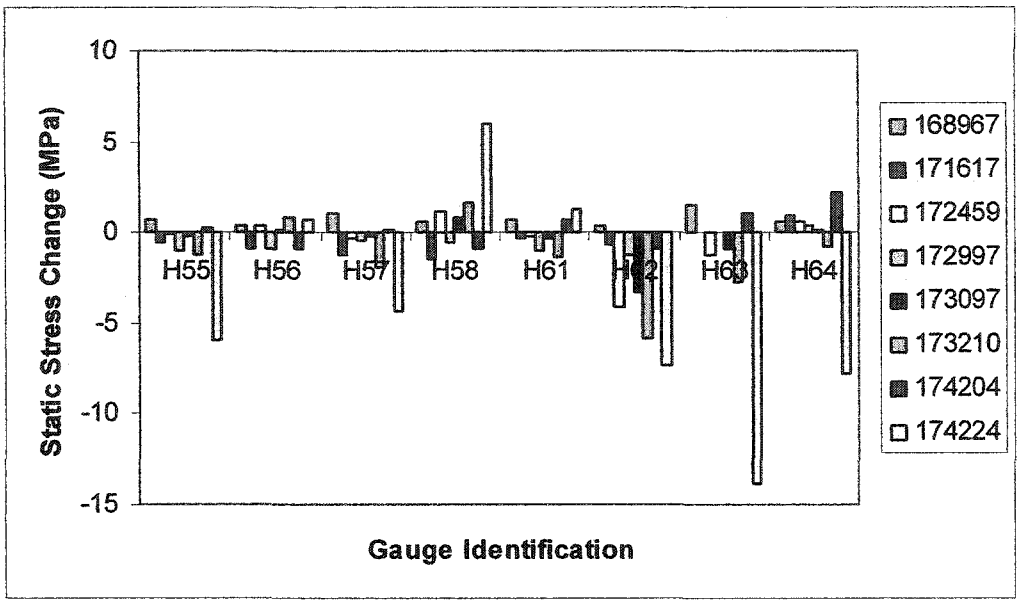

Figure 5-5: Hopper Stress Distribution October Events 10-17

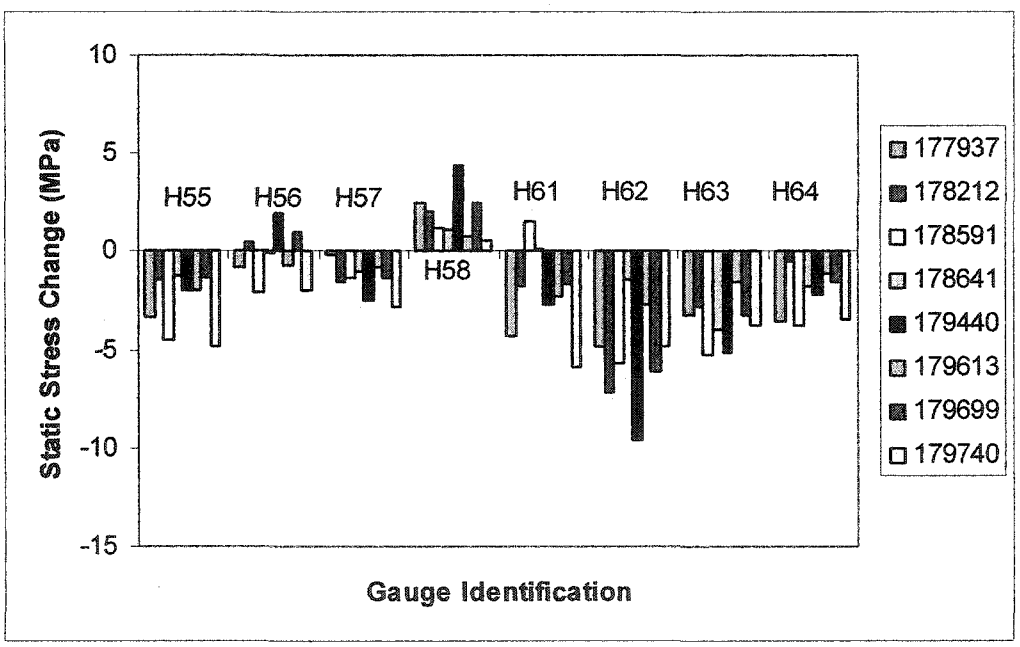

Figure 5-6: Hopper Stress Distribution October Events 18-25

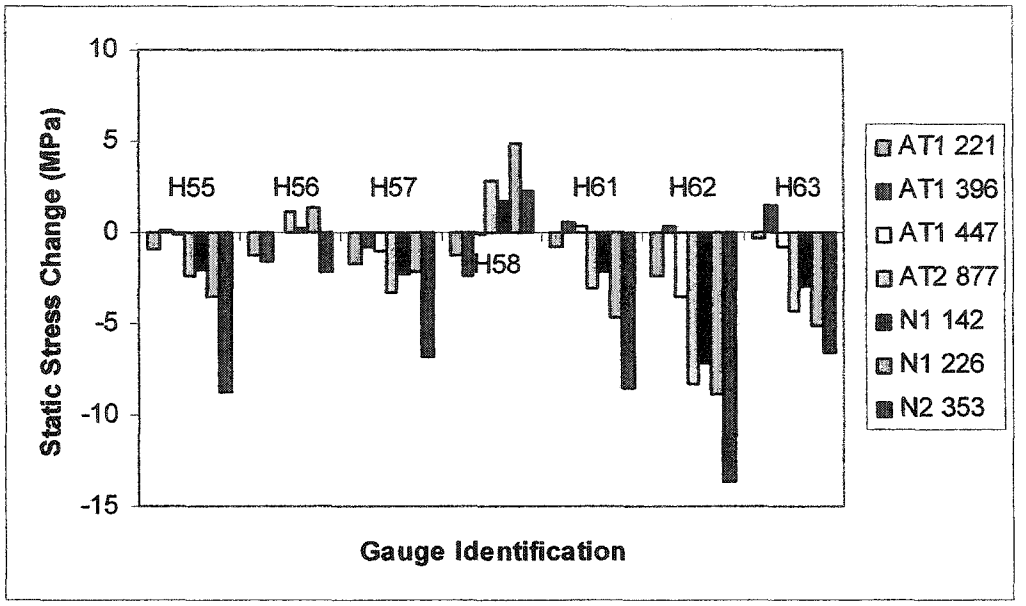

Figure 5-7: Hopper Stress Distribution April Testing

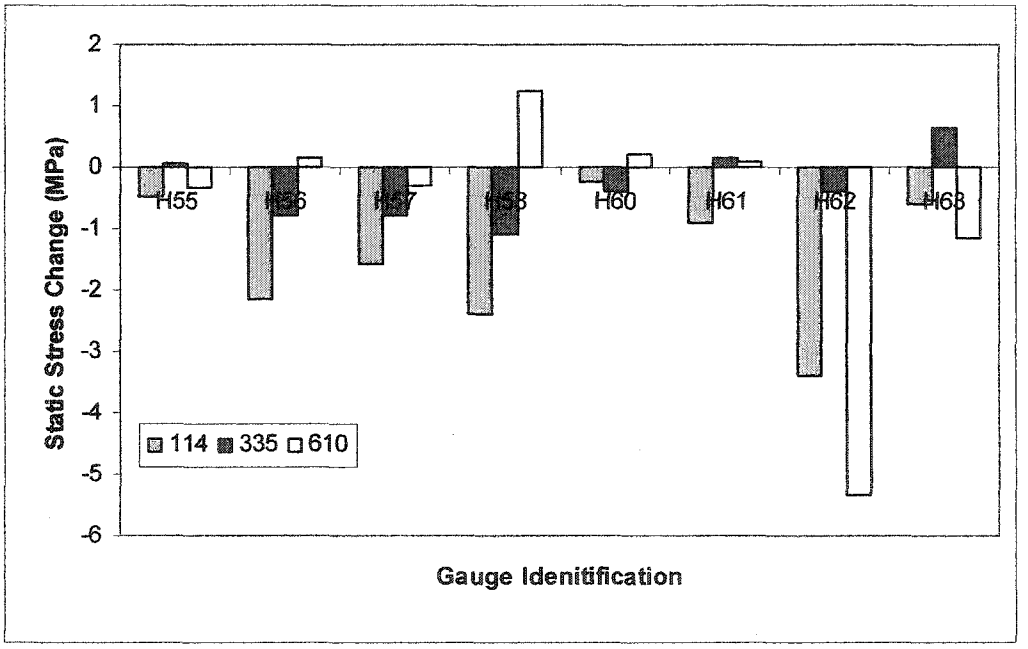

Figure 5-8: Hopper Stress Distribution April Control Tests

The gauges at the intersection of the horizontal and vertical stiffeners (H62-H64) show the largest response to the events. Twenty percent of the events show a stress change greater than 5 MPa. Gauge H62 shows the largest response on a consistent basis having 34 percent of the events over 5 MPa. Gauges located on the vertical stiffeners have stresses ranging from 0.75 MPa to -8.80 MPa, with over 90 percent of them being below 5 MPa. Gauges on the horizontal stiffeners have stresses ranging from -3.26 MPa to 6.10

MPa, with 95 percent of them being below 5 MPa. Hopper stresses were quite varied for each gauge due to the high variability in loading of the hopper. The stress observed at each location would depend on exact location of impact of the oilsand. Gauge H62 did give the highest response on a consistent basis and could be used to identify an event occurring in the hopper. In Section 6.2, patterns will be examined to see if different types of events create different responses in the gauges.

5.3. Column Results

5.3.1. Stresses

Forty strain gauges installed on the columns recorded strain at 100 Hz. The strain was plotted versus time. Gauges were selected for analysis based on their significance. Gridlines 2 and 4 were deemed the most important as this is where dumping is occurring. With the large amount of noise on Gridlines 5 and 6 the following gauges were selected for analysis: C1-C4, C5, C6, C9, C10, C15, C16, C25-C30, C31, C32, C35, C39 and C40. These gauges provided the vertical loads transmitted to the pontoon on Gridlines 2 (C1-C4 and C25-C28) and Gridline 4 (C5, C6, C9, C10, C31, C32 and C35) as well as a sample of the stresses at the top of the column (C29 and C30) and the inclined members at the bottom of the exterior columns on Gridline 5 (C15, C16, C39 and C40).

Using the same process as described for the hopper stresses, twenty-nine events were identified in the column gauges for the October testing and twelve events were identified in the April testing. The stress for each event at each gauge location was calculated. Static stresses for all of the events at each of these gauge locations were calculated. Figure 5-9, Figure 5-10 and Figure 5-11 show the results of the column stress distribution on Gridline 2 for the October testing. The normal operations results for April testing on Gridline 2 are shown in Figure 5-12.

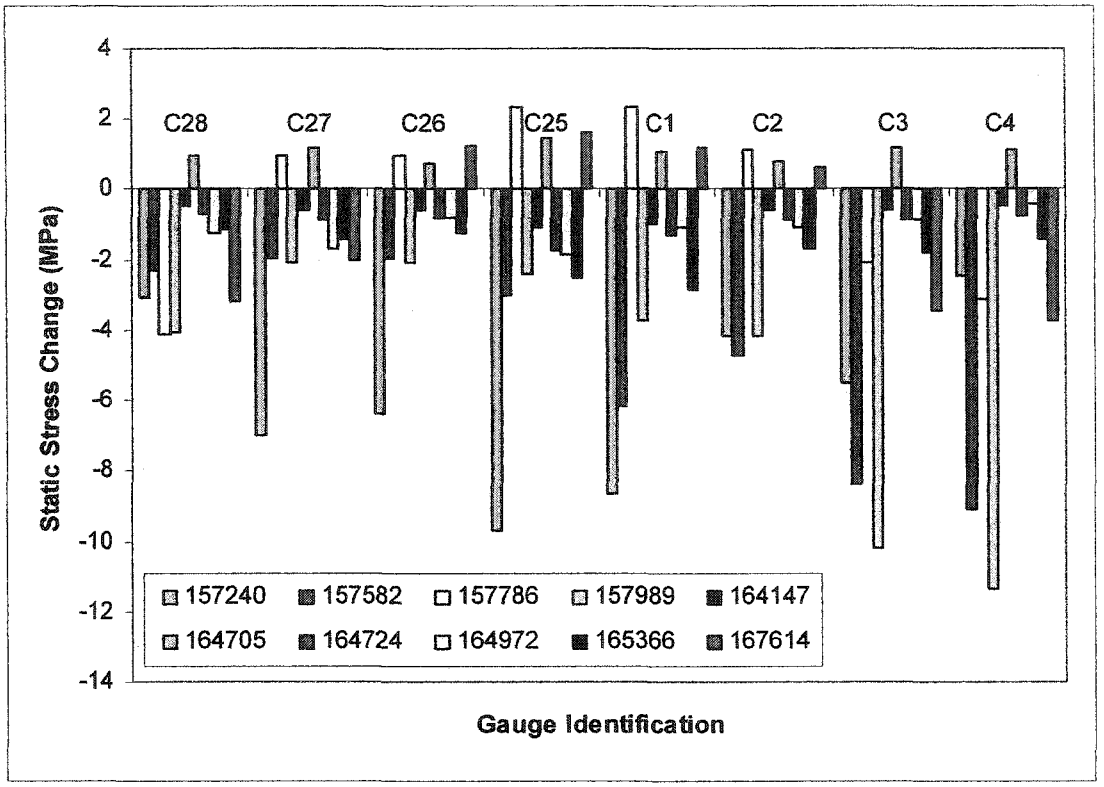

Figure 5-9: Gridline 2 Column Stress Distribution October Events 1 – 10

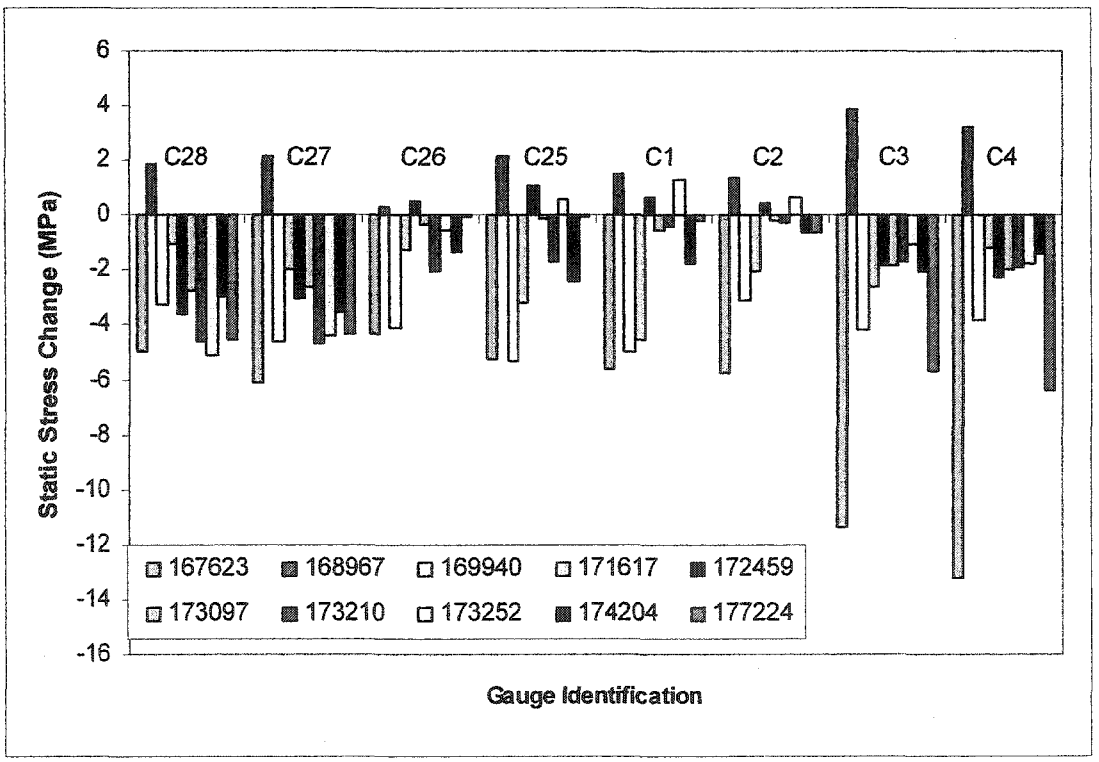

Figure 5-10: Gridline 2 Column Stress Distribution October Events 11 – 20

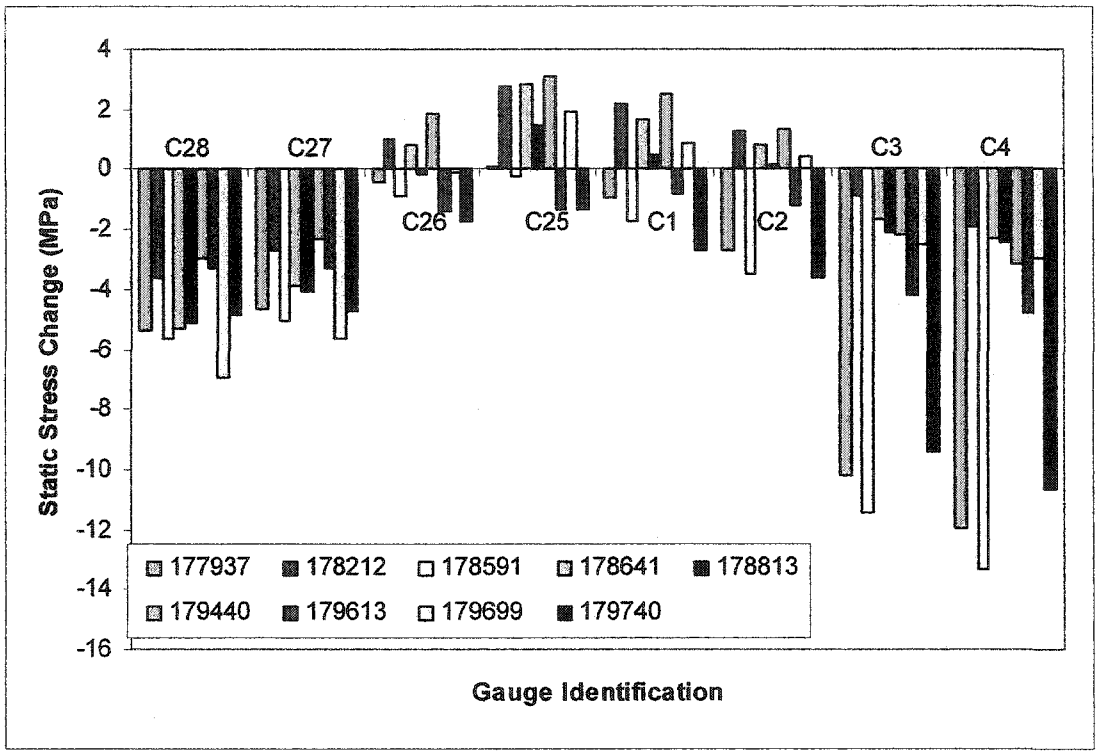

Figure 5-11: Gridline 2 Column Stress Distribution October Events 21 – 29

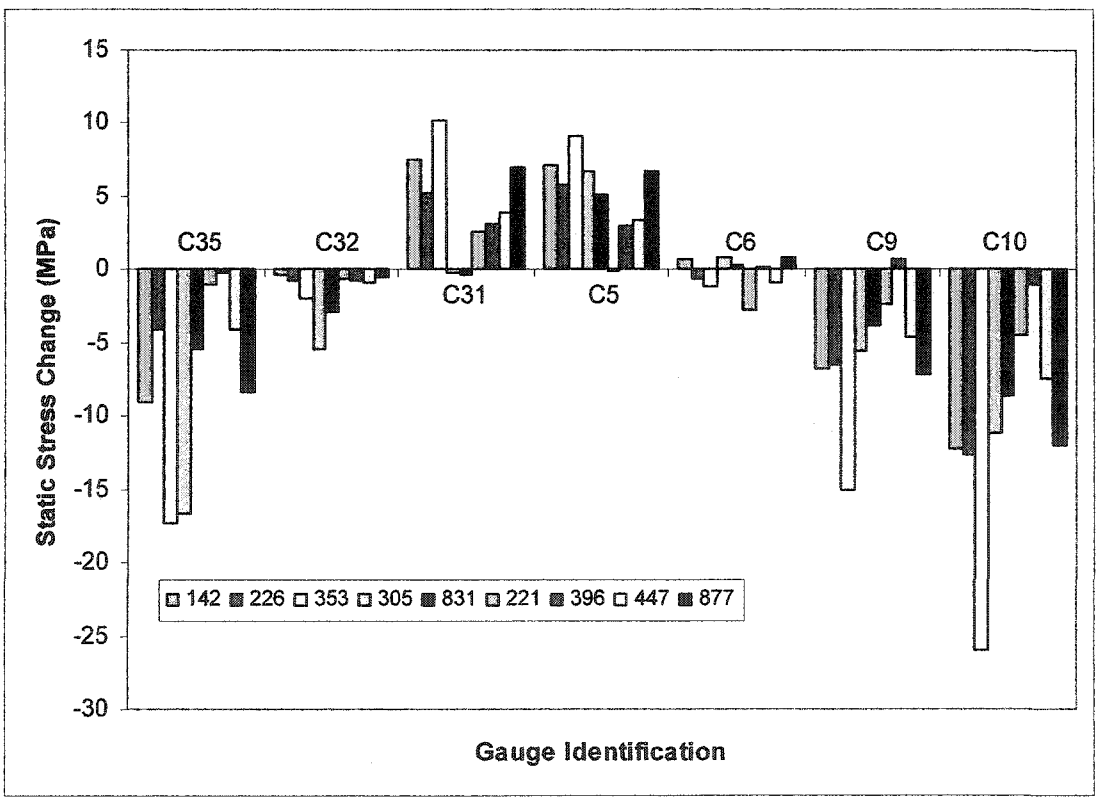

Figure 5-12: Gridline 2 Column Stress Distribution April Normal Operations

The largest stress changes on Gridline 2 are often in the outer vertical columns, but there are many instances where the inner columns also show high stress changes. All columns on Gridline 2 most often show a compressive stress change in response to an event; however, there are many variations which will be examined in Section 6.2. to create an event signature for different types of events. Figure 5-13, Figure 5-14, Figure 5-15 show the results of the column stress distribution on Gridline 4 for the October testing. The normal operations results for April testing on Gridline 4 are shown in Figure 5-16.

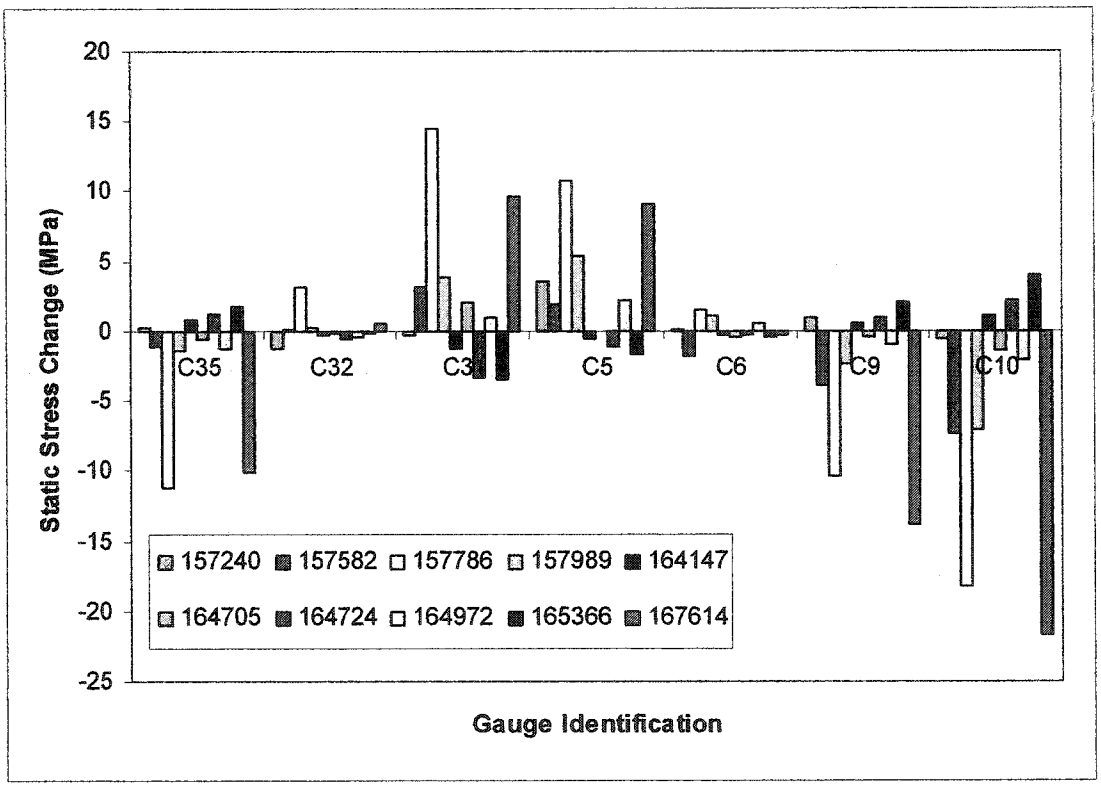

Figure 5-13: Gridline 4 Column Stress Distribution October Events 1 – 10

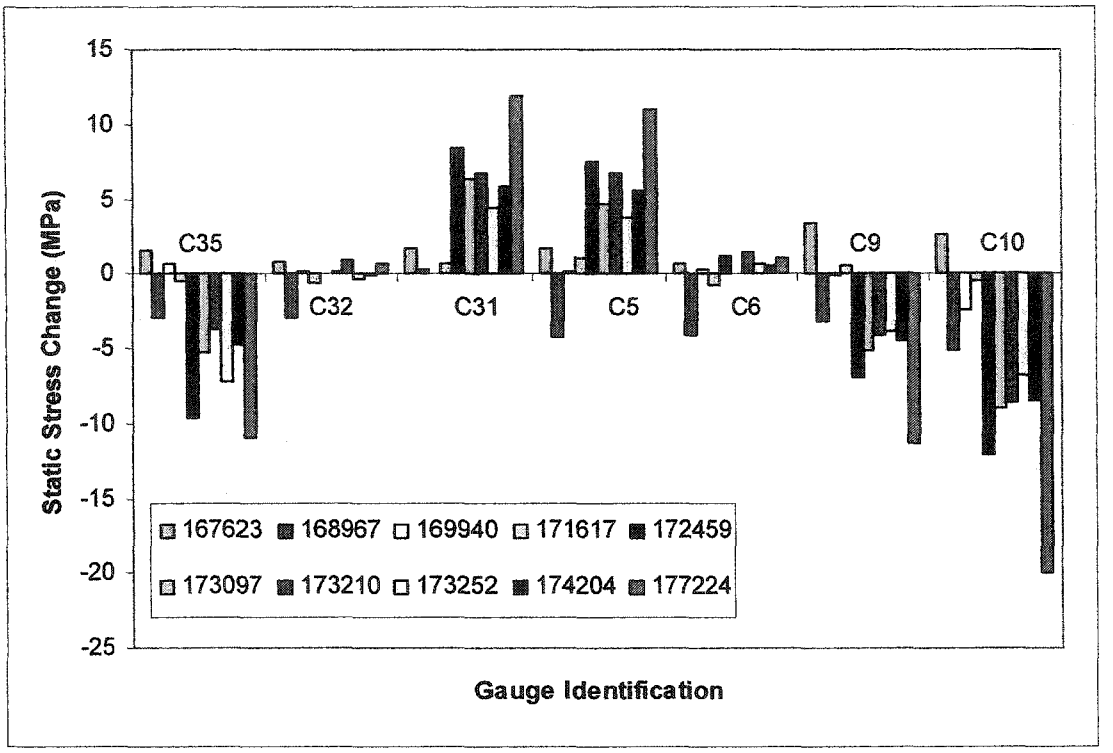

Figure 5-14: Gridline 4 Column Stress Distribution October Events 11 – 20

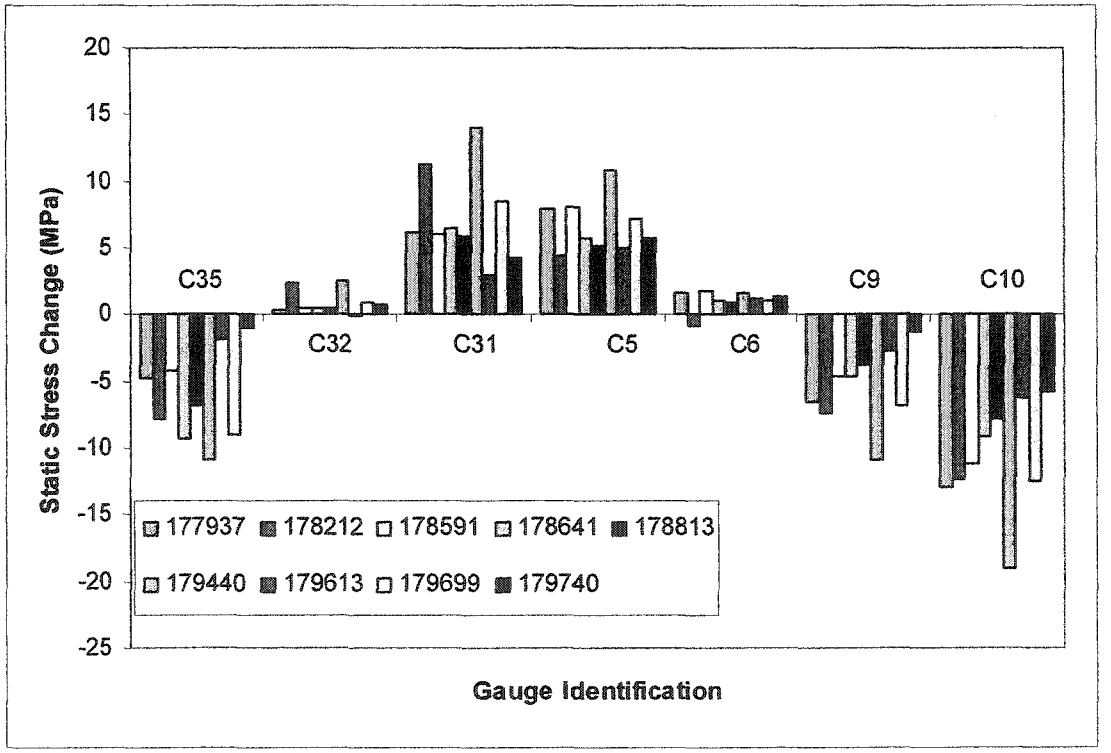

Figure 5-15: Gridline 4 Column Stress Distribution October Event 21 - 29

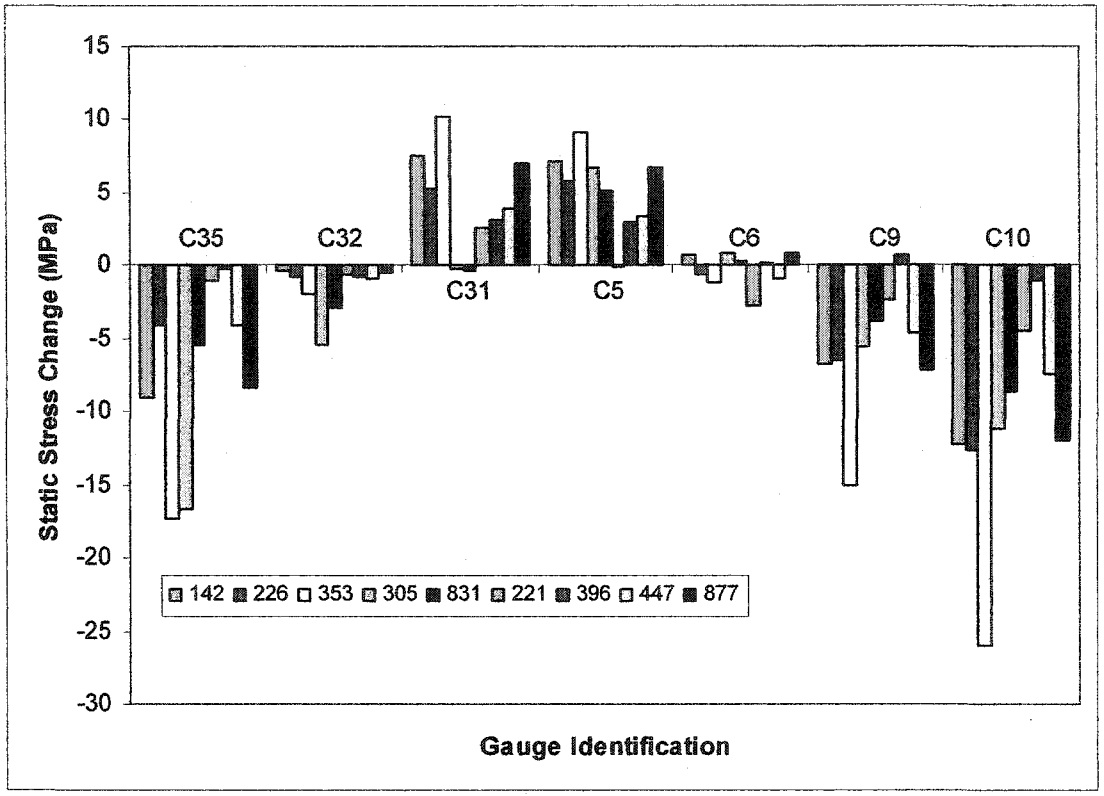

Figure 5-16: Gridline 4 Column Stress Distribution April Normal Operations

The outer column gauges on Gridline 4 have the largest stresses of the vertical columns. The inner columns most often show a tensile stress change in response to an event. The gauges on the outer part of the inner column (C32 and C6) often show little to no change. This would indicate the columns on either side of the hopper are bending as a group but the entire gridline of columns are not bending as a large built-up column.

The column stress distributions for the control testing are shown in Figure 5-17 and Figure 5-18. The distribution on Gridline 2 shows the largest stress changes in the inner columns. The distribution for Gridline 4 is similar to the normal operating results.

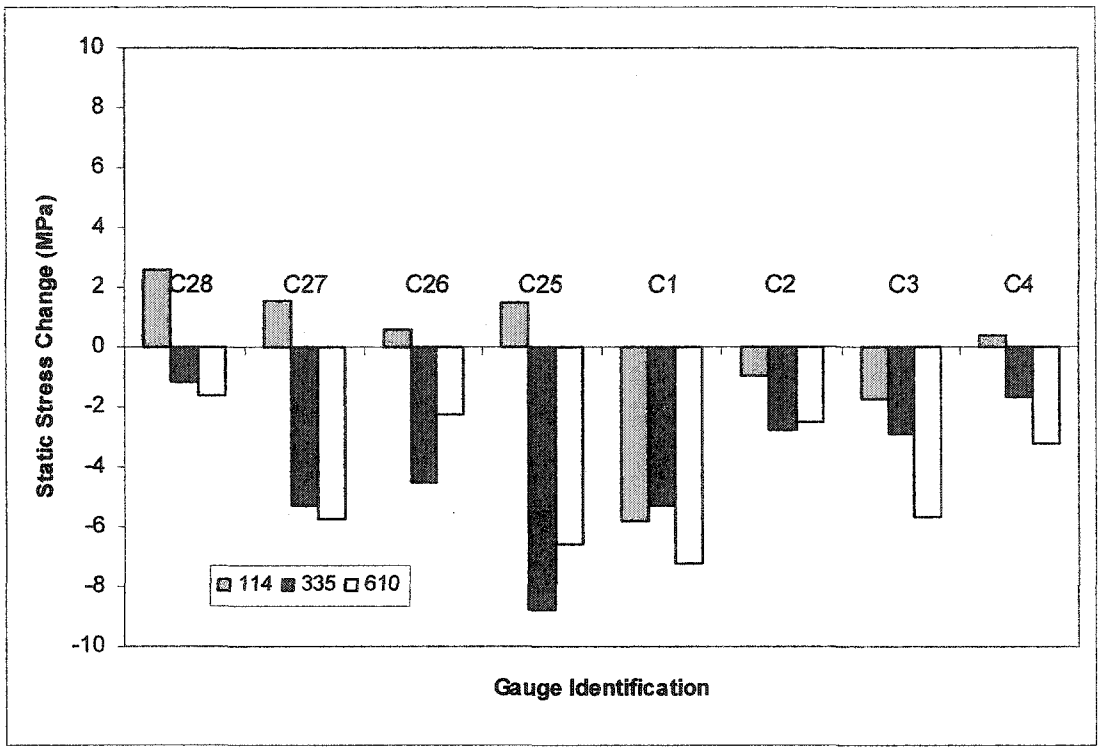

Figure 5-17: Gridline 2 Column Stress Distribution for Control Test

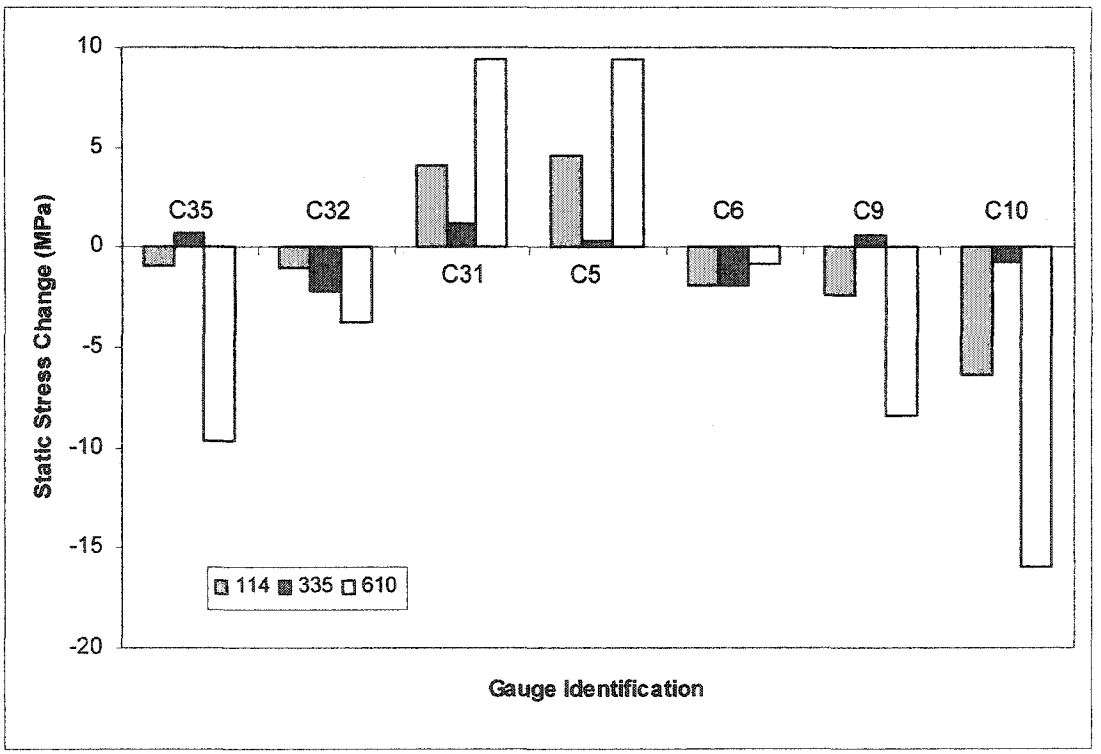

Figure 5-18: Gridline 4 Column Stress Distribution for Control Test

A comparison between the stress at the top and bottom of the columns was done to see if higher stresses occurred near the top as predicted by the model. Figure 5-19, Figure 5-20 Figure 5-21 and Figure 5-22 show the average stress at the bottom of the outer column on Gridline 2 (C27&C28) and the top of the column (C29 & C30). Approximately half of the time the top of the columns experience higher stresses than the bottom of the column. Mostly these differences are with 1.5 MPa, therefore are not a major concern. Four out of 38 times the column at the top and bottom experience opposite stress changes. The difference in the stress at the top and the bottom is due to a bending moment distribution in the column caused by the outward drift of the column top.

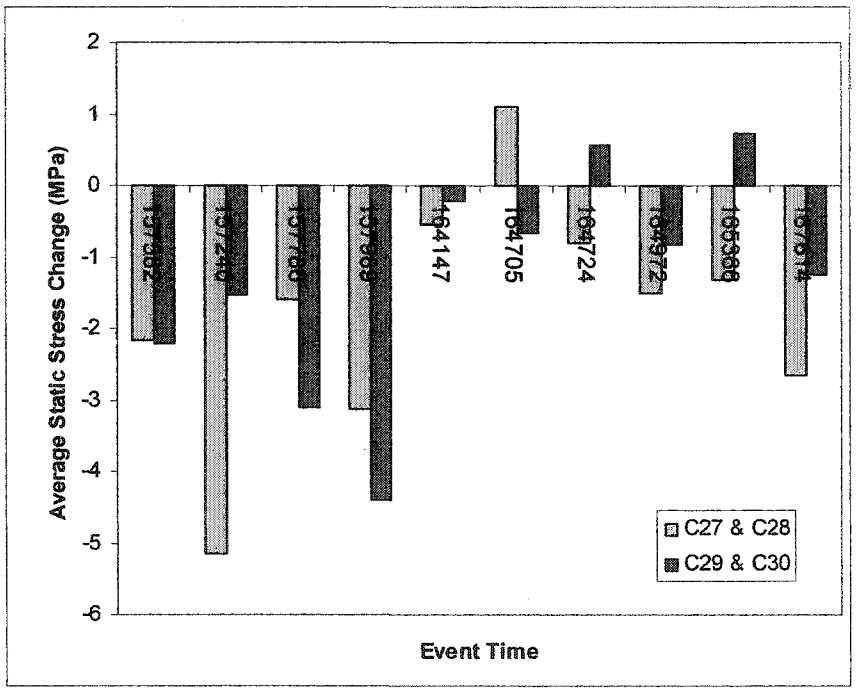

Figure 5-19: Top and Bottom of Column Stress Distribution for October Event 1 - 10

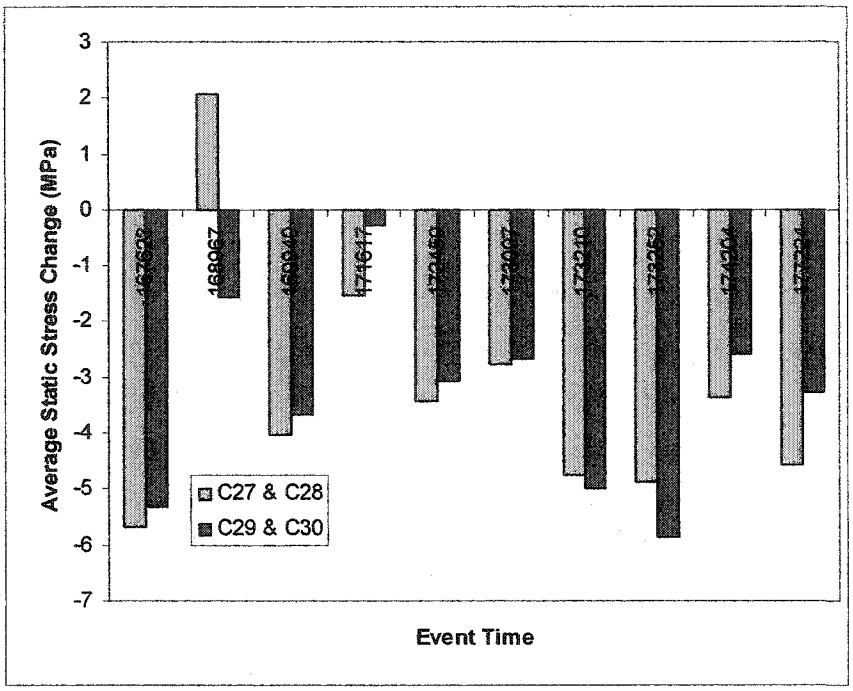

Figure 5-20: Top and Bottom of Column Stress Distribution for October Event 11 - 20

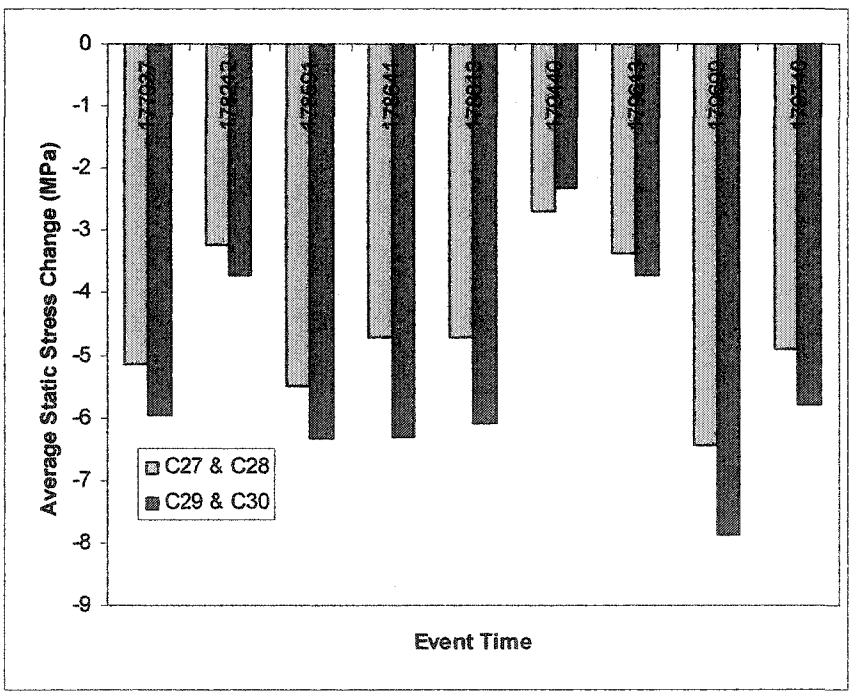

Figure 5-21: Top and Bottom of Column Stress Distribution for October Event 21 - 29

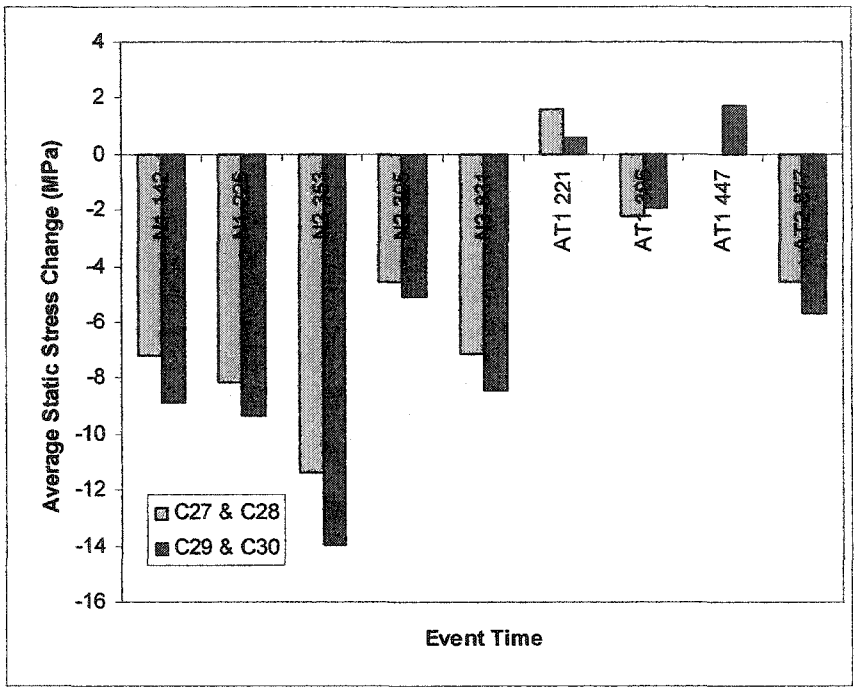

Figure 5-22: Top and Bottom of Column Stress Distribution for April Normal Operations Testing

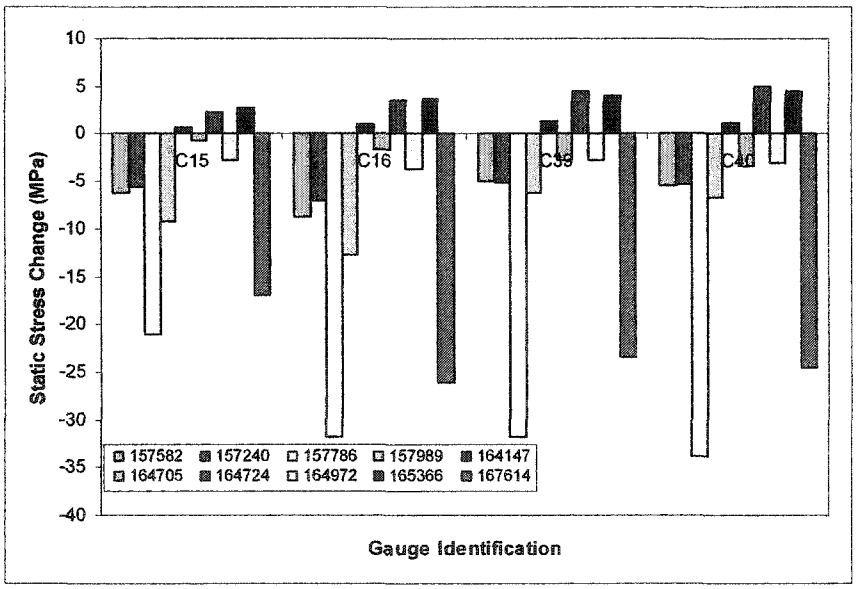

Figure 5-23: Bottom Inclined Member Stress Distribution for October Tests 1 - 10

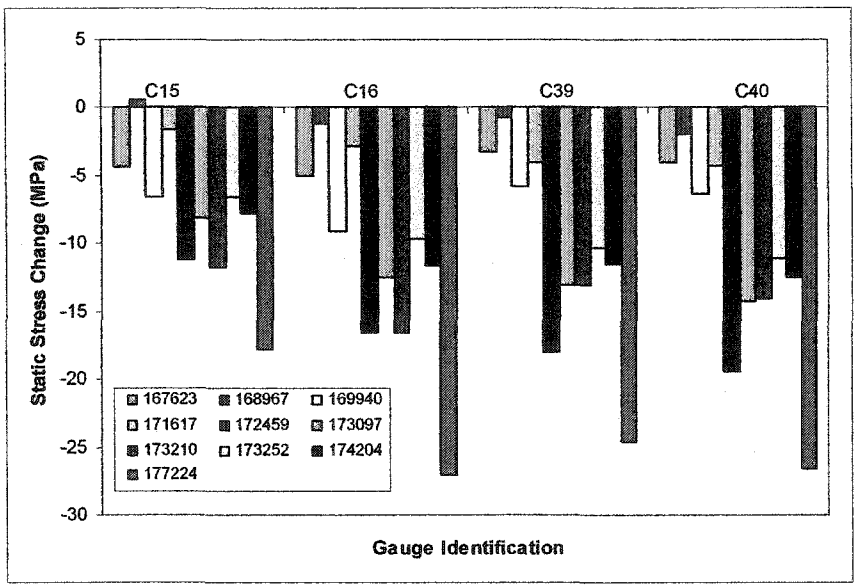

Figure 5-24: Bottom Inclined Member Stress Distribution for October Tests 11 - 20

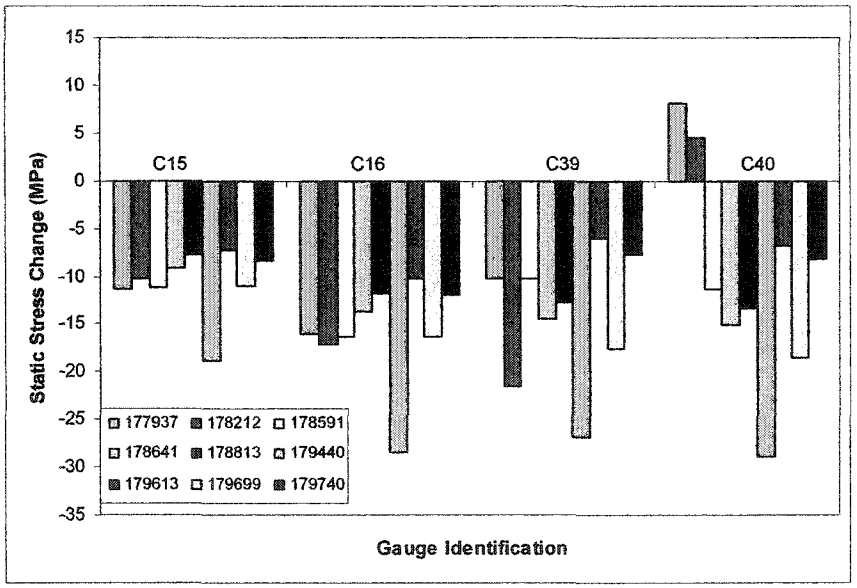

Figure 5-25: Bottom Inclined Member Stress Distribution for October Tests 21 - 29

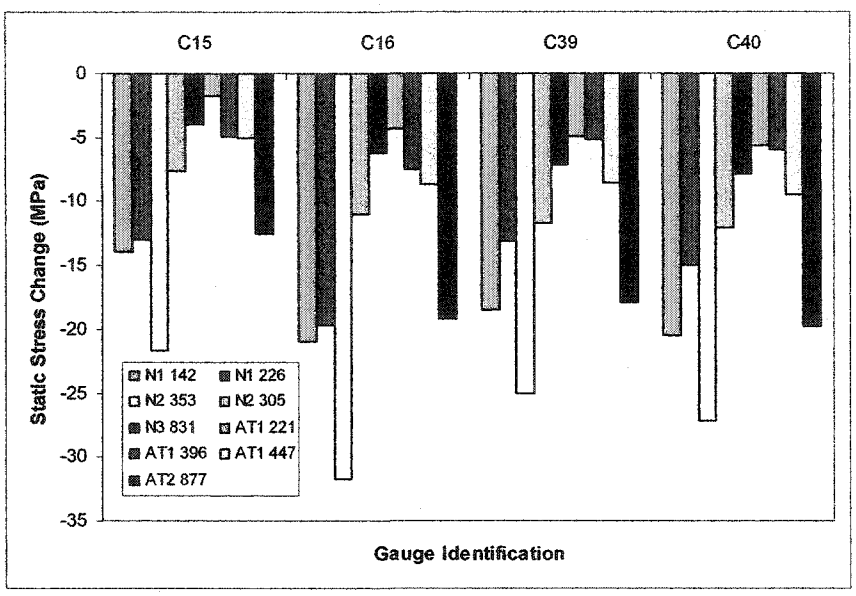

Figure 5-26: Bottom Inclined Member Stress Distribution for April Normal Operations Testing

Because the bottom inclined members on Gridlines 5 and 6 are smaller sections, they show the largest static stress change for events. See Figure 5-23, Figure 5-24, Figure 5-25 and Figure 5-26. These gauges could be used to identify events as they rarely have stress changes less 5 MPa for an event, which would correspond to 25 microstrain, which is 2.5 times the maximum noise observed in the gauges of 10 microstrain. Often gauges on either side of the columns do not show the same static stress change. To eliminate bending effects, the average of these two gauges will be used to determine if there is a pattern in the column stress distribution for different types of events, in Section 6.2.

5.3.2. Displacements

The displacements were calculated in much the same manner as static stress change. The accelerometers were not used to calculate any displacements because of problems. During initial set-up a number of the accelerometers were found to have no response and a few were thought maybe to have wires crossed and therefore not measuring the acceleration for which they were installed. A95 was removed to determine the problem. The problem could not be determined before the next set of testing in April; therefore I have chosen not to use any accelerometer data due to a lack of confidence in it. Results from the LVDTs are in the form of voltage output. Events identified while calculating static stress changes were also analyzed to determine static displacement. Voltage versus

time was plotted for the LVDTs (Figure 5-27), a beginning and ending average was taken over one minute, the voltage difference multiplied by the calibration number for each gauge is the static displacement.

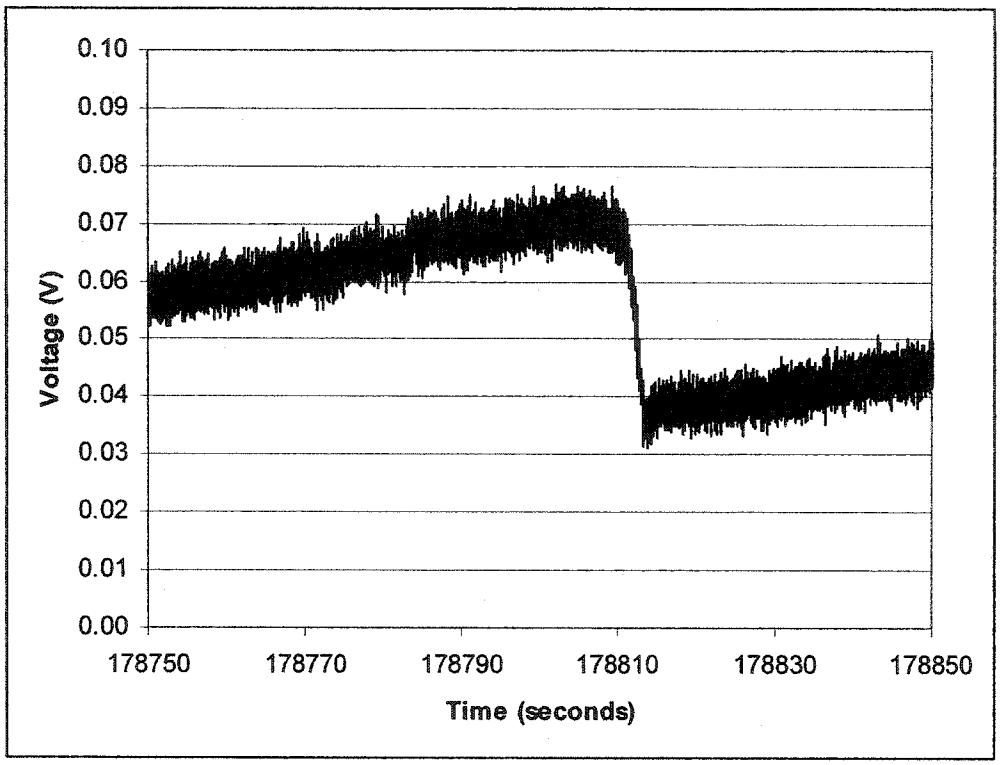

Figure 5-27: Event in L76

The LVDTs measured the relative displacement with respect to the retaining wall. L78 was faulty during October testing; therefore there are no results for the z-displacement on the left side of the apron feeder. Prior to the April Testing L79 fell down from the crusher; therefore they are no results for L79 for the April Testing. Table 5-4 summarizes the calculated static displacements of the top of the columns.

Table 5-4: Column Displacements

Event	L74 (x)	L75 (y)	L76 (z)	L77 (y)	L79 (x)
157240	1.269	-0.856	0.099	0.124	1.716
157582	0.102	0.102	0.109	0.031	0.053
157786	-0.639	-1.048	-2.193	-2.920	-0.266
157989	0.211	-0.951	-0.923	-0.204	0.368
164147	0.153	0.044	0.131	0.079	0.175
164705	-0.443	-0.040	-0.416	-0.147	-0.408
164724	0.245	0.058	0.398	0.121	0.239
164972	0.220	-0.079	-0.225	-0.531	0.253
165366	0.607	0.150	0.520	0.149	0.522
167614	-0.266	-0.940	-0.637	-7.450	0.176

167623	4.854	-10.321	0.689	-9.510	3.892
168967	-1.204	-0.246	-0.183	-1.067	-1.227
169940	0.447	-0.624	-0.107	0.096	0.701
171617	0.584	0.059	-0.019	-2.464	0.600
172459	-0.190	-0.595	-0.461	-7.340	-0.242
173097	-0.131	-0.464	-0.352	-4.692	-0.070
173210	-0.129	-1.073	-0.355	-1.308	0.065
173252	-0.142	-0.340	-0.239	-4.442	-0.248
174204	0.098	-0.327	-1.037	-1.465	0.183
177224	-0.467	-1.075	-2.353	-2.459	-0.254
177937	-0.234	-1.353	-1.406	-0.506	0.046
178212	-0.307	0.451	-1.274	-1.853	-0.406
178591	-0.085	-1.242	-1.382	-0.474	0.102
178641	-0.325	-0.508	-1.037	-1.750	-0.622
178813	-0.121	-0.374	-0.935	-1.455	-0.305
179440	-0.631	-1.000	-2.081	-2.371	-0.479
179613	-0.070	-0.751	-0.733	-0.245	0.052
179699	-0.291	-0.598	-1.353	-1.687	-0.256
179740	0.172	-0.764	-0.860	-0.202	0.272
Apr 14 142	-0.106	-0.547	-1.411	-1.643	
Apr 14 226	-0.023	-1.052	-1.405	-0.363	
Apr 14 353	-0.705	-1.747	-2.499	-2.269	
Apr 15 305	0.026	-0.506	-1.399	-2.081	
Apr 15 831	0.097	-0.371	-1.159	-0.812	
Test 114	-0.322	-0.222	-1.336	-0.733	
Test 335	0.487	-0.312	0.180	0.035	
Test 610	-0.246	-1.198	-1.291	-1.192	
After Test 221	-0.118	-0.339	-0.647	-0.466	
After Test 396	0.572	-0.471	-0.131	-0.044	
After Test 447	-0.148	-0.509	-0.994	-0.737	
After Test 877	-0.453	-0.717	-1.451	-1.526	

The largest column displacement was 10.32 mm down. 91 percent of the x-displacements were less than 1 mm and only 4 percent were larger than 2 mm. 62 percent of the y-displacements were less than 1 mm and 5 percent were larger than 2 mm. 58 percent of the z-displacements were less than 1 mm and 10 percent were over 2 mm. Because the retaining wall is not stationary and there would be vibration in the brackets that the LVDTs measure between the exact displacements are not known. However, over 80 percent of the z-displacements were negative indicating that the columns are displacing outwards. The difference between the vertical displacements will be examined in Section 6.2 to help to characterize events.

5.4. Pontoon Results

5.4.1. Stress Distribution

The pontoon data was handled in the same manner as the column and hopper results. All ten gauges were plotted for the first event identified by looking at the columns. The October results are shown in Figure 5-28, Figure 5-29 and Figure 5-30. April's normal operation results are shown in Figure 5-31. Figure 5-32 shows the pontoon stress results from the April control testing.

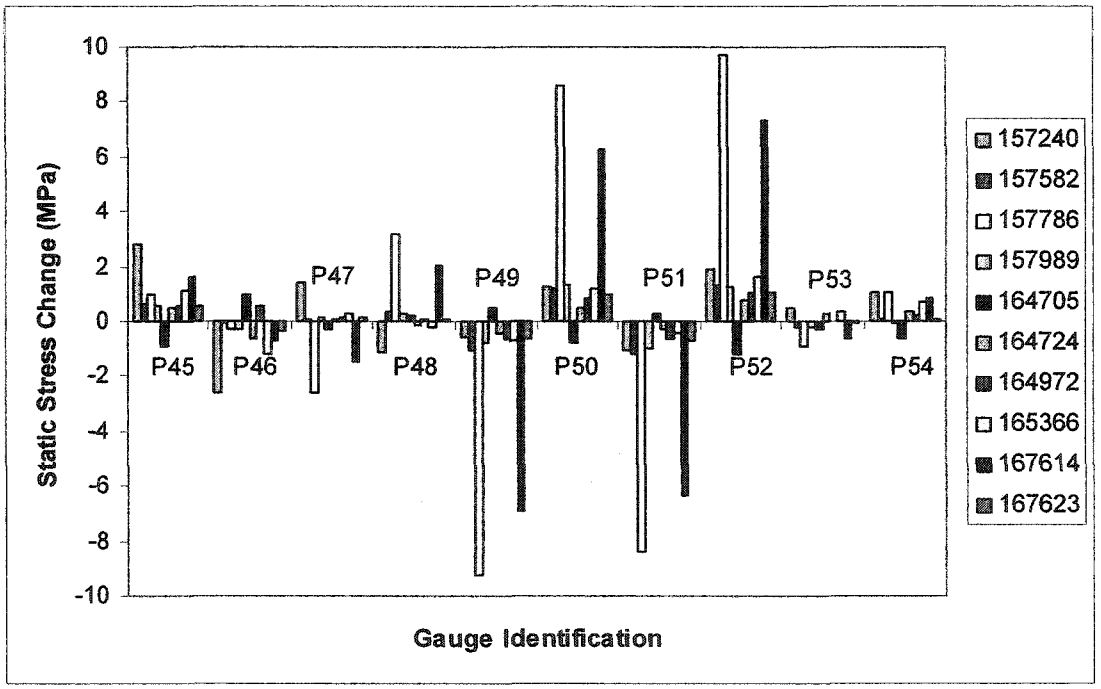

Figure 5-28: Pontoon Stress Distribution October Events 1-10

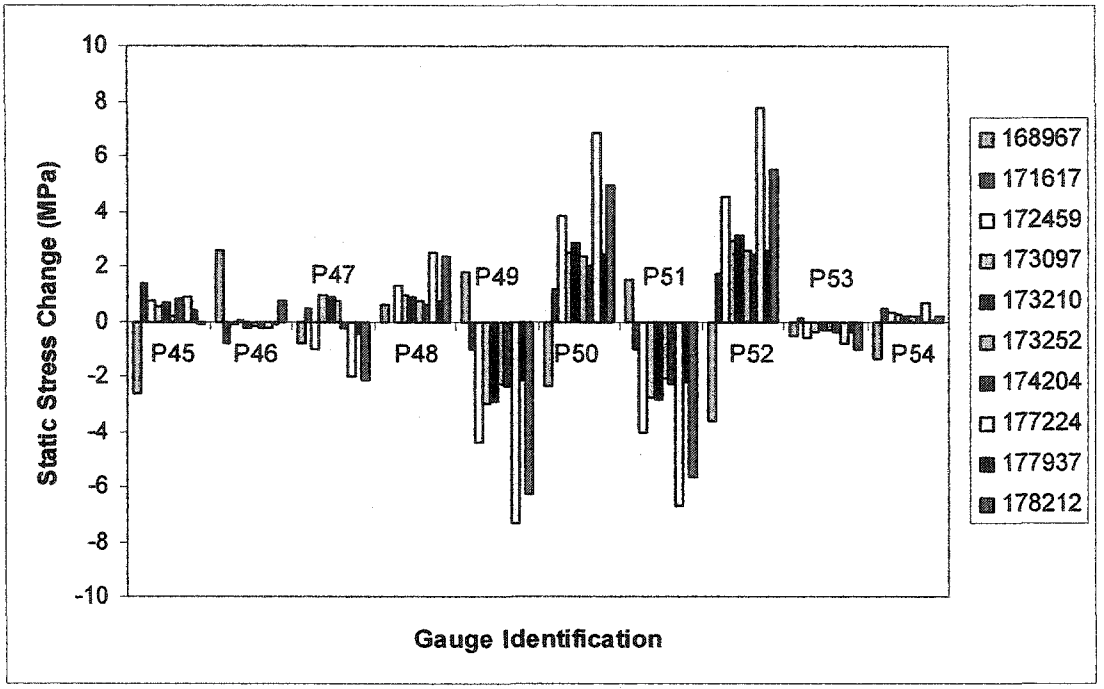

Figure 5-29: Pontoon Stress Distribution October Events 11-20

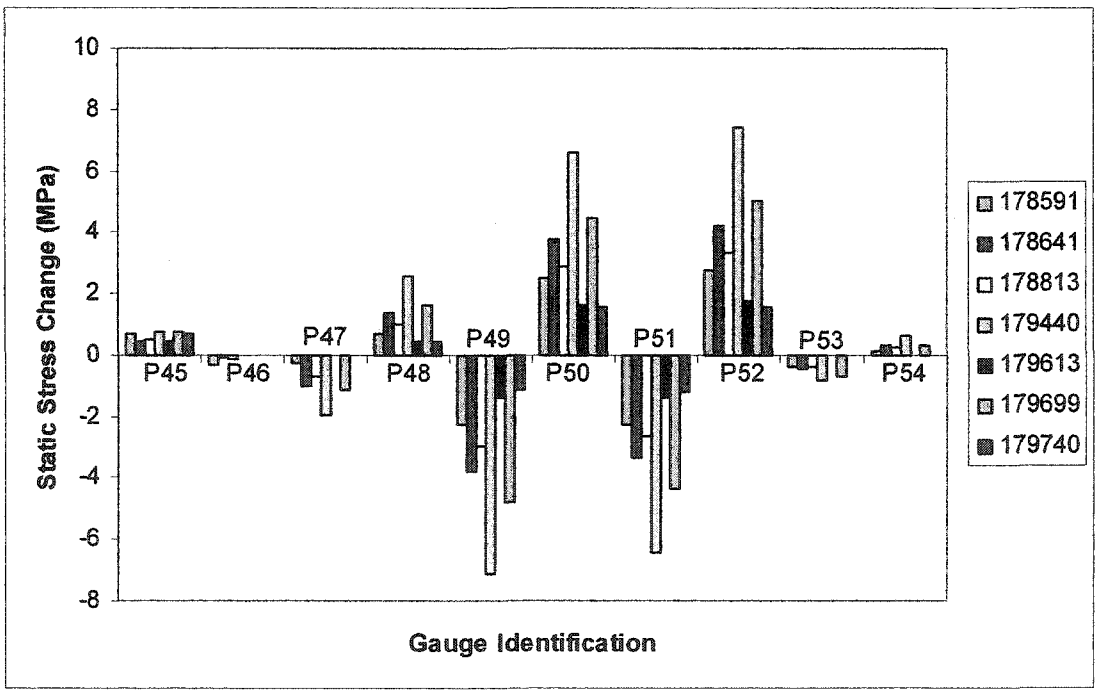

Figure 5-30: Pontoon Stress Distribution October Events 21-27

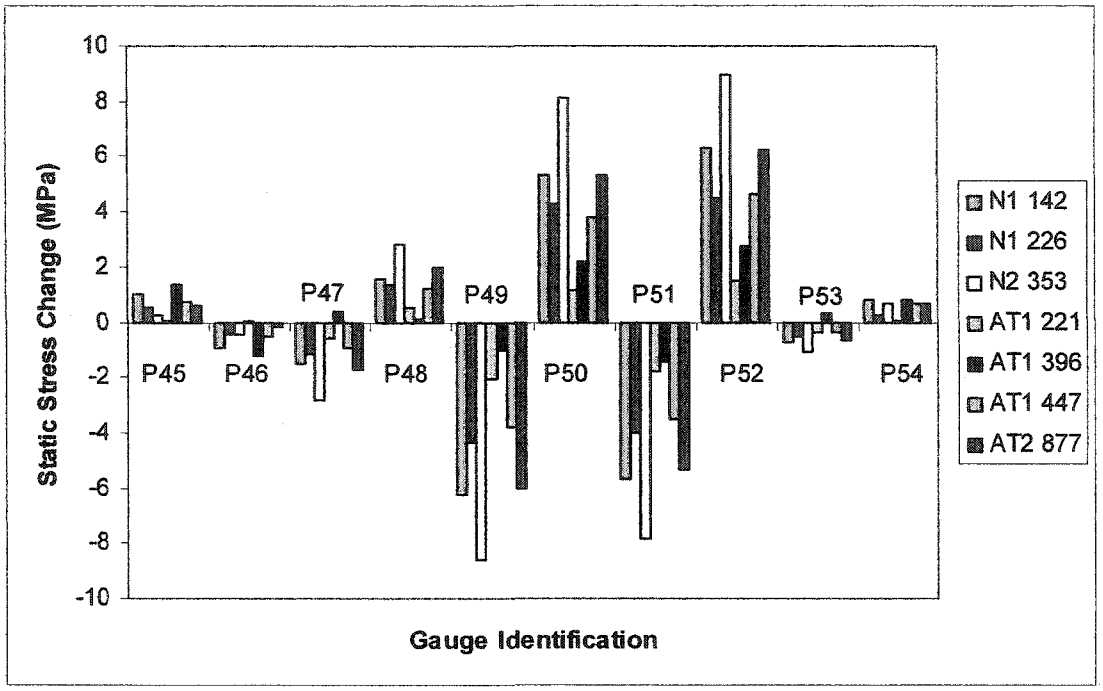

Figure 5-31: Pontoon Stress Distribution April Testing

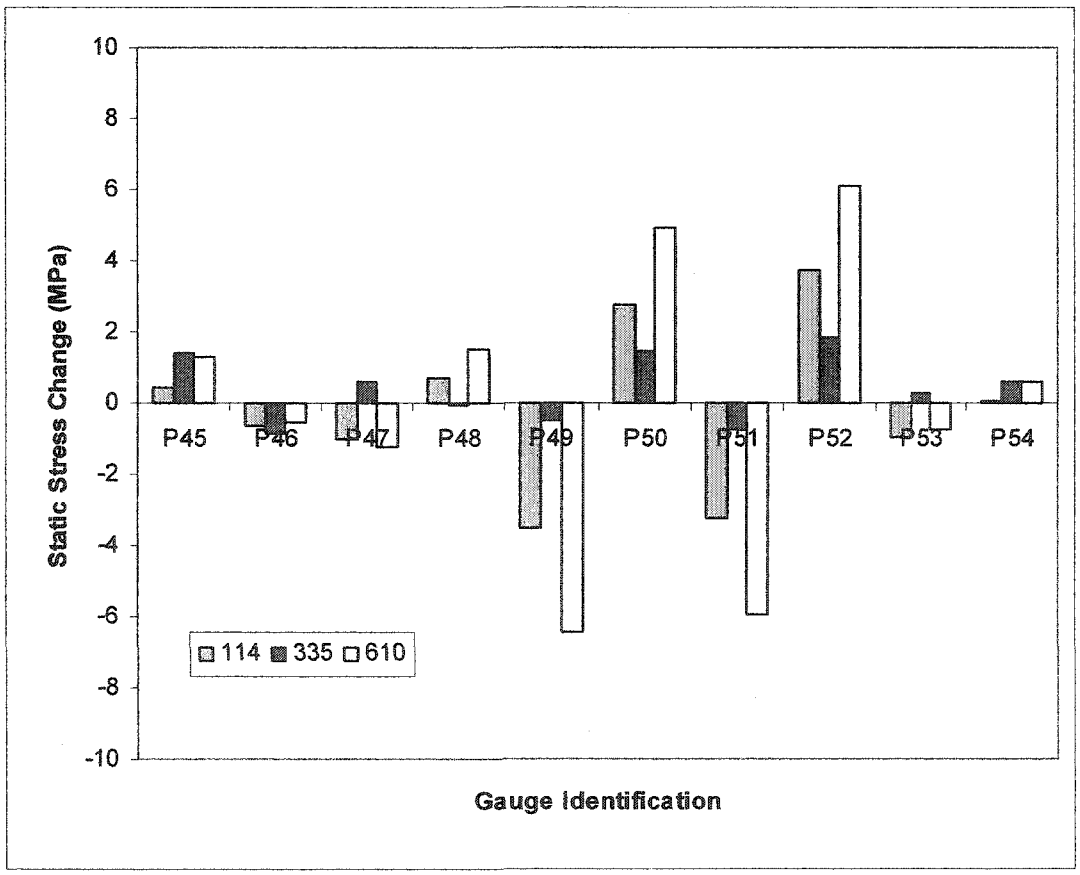

Figure 5-32: Pontoon Stress Distribution April Control Tests

In general, the top gauges (odd numbered) show compressive stress changes and the top gauges (even numbered) show tensile stress changes when an event takes place. Gauges at the same x-location showed very similar stress changes, but in the opposite sense. This indicates bending in the pontoon. The stress change is larger at the gauges located in the middle of the pontoon and decreases towards the ends. The gauges at the end closest to the dumping location show an opposite change as the rest. The top gauge (P45) shows a tensile change and the bottom gauge (P46) shows a compressive change. This indicates that the pontoon is in a double curvature bending, experiences positive moment in the middle of the span and negative moment at the support location.

5.4.2. Displacements

Displacements were calculated for the pontoon at the end closest to the retaining wall. Like the column displacements, they were measured with respect to the retaining wall. Prior to the April Testing, three of the four LVDTs were removed and used for other Syncrude projects. Displacements were calculated by determining the static voltage change and multiplying it by the calibration factor. Table 5-5 summarizes the pontoon displacements.

Table 5-5: Pontoon Displacements

Event	L70 (x)	L71 (z)	L72 (z)	L73 (x)
157240	-0.133	0.129	0.129	-0.368
157582	-0.002	0.000	0.007	0.005
157786	0.184	-0.022	-0.105	0.392
157989	0.028	0.004	0.019	-0.012
164147	-0.011	-0.002	-0.004	-0.020
164705	0.028	0.002	-0.005	0.046
164724	-0.014	0.000	0.008	-0.020
164972	-0.002	0.015	0.016	0.003
165366	-0.046	-0.001	0.017	-0.085
167614	0.148	-0.027	-0.121	0.248
167623	-0.014	0.748	0.387	2.438
168967	0.033	-0.003	-0.010	0.067
169940	0.012	0.045	0.058	-0.117
171617	-0.067	-0.027	-0.034	-0.099
172459	0.070	0.011	-0.019	0.159
173097	0.041	-0.018	-0.062	0.117
173210	0.110	0.038	0.043	0.069
173252	0.032	0.019	0.017	0.088
174204	0.018	-0.019	-0.062	0.067
177224	0.184	-0.010	-0.114	0.318
177937	0.099	0.036	0.006	0.070

178212	0.111	-0.062	-0.111	0.329
178591	0.108	0.027	0.001	0.062
178641	0.063	-0.007	-0.036	0.173
178813	0.049	-0.012	-0.037	0.114
179440	0.156	-0.014	-0.075	0.336
179613	0.081	0.019	0.038	0.053
179699	0.070	-0.044	-0.108	0.175
179740	0.057	-0.002	0.012	0.018
Apr 14 142				0.145
Apr 14 226				0.098
Apr 14 353				0.350
Apr 15 305				0.066
Apr 15 831				0.019
Test 114				0.089
Test 335				-0.135
Test 610				0.107
After Test 221				0.040
After Test 396				-0.156
After Test 447				0.172
After Test 877				0.247

The pontoon displacements were very small with 93 percent of them being less than 0.25 mm. Only 1.5 percent of the displacements were greater than 0.5 mm.

6. Analysis and Discussion

6.1. Thermal Strains

Due to the large redundancy in the system, the amount of thermal strains observed varies. The response in the columns varied between 1.31 and 5.47 με/°C. The pontoon's response varied between 2.43 and 4.26 με/°C, and the hopper's response varied between 5.08 and 6.43 με/°C. No restraint in the system would result in 11.6 με/°C and a perfectly rigid structure would result in no strain differences. The lower strain change per degree Celsius means a more rigid system. This would suggest that the pontoon and the columns are more rigid than the hopper. These values were to be compared with a one degree temperature change in the model; however STAAD's output is only in stress not strain and a direct comparison could not be conducted. Although the strain could not be compared to the model, the thermal coefficients calculated for each gauge provide a basis for boundary condition changes. At a future date when the crusher is not running, data can be collected every ten minutes. The relationship between the temperature and strain change is the new thermal coefficients. If these coefficients differ significantly, a change in the boundary conditions has occurred.

6.2. Event Characterization

In order to characterize events the column stress distribution was examined to see if patterns were evident. Video taken on April 14, 2004 and April 15, 2004 during normal operating conditions was used to determine side of dumping and if the load remained on that side or moved for events identified by the Excel plots. Table 6-1 shows the observations from the video and their event times in the data file.

Five types of events were identified: right side dumping, left side dumping, both sides dumping, right side dumping with the load moving across, and left side dumping with the load moving across. Because not enough channels were available to accurately determine the amount of bending stress, the average stress was calculated for each column by averaging the static stress change calculated on each side of the column. The

column average stress distribution on Gridlines 2 and 4 were examined and distinct patterns were observed for the five types of events. The difference in vertical displacement on either side of the hopper was also used to determine the side of dumping. Hopper stresses were examined to determine any differences between events.

Table 6-1: Video Observations compared with Data

Date	Time	Dump Side	Duration (sec)	Observations	Time in File (sec)
April 14	15:50	Left	~10	Load stays	142
	15:52	Right	~6	Load stays	226
	15:54	Both	~13	Load stays	353
April 15	10:10	Left	~10	Stays	305
	10:14	Both	~40	Stays	not seen
	10:19	Left	~30	Stays	831
	10:21	Right	~40	Stays	Not seen
April 15 (Control Tests)	13:53	Left	~2	Moves Across	114
	13:56	Right	~13	Stays	335
	14:01	Both	~ 8	Stays	610
April 15 (After Test)	14:17	Left	~60 sec	Moves Across	221
	14:21	Right	~8 sec	Moves Across	396
	14:22	Left	~2 sec	Moves Across	447

6.2.1. Right Side Dumping

Events identified as dumping on the right hand side with the load staying on the right, had higher stresses in the outer columns on the right side. The inner columns on Gridline 4 experienced tensile stress changes for this type of event. Figure 6-1 shows the stress distributions for right side dumping. The difference in the vertical displacement at the top of the columns also helps to characterize events. By subtracting the left vertical displacement (L77) from the right vertical displacement (L75), if this value negative, it indicates that the right side of the hopper is deflecting more vertically than the left. See Table 6-2 for these values. By using these two characteristics, seven events were identified as right side dumping, 157582, 157989, 177937, 178591, 179613, 179740 and April 14 226.

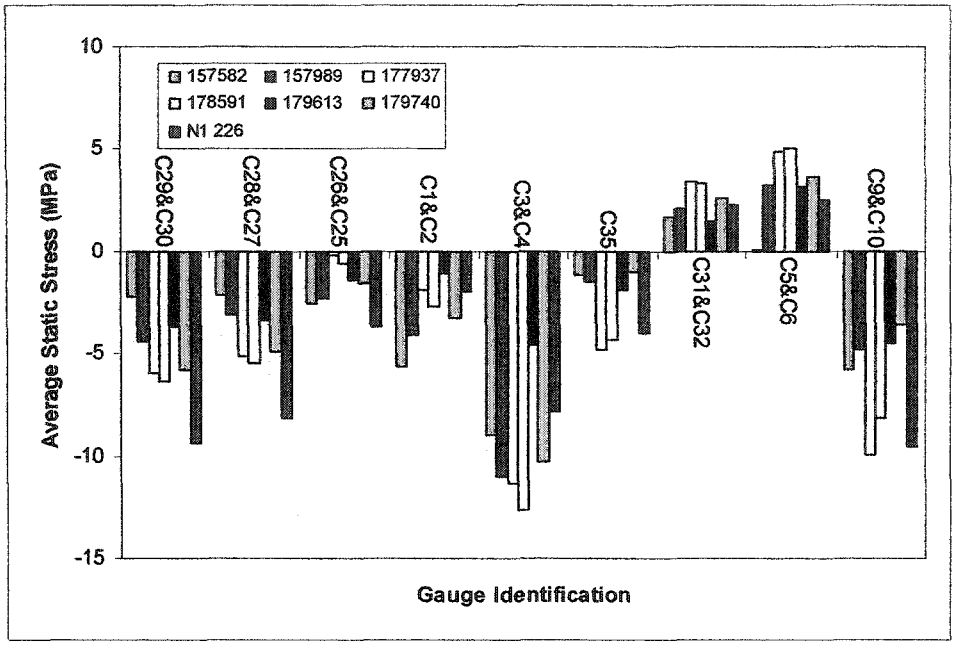

Figure 6-1: Right Side Dumping Column Stress Distribution

Table 6-2: Vertical Displacement Differences for Right Side Dumping

Event	L77 (mm)	L75 (mm)	Right - Left
157582	0.031	0.102	0.072
157989	-0.204	-0.951	-0.747
177937	-0.506	-1.353	-0.848
178591	-0.474	-1.242	-0.768
179613	-0.245	-0.751	-0.505
179740	-0.202	-0.764	-0.562
April 14 226	-0.363	-1.052	-0.689

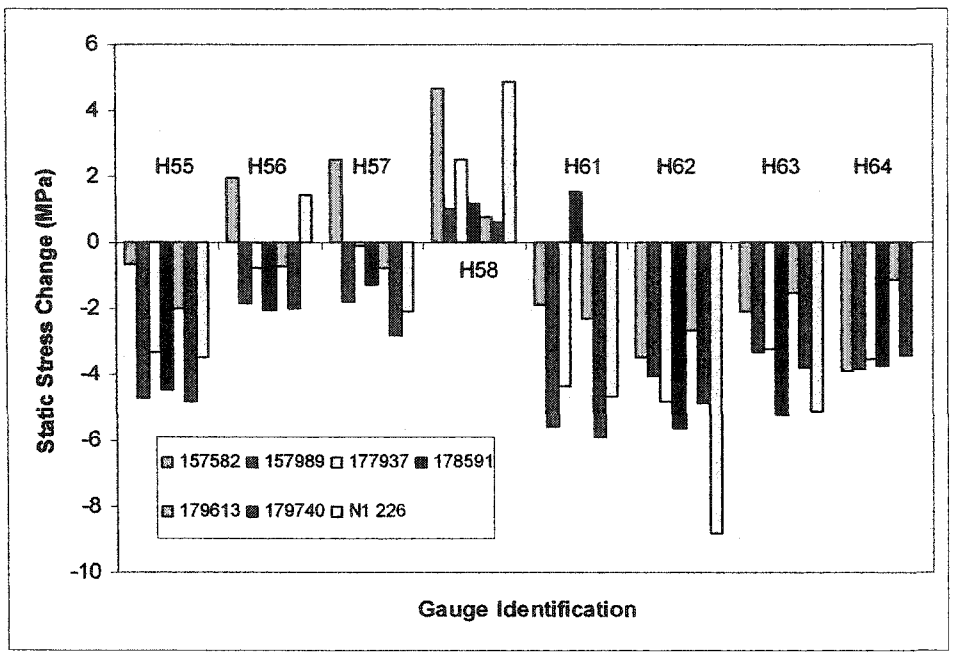

Figure 6-2: Right Side Dumping Hopper Stresses

Gauge H58, located on a horizontal stiffener experiences tensile stress changes for all events deemed to be right side dumping. Gauges at the intersection of the stiffeners experience compressive stress changes with gauge H62 almost always having the largest stress change. See Figure 6-2.

6.2.2. Left Side Dumping

Column stress distributions that have higher stresses in the outer columns on the left side and tensile stress changes in the inner columns on both Gridline 2 and Gridline 4 indicate dumping from the left side with the load staying on the left. Because gauge C36 was damaged prior during installation, the average stress does not always look higher on Gridline 4. However, by looking at both gridlines and the unaveraged stresses if necessary, a specific stress pattern can be found for left side dumping. See Figure 6-3. The difference in the vertical column displacements were also used to help determine the type of event. If the difference between the right and left vertical displacements is negative (see Table 6-3) and the column stress distribution matches the one shown in Figure 6-3, an event can be characterized as left side dumping. These two characteristics together identified thirteen events as left side dumping, 16492, 173097, 173210, 174204,

172459, 173252, 178212, 178641, 178813, 179699, April 14 142, April 15 305, and April 15 831.

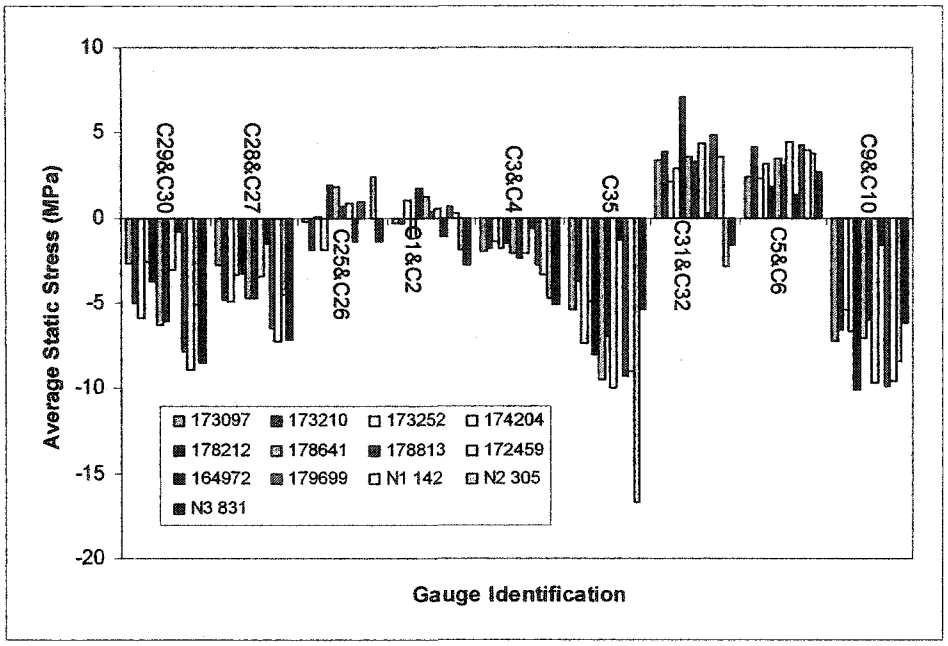

Figure 6-3: Left Side Dumping Column Stress Distribution

Table 6-3: Vertical Displacement Differences for Left Side Dumping

Event	L77 (mm)	L75 (mm)	Right - Left
164972	-0.531	-0.079	0.452
172459	-7.340	-0.595	6.745
173097	-4.692	-0.464	4.228
173210	-1.308	-1.073	0.235
174204	-1.465	-0.327	1.138
178212	-1.853	0.451	2.303
178641	-1.750	-0.508	1.242
178813	-1.455	-0.374	1.081
179699	-1.687	-0.598	1.089
April 14 142	-1.643	-0.547	1.096
April 14 305	-2.081	-0.506	1.575
April 14 831	-0.812	-0.371	0.441

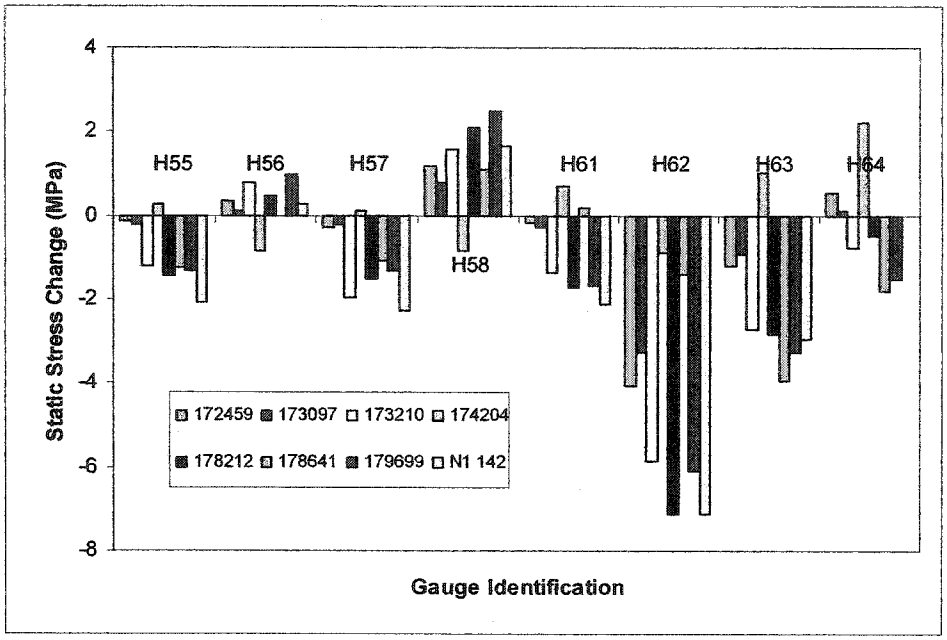

Figure 6-4: Left Side Dumping Hopper Stresses

Gauge H58 has all tensile changes except for one event, and gauge H62 consistently has the largest stress change. See Figure 6-4.

6.2.3. Both Sides Dumping

Events that have dumping on both sides of the hopper simultaneously, experience higher stresses than just left or right side dumping. The stresses on both sides are similar and the inner columns have tensile stress changes. See Figure 6-5 for the stress distribution of events identified as both side dumping. The difference in the vertical displacements on either side of the hopper is expected to be close to zero for these events; however, it is not. This is indicated Table 6-4. The column stress distribution on Gridlines 2 and 4 is used to identify six events as both sides dumping, 157786, 167614, 177224, 179440, April 14 353 and After Test 396.

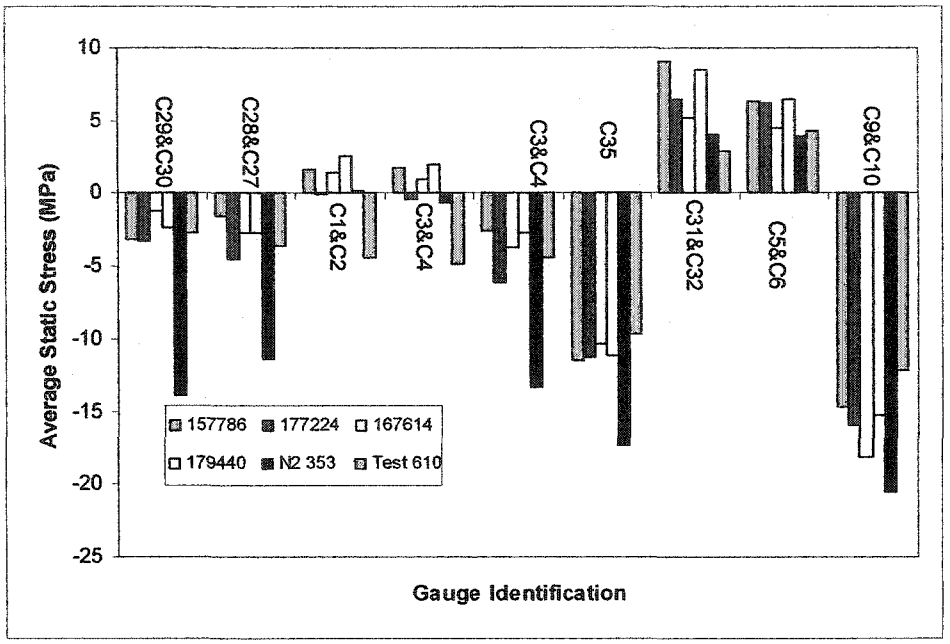

Figure 6-5: Both Sides Dumping Column Stress Distribution

Table 6-4: Vertical Displacement Differences for Both Sides Dumping

Event	L77 (mm)	L75 (mm)	Right - Left
157786	-2.920	-1.049	1.872
167614	-7.450	-0.940	6.510
177224	-2.459	-1.075	1.384
179440	-2.371	-1.000	1.370
April 14 353	-2.269	-1.747	0.522
Test 610	-1.192	-1.198	-0.006

The hopper stresses were examined for any pattern for both sides dumping events. Gauge H58 has tensile changes for all events characterized as both sides, and gauge H62 again has the largest static stress change. See Figure 6-6.

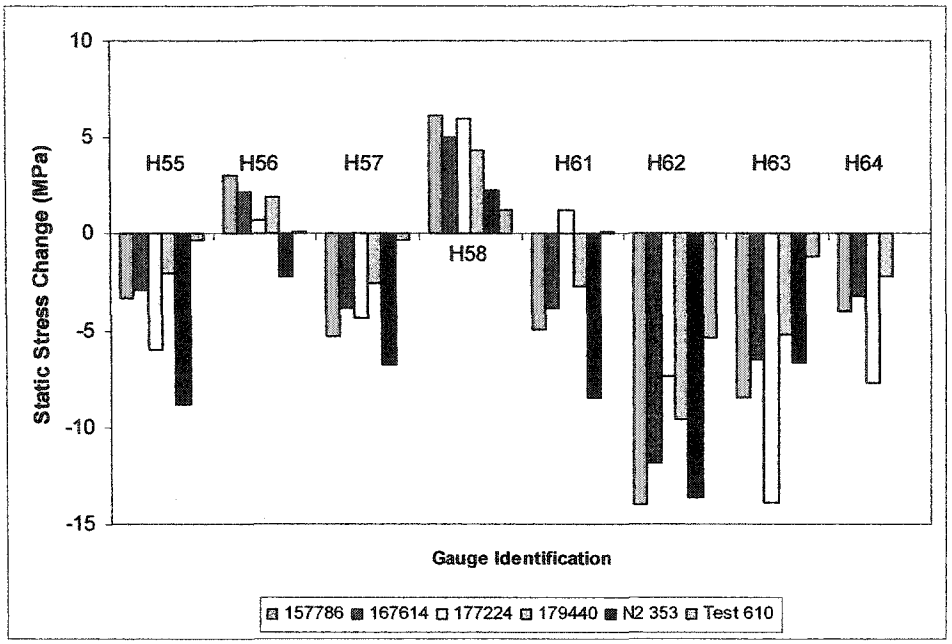

Figure 6-6: Both Sides Dumping Hopper Stresses

6.2.4. Moving Across Events

The control tests that were conducted in April were conducted on an empty hopper. This resulted in the load sliding across the hopper and impacting the opposite side from which the load was dumped. The stress distribution in the columns for the control tests show the higher stress in the columns being in the inner column rather than the outer ones as for left, right or both side dumping. When the load was dumped from the right, the inner column on the left of Gridline 2 experienced the highest stress, as shown in Figure 6-7. If the load is dumped from the left the inner column on the right side of Gridline 2 shows the highest stress. See Figure 6-7. The difference between the displacement on the right and left is negative for right side dumping events and positive for left side dumping events. See Table 6-5. Events 157240, 169940, Test 335, and After Test 396 were identified as right side dumping with the load moving across and events 171617, Test 114, After Test 221 and After Test 447 were identified as left side dumping with the load moving across.

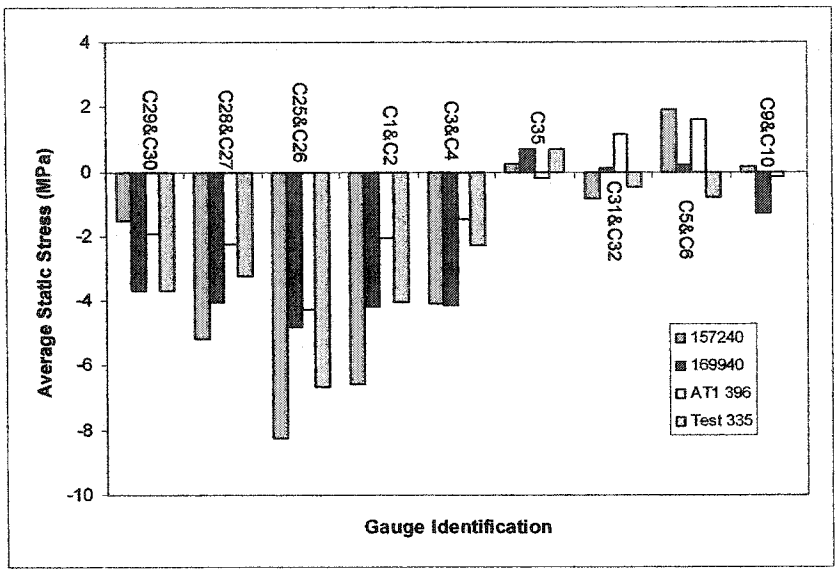

a) Right to Left

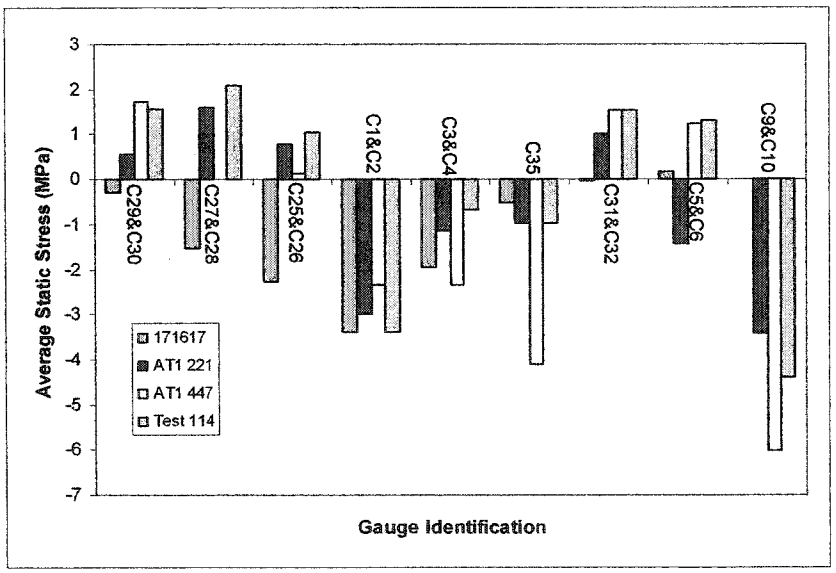

b) Left to Right

Figure 6-7: Moving Across Events Column Stress Distribution

Table 6-5: Vertical Displacement Differences Moving Across Events

Event	L77 (mm)	L75 (mm)	Right - Left	Dump
157240	0.124	-0.856	-0.980	Right Across
169940	0.096	-0.624	-0.720	Right Across
Test 335	0.035	-0.312	-0.347	Right Across
After Test 396	-0.044	-0.471	-0.428	Right Across
171617	-2.464	0.059	2.523	Left Across
Test 114	-0.733	-0.222	0.511	Left Across
After Test 221	-0.466	-0.339	0.127	Left Across
After Test 447	-0.737	-0.509	0.229	Left Across

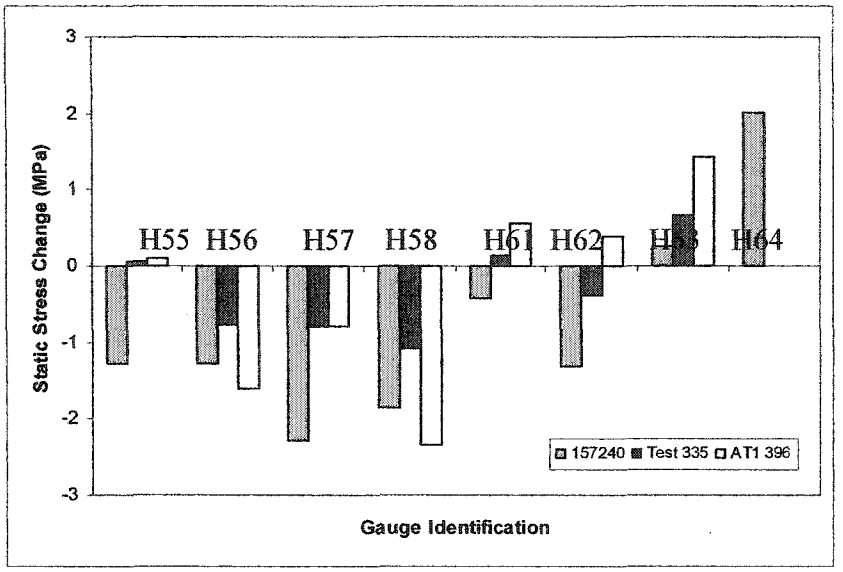

a) Right to Left

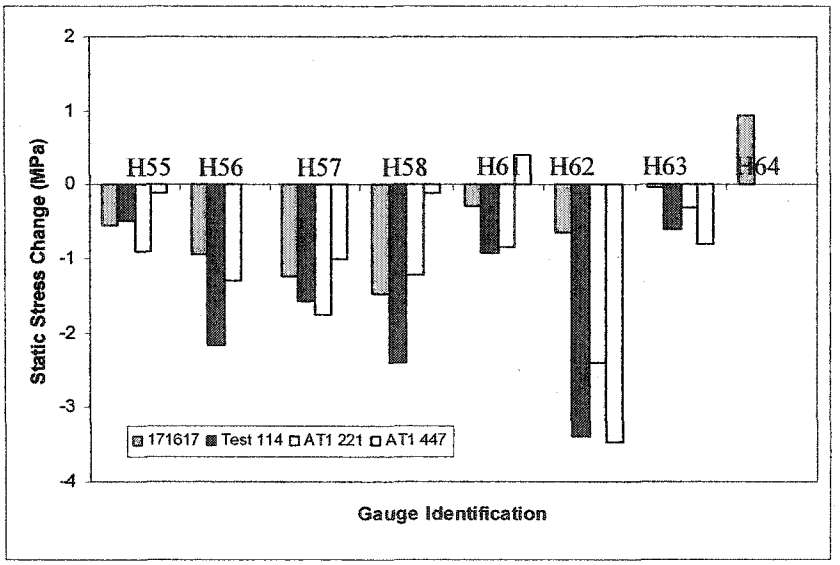

b) Left to Right

Figure 6-8: Moving Across Events Hopper Stresses

Figure 6-8 shows the hopper stresses for moving across events. These events result in smaller hopper stresses than left, right or both sides dumping events. Because these events occur when the hopper is empty or near empty, the load impact the hopper at a lower location. This could mean that the load impacts below the location of the gauges. Gauge H58 experiences a compressive stress change for all moving across events unlike the tensile changes it experiences for the other types of events.

6.2.5. *Summary*

Column stress distribution and the difference between the vertical displacements can be used to identify different types of events due to different signatures. For right side dumping, the outer right columns have the higher stress distribution and the difference between the right and left vertical displacements is negative. Left side dumping has a similar distribution; however, the left outer columns have the highest stress and the difference in displacements is positive. Events that occur when dumping happens on both sides simultaneously experience similar stresses on both sides. These stresses are higher than the left and right dumping. The difference in displacement does not help to identify these events. For all of these events gauge H58 in the hopper experiences tensile changes. The events that occur when the hopper is empty or near empty are characterized as moving across events because the load slides across the hopper and impacts the side opposite to the dumping. Higher stresses are observed in the inner columns for these types of events; high stress on the inner right column left side dumping and high stress on the inner left column for right side dumping. Another distinct feature of these events is gauge H58 experiences compressive changes unlike the tensile change experienced for right, left and both sides events. There are not any noticeable differences in the pontoon stresses for different types of events, other than the stresses being slightly higher for both sides dumping events. Using the column stress distribution, difference in vertical displacement, and gauge H58 event signatures have be identified for five different types of events.

6.3. *Impact Factor*

The impact factor measures the amount of extra strain in the system due to the dynamic response of the crusher. In design, only a static analysis was done and the impact factor was used to adjust loads to better simulate expected stresses in the system. Knowledge of actual impact factor the crusher experiences will allow for a refined and improved design. The impact factor was determined by plotting a strain versus time graph. Events were then identified by looking for large sudden changes in stress. When an event occurred, the beginning and ending were identified by the point where the strain levels out. A one-minute average of the strain at these points was taken for the average static strain before

and after the event. The difference in these strains is the static strain change. In order to determine the dynamic strain change, a maximum and minimum strain value was calculated during the event. If the static strain change was positive, the difference between the maximum strain and the average before the event was taken as the dynamic strain change. Had the static strain change been negative, then the minimum value would be used. The impact factor is the ratio of dynamic strain change to static strain change. This process is illustrated in Figure 6-9. The sampling rate of 100 Hz was able to catch the peak dynamic response as illustrated in Figure 3-1Figure 6-10 as there are numerous data points around the peak.

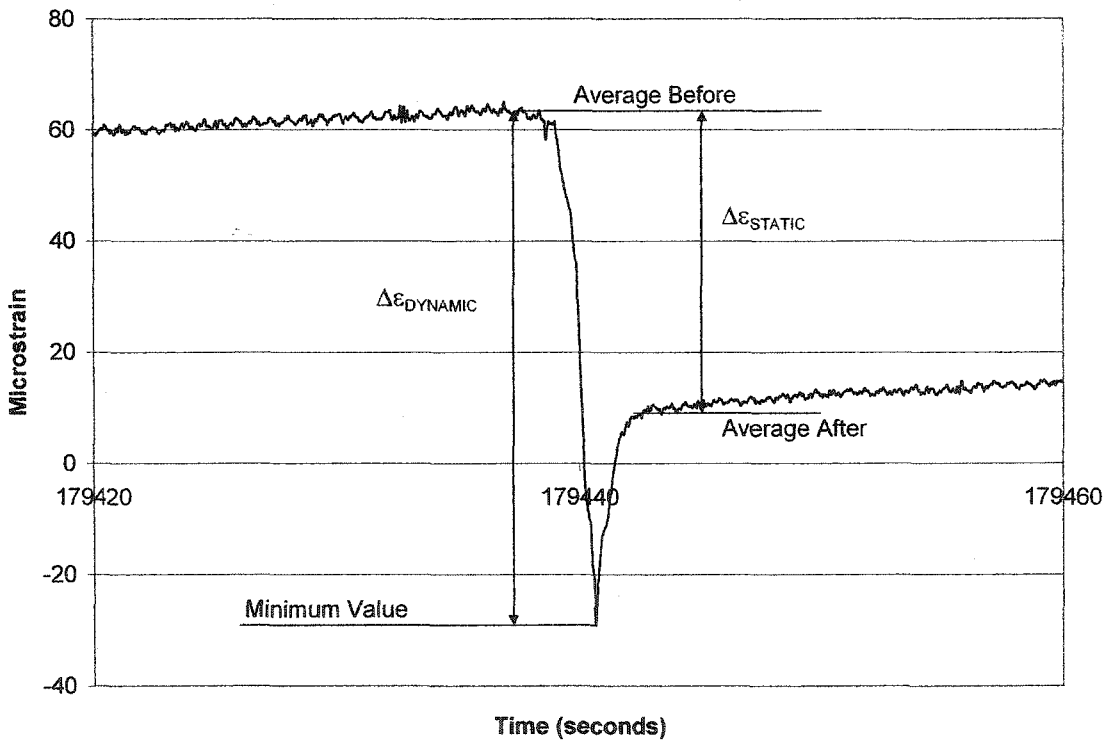

Figure 6-9: Strain vs. Time for Gauge C9

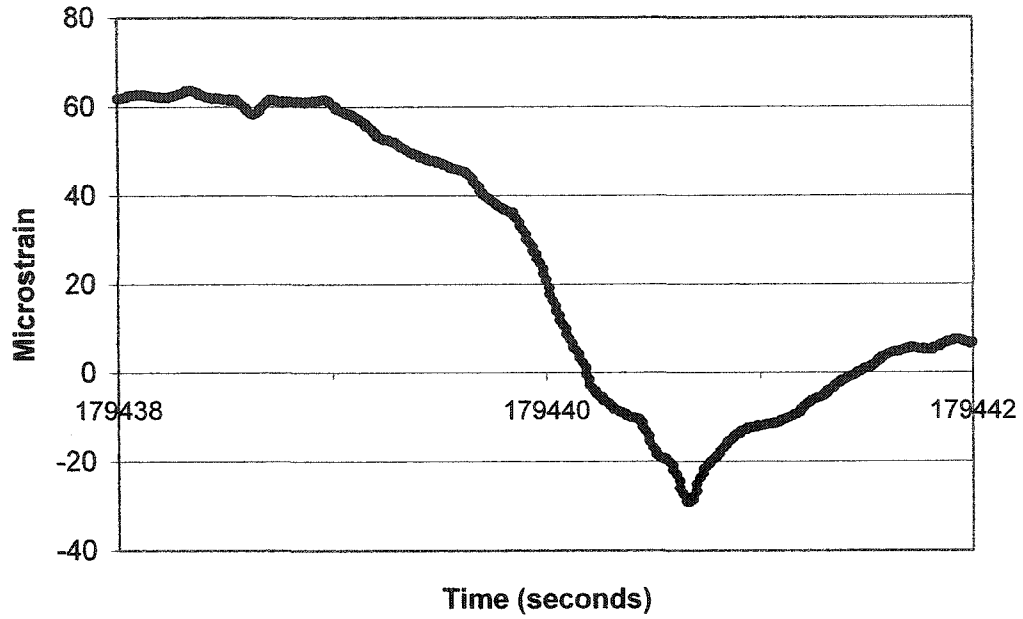

Figure 6-10: Close-up of Peak of strain change

6.3.1. Columns

The impact factor was calculated for the same gauges used to calculate static stress change. Using the method described, the impact factor was calculated for each gauge during each event. The impact factors calculated varied considerably with stress range, type of member and type of event. Table 6-6, Table 6-7, and Table 6-8 summarize the impact factors observed in the columns gauges for events identified as left, right or both sides dumping. Table 6-9, Table 6-10 and Table 6-11 summarize the impact factors for moving across events.

Table 6-6: Vertical Columns Summary

$\Delta\sigma_{STATIC}$ (MPa)	Average Impact Factor	Standard Deviation	Number of Events
$0 < \sigma < 2$	3.02	2.543	120
$2 < \sigma < 5$	2.05	0.850	109
$5 < \sigma < 10$	1.46	0.476	82
$10 < \sigma < 15$	1.37	0.275	35
$\sigma > 15$	1.35	0.270	8

Table 6-7: Gauges at the Top of Columns Summary

$\Delta\sigma_{STATIC}$ (MPa)	Average Impact Factor	Standard Deviation	Number of Events

$0 < \sigma < 2$	4.38	1.784	5
$2 < \sigma < 5$	2.65	1.142	27
$5 < \sigma < 10$	1.70	0.717	12
$10 < \sigma < 15$	1.49	0.660	5

Table 6-8: Inclined Members at bottom of Columns Summary

$\Delta\sigma_{STATIC}$ (MPa)	Average Impact Factor	Standard Deviation	Number of Events
$0 < \sigma < 2$			
$2 < \sigma < 5$	1.39	0.305	7
$5 < \sigma < 10$	1.22	0.143	23
$10 < \sigma < 15$	1.12	0.078	33
$\sigma > 15$	1.08	0.057	37

Table 6-9: Vertical Columns Summary for Moving Across Events

$\Delta\sigma_{STATIC}$ (MPa)	Average Impact Factor	Standard Deviation	Number of Events
$0 < \sigma < 2$	8.59	8.286	37
$2 < \sigma < 5$	4.20	5.220	31
$5 < \sigma < 10$	2.96	1.018	9

Table 6-10: Gauges at the Top of Columns Summary for Moving Across Events

$\Delta\sigma_{STATIC}$ (MPa)	Average Impact Factor	Standard Deviation	Number of Events
$0 < \sigma < 2$	7.80	6.785	6
$2 < \sigma < 5$	2.46	2.546	5

Table 6-11: Inclined Members at bottom of Columns Summary for Moving Across Events

$\Delta\sigma_{STATIC}$ (MPa)	Average Impact Factor	Standard Deviation	Number of Events
$0 < \sigma < 2$	5.00	4.258	2
$2 < \sigma < 5$	3.22	1.838	6
$5 < \sigma < 10$	2.22	0.785	16

The gauges at the top of the columns (C29 and C30) experience a higher impact factor with more scatter because the top of the columns may or may not be influenced by each event. This is similar to the impact factor calculated in the hopper. Similar impact factors are observed in the inclined members at the bottom of the columns (C15, C16, C39 and C40) and the pontoon gauges. The calculated impact factor at these locations is much lower than the vertical columns and the scatter is also much lower. Impact factor for stress changes over 10 MPa is approximately 1.1. This observation is most likely because these gauges are far away from the direct impact site and therefore the variability

in the load is reduced. The vertical columns experience a wide range of impact factors. If the lower stress changes are not considered and only stress changes above 5 MPa are considered, the impact factor ranges between 1.37 and 1.46. Although the impact factor is higher, the lower stress changes are less of a concern because the static stress change is lower and these two combine to be lower than the higher stress changes with a lower impact factor. In a limit states design, only the limit state is considered. If a fatigue analysis were being conducted, perhaps the lower stress ranges would need to be considered. For events identified as moving across events, which are typical when the hopper is empty or near empty, the impact factor was much higher.

6.3.2. Pontoon

Gauges P49, P50, P51 and P52 were only considered when calculating the impact factor in the pontoon because they showed the largest changes. The remaining gauges rarely had static stress changes over 2 MPa; therefore, were not used to calculate the impact factor in the pontoon. The impact factors calculated varied in the pontoon as well; however, the scatter was much less than observed in the columns or the hopper. The reduction in scatter is most likely due to the pontoon being the furthest away from the direct impact of the dump trucks loading oil sand into the hopper. The impact factor still varied with static stress change and location. The largest variable in impact factor is the stress range. There were slight differences between average impact factors when comparing the gauges located at the top of the pontoon versus the bottom of the pontoon. Table 6-12 summarizes the impact factor for the pontoon for left, right and both sides dumping events. Table 6-13 summarizes the impact factor for the moving across events.

Table 6-12: Pontoon Impact Factor by Location and Stress Range

Top Gauges (P49 & P51)				Bottom Gauges (P50 & P52)			
$\Delta\sigma_{STATIC}$ (MPa)	Average Impact Factor	Standard Deviation	Number of Events	$\Delta\sigma_{STATIC}$ (MPa)	Average Impact Factor	Standard Deviation	Number of Events
$0<\sigma<1$	1.64	0.080	4	$0<\sigma<1$	1.99		1
$1<\sigma<2$	1.53	0.160	6	$1<\sigma<2$	1.54	0.221	10
$2<\sigma<5$	1.27	0.149	22	$2<\sigma<5$	1.34	0.178	21
$5<\sigma<10$	1.22	0.100	14	$5<\sigma<10$	1.28	0.102	14

Table 6-13: Pontoon Impact Factor for Moving Across Events

Top Gauges (P49 & P51)				Bottom Gauges (P50 & P52)			
$\Delta\sigma_{STATIC}$ (MPa)	Average Impact Factor	Standard Deviation	Number of Events	$\Delta\sigma_{STATIC}$ (MPa)	Average Impact Factor	Standard Deviation	Number of Events
$0<\sigma<1$	6.20		1	$0<\sigma<1$			
$1<\sigma<2$	4.01	2.038	6	$1<\sigma<2$	6.01	4.819	6
$2<\sigma<5$	3.06	1.344	3	$2<\sigma<5$	2.84	0.941	5
$5<\sigma<10$	1.10		1	$5<\sigma<10$	1.08		1

For events that are not moving across, the scatter and the impact factor for the pontoon is very low. Looking at stress changes greater than 5 MPa, the impact factor is approximately 1.25 with a standard deviation of approximately 0.10. The impact is low in the pontoon because it is farthest away from direct impact. This results in the dynamic effects being filtered out by the hopper and columns.

6.3.3. Hopper

Gauges installed directly on the plate wall of the hopper were not used to calculate the impact factor. One of these gauges was faulty (H59) and the other gauge (H60) did not record a significant change in strain during identified events. Without a significant strain change ($\Delta\varepsilon > 5\mu\varepsilon$), the impact factors calculated are not reliable and therefore not considered. Gauges located on the hopper are on three different locations: the vertical stiffeners (H56, H58), the horizontal stiffeners (H55, H57, and H61) and at the intersection of both stiffeners (H62-H64). During April Testing gauge H64 was not working. Because the hopper experiences localized behaviour, the scatter in the data is quite large. Although an event may be similar in the amount of stress it creates, the location of the exact impact may be different resulting in varying impact factors observed. The impact factor is also higher in the hopper than the columns or the pontoon because it is directly impacted by the oil sand. Table 6-14 and Table 6-15 summarize the impact factors calculated by location and stress range.

Table 6-14: Hopper Impact Factor Summary by Location and Stress Range

	Horizontal Stiffeners		Vertical Stiffeners		Intersection of Stiffeners	
$\Delta\sigma_{STATIC}$ (MPa)	Average Impact Factor	Standard Deviation	Average Impact Factor	Standard Deviation	Average Impact Factor	Standard Deviation

$0 < \sigma < 2$	1.79	0.983	2.95	1.758	3.33	2.162
$2 < \sigma < 5$	1.74	0.711	1.81	0.580	1.46	0.670
$5 < \sigma < 10$	1.18	0.126	2.26	0.614	1.45	0.444
$\sigma > 10$					1.65	0.444

Table 6-15: Hopper Impact Factor Summary for Moving Across Events

	Horizontal Stiffeners		Vertical Stiffeners		Intersection of Stiffeners	
$\Delta\sigma_{STATIC}$ (MPa)	Average Impact Factor	Standard Deviation	Average Impact Factor	Standard Deviation	Average Impact Factor	Standard Deviation
$0 < \sigma < 2$	5.63	5.265	4.22	2.789	9.06	8.768
$2 < \sigma < 5$	2.65	-	2.58	-	5.36	2.055

Events that were characterized by the load moving across experienced higher impact factors than the left, right, and both sides dumping events. The scatter in these events was also very high. The stress ranges calculated for the hopper gauges were lower than the other events because the moving across events occur when the hopper is empty or near empty and the load impacts below the location of the gauges. The impact factor is higher because there is no oil sand in the hopper to filter the impact of the oil sand and the oil sand is falling from a greater height.

6.3.4 Conclusions

Because of the variety of loading, the hopper and the top of the columns experience the largest impact factors with the most variance. Small changes in the location of the load application will have a large influence in the response of these gauges. The larger impact factors occur because these locations experience direct contact with the load and therefore the largest dynamic response. The columns experience variation in impact factor but the variation decreases as the load increases. The pontoon and the inclined members that connect a few of the columns to the pontoon experience similar impact factors. These impact factors are lower because there is less variance in the load application. The load variation and dynamic effect is filtered out in the hopper and the vertical columns. Events where the load moves across the hopper have much higher impact factors and much more scatter. This would suggest that dumping on an empty hopper should be avoided if possible to avoid the higher impact stresses experienced.

6.4. Model Calibration

6.4.1. Model and Data Comparison

Krupp's model of the hopper was compared to the data collected by creating three load cases to simulate right, left and both sides dumping. The video collected from April's normal operation was used to determine the location that the load impacts the hopper. The static stress changes calculated on Gridline 4 were compared to the average stress in the columns in the model at the same location as the gauges. An event on April 14 at T = 226 sec was used to calibrate the model for right side dumping events. This event was chosen because video was available to ensure the location of dumping. The load case created to compare to right side dumping involved linear varying local y – direction loads applied to the stiffeners and local y-direction pressure on the plates in the hopper. Figure 6-11 shows the loads applied to the hopper model. Loads were applied to both sides of the hopper, increasing towards the right. Linear varying loads ranged from 0 to 30 kN/m to 60 to 75 kN/m in the negative local y-direction. The plate pressures were 10 kPa. Figure 6-12 shows the comparison between the model output and this event. The data and the model compare quite well on Gridline 4, but the model was unable to model the stress changes on Gridline 2. Gridline 4 was determined to be the stresses to compare because many variables could influence the stress on the other gridlines such as the level of oil sand in the hopper. Figure 6-13 shows the comparison of the model's output on Gridline 4 with all right side dumping events.

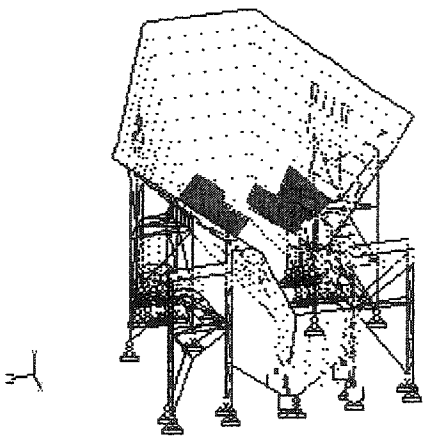

Figure 6-11: Right Side Dumping Loads

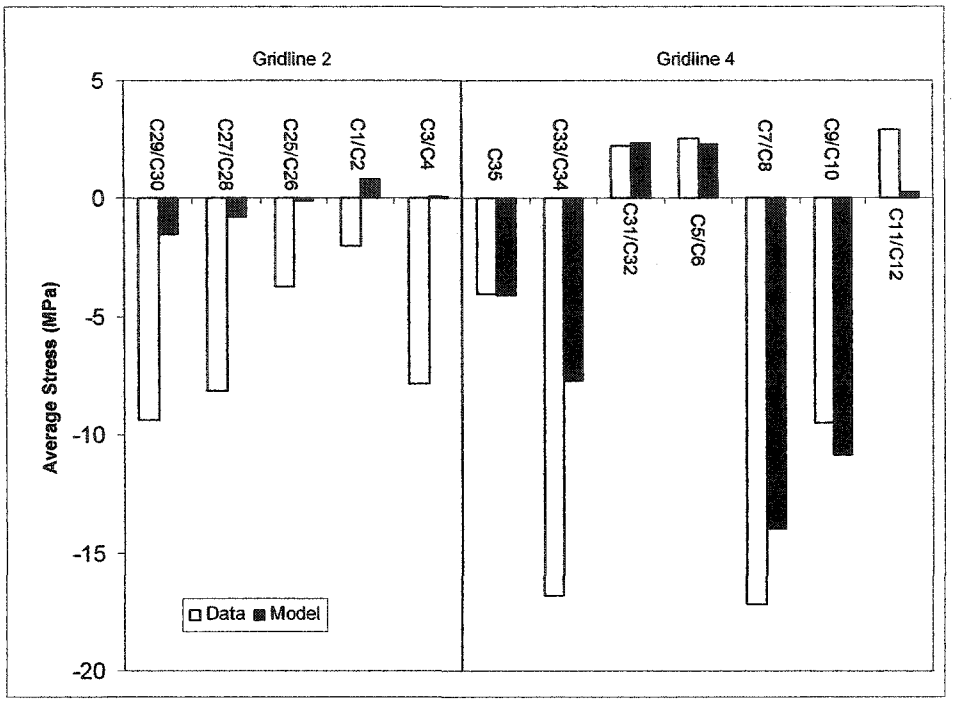

Figure 6-12: Right Side Dumping Model and April 14, Dump 226 Comparison

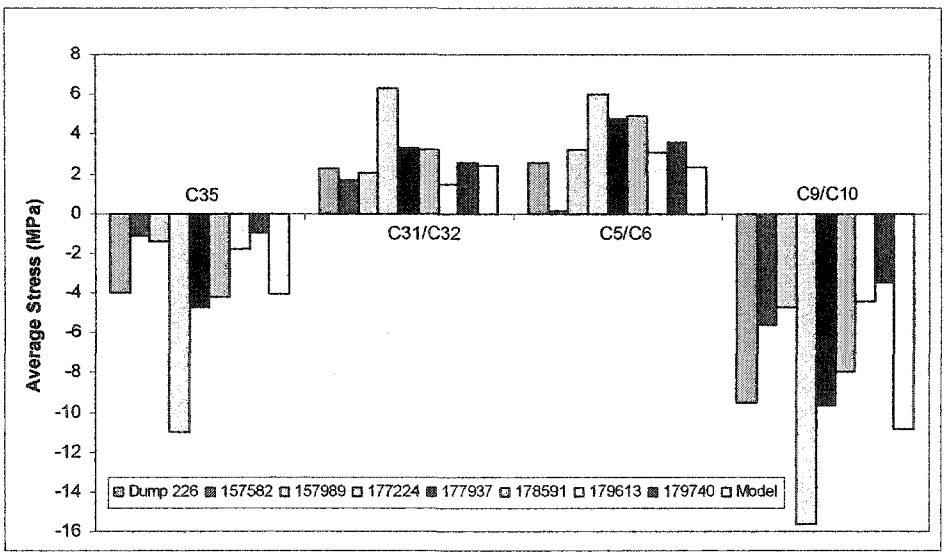

Figure 6-13: Gridline 4 Model and Data Comparison

Good agreement between the model and the data on Gridline 4 provides confidence in the model to predict and model stresses in the crusher. The maximum stresses and locations in the hopper model for this load case were calculated. Figure 6-14 shows the plate

stresses. The maximum plate stress is 11.4 MPa and it occurs on Gridline 4 where the inner right column connects to the hopper.

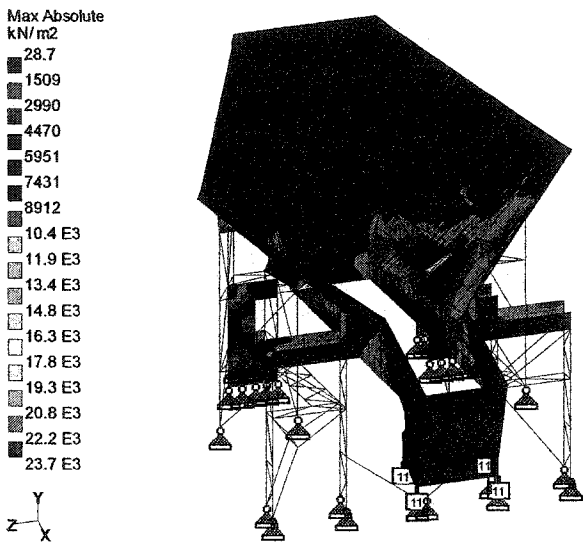

Figure 6-14: Plate Stresses for Right Side Dumping

Maximum beam stresses were also low. The maximum compressive stress is 44.4 MPa and the maximum tensile stress is 37.7 MPa. The maximum compression occurs at the top of the inner right column on Gridline 4 and the maximum tensile stress is in an inclined member where the inner right column connects to the hopper on Gridline 2.

A load case was created to simulate left side loading, by using linear varying loads and plate pressure increasing towards the left. Linear varying loads ranged from 0 to 50 kN/m to 70 to 80 kN/m and plate pressures ranged from 10 kPa to 15 kPa. Figure 6-15 illustrates the load case.

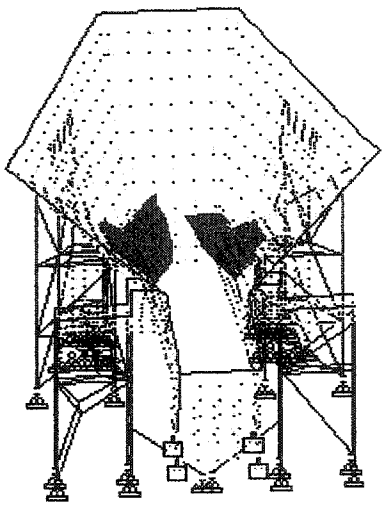

Figure 6-15: Left Side Dumping Loads

Event 178813 was chosen for a comparison to the model. It had the most distinct difference between the left and right side column stresses. Because gauges C36 was damaged the average stress in the outer column on the left side seems lower than it actually is. Typically the outer gauge on the outer column shows a higher stress change than the inner gauge. When the averaged stress on the right is compared to the only the inner gauge on the left side, they are similar for different types of events. Figure 6-16 shows the comparison between event 178813 and the model's output. The stress in the model is higher on the left than the data, but the right side stresses are very close. Because one cannot average the stress on the left column, the results from the data are lower than the model. Figure 6-17 shows the comparison between the model and all the left side dumping events on Gridline 4. The distributions are similar with variations due to the many variables in loading.

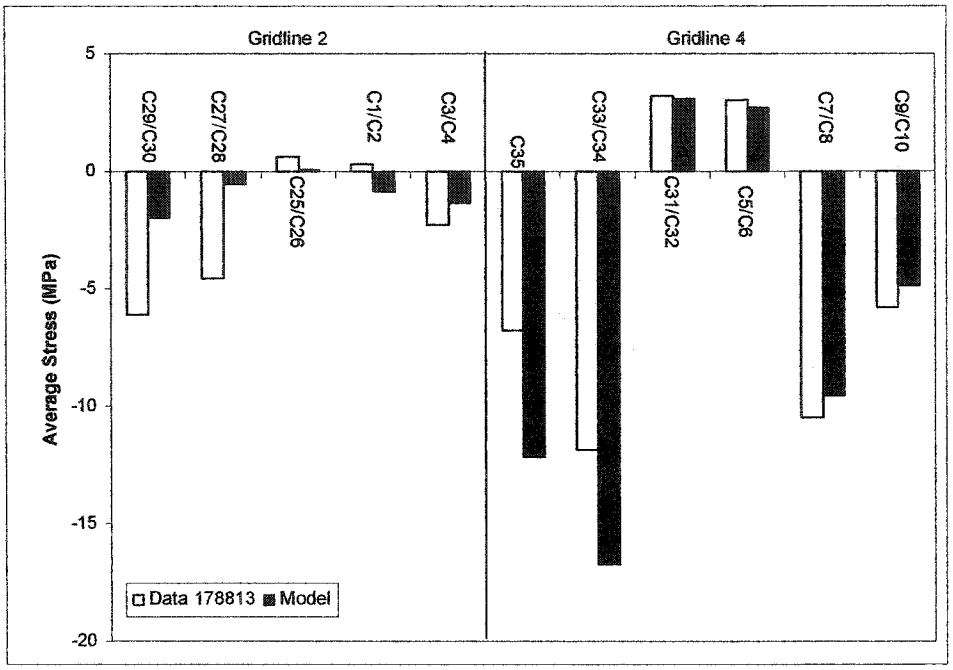

Figure 6-16: Left Side Dumping Data and Model Comparison

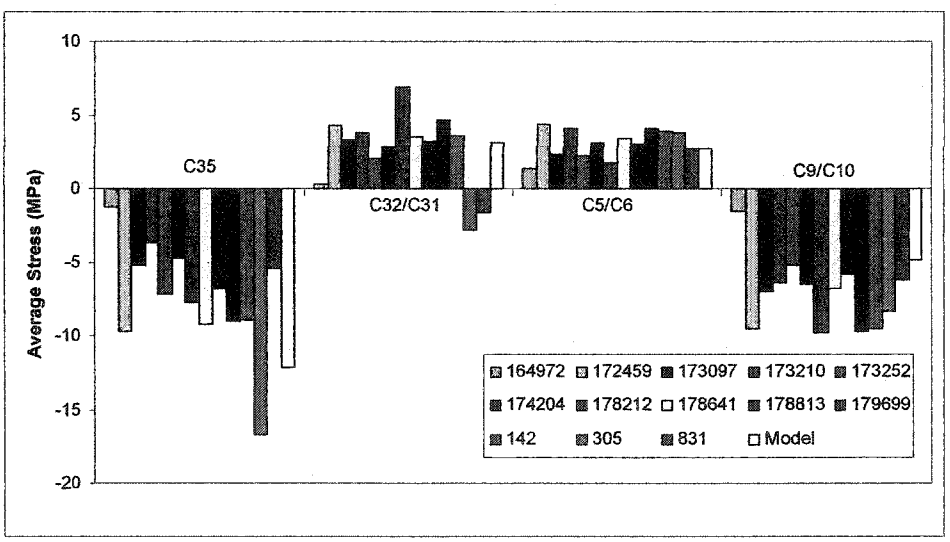

Figure 6-17: Gridline 4 Left Side Dumping and Model Comparison

The maximum stresses and location were determined for this load case. The stresses were quite small, all plate stresses below 15 MPa, with the largest being 13.2 MPa on Gridline 4 where the inner column connects to the hopper on the left side. See Figure 6-18. This is the same location as for the right loading only on the left side. The maximum beam stress in compression is 49.9 MPa and it occurred in an inclined member where the inner column on the left connects to the hopper on Gridline 2. The maximum tensile stress of 50.6 MPa also occurred in this member.

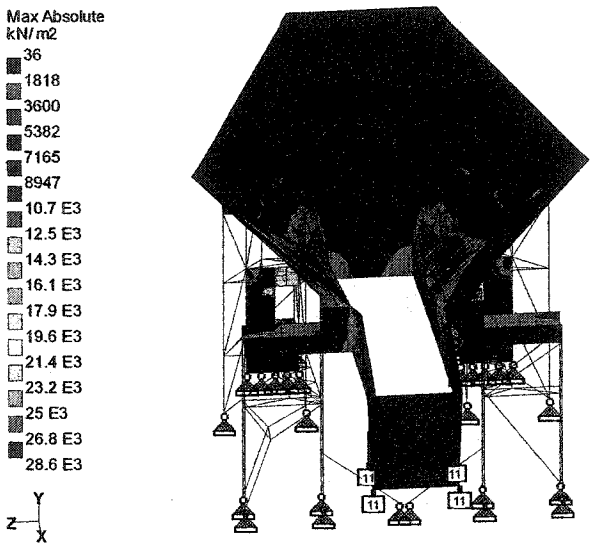

Figure 6-18: Hopper Plate Stresses Left Side Dumping

The final load case created in Krupp's hopper model simulates dumping on both sides. Linear varying loads and plate pressures were used, with values increased from those used in left or right side dumping. Plate pressures ranged from 15 to 20 kPa, and the linear varying loads increased to 85 kN/m. The values were increased towards the top of the hopper. See Figure 6-19.

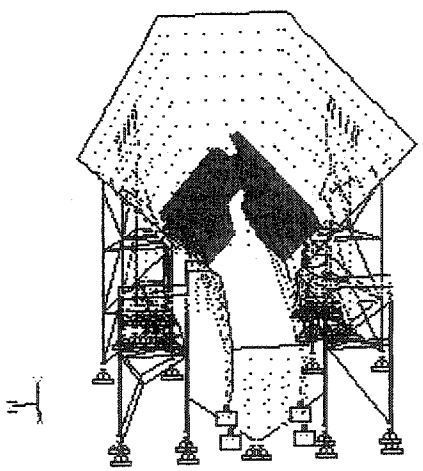

Figure 6-19: Both Sides Dumping Loads

Figure 6-20 compares the model's output to an event from October at T = 179940. The model's output compares well to the data on Gridline 4. See Figure 6-21. The outer left

column data is slightly lower most likely due to the lack of the outer gauge to compare the average stresses. The inner columns have higher stresses in the data and on Gridline 2 the stresses are higher than modelled. This is perhaps due to the large amounts of variables in loading.

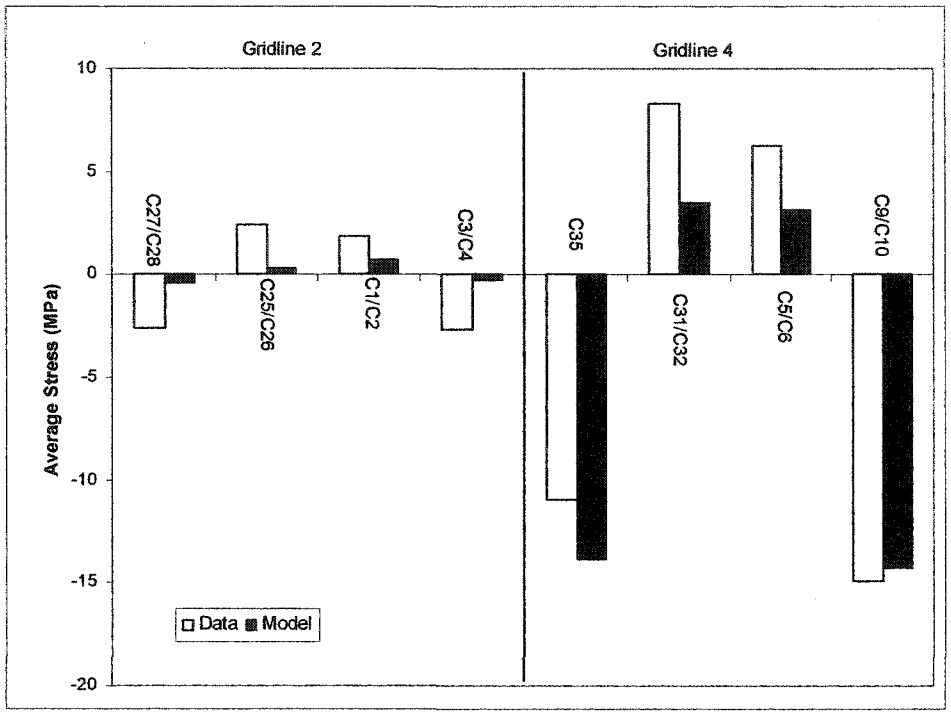

Figure 6-20: Model and Data 179440 Comparison

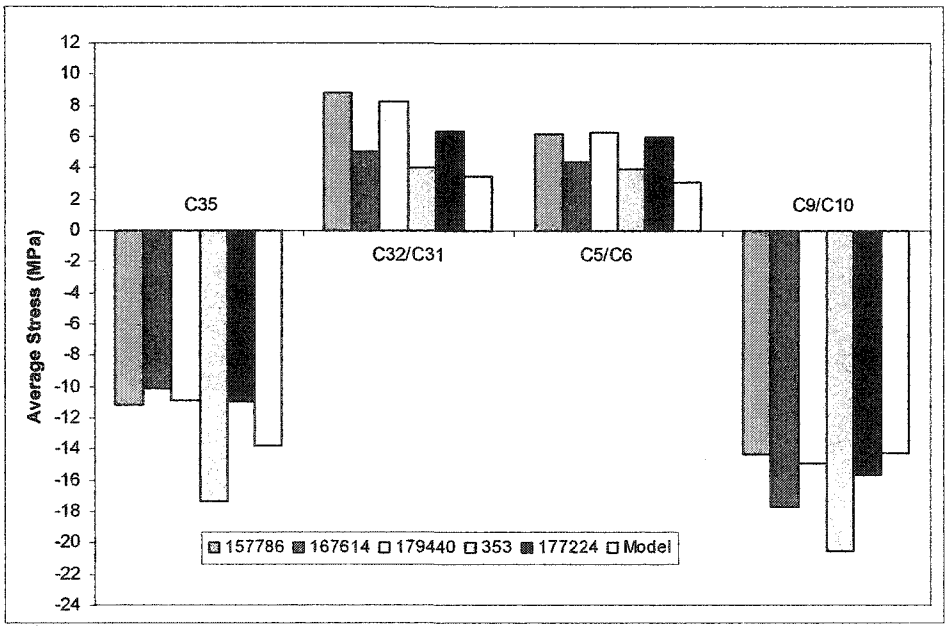

Figure 6-21: Both Sides Dumping Gridline 4 Data and Model Comparison

When examining only Gridline 4, the model and the data compare well. The inner columns have higher stresses than modelled, but the outer columns are very close. Confidence in predicting stress in the crusher using this load case to simulate both sides dumping events, allowed maximum stresses and locations to be determined from the model. Figure 6-22 shows the maximum plate stresses. The maximum plate stress was 18.0 MPa and the maximum plate stresses occurred on Gridline 4 where the inner column connects to the hopper on both sides. This is the same location for left and right side dumping.

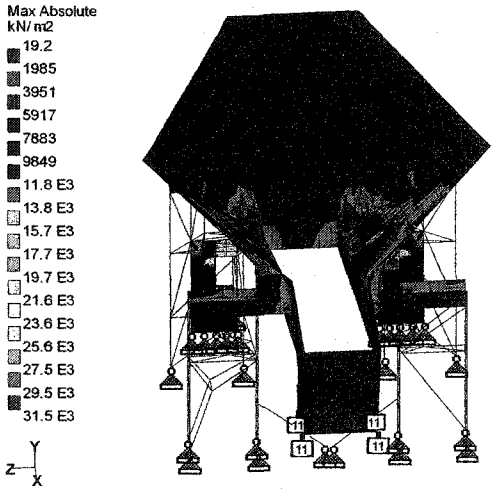

Figure 6-22: Both Sides Dumping Plate Stresses

The maximum beam stresses are 68.5 MPa in compression and 67.0 MPa in tension. Seven beams have compressive stresses over 50 MPa. Four of these beams are the top of the inner columns on Gridlines 3 and 4 on both sides. Three stiffeners at the bottom of the hopper have stresses over 50 MPa. Two beams have stresses over 50 MPa in both compression and tension. These beams are located on Gridline 2 at connection between the inner column and the hopper.

6.4.2. Krupp's Load Cases

Krupp's model compared well with the data. Column stress distribution on Gridline 4 was used to validate load cases created to simulate left, right and both sides dumping events. Maximum stresses and locations were determined. The top of the inner columns on Gridlines 3 and 4 as well as the plates that connect the inner column and the hopper

experienced the highest stresses. These locations were predicted to have the highest stress during the analysis of Krupp's Syncrude Load Case prior to testing. The stresses observed were much lower than predicted. The maximum plate stresses were less than 20 MPa and the maximum beam stresses were less than 70 MPa, unlike the predictions of 148 MPa for a maximum plate stress and 615 MPa as the maximum beam stress.

Krupp used nineteen primary load cases to model parts of loads that were expected to occur in the crusher. Load 1 is the self-weight with a factor of 1.1, which allows for connections. Load 2 is a superimposed dead load of 3 kPa vertically on all plates, which I suspect is for material encrusted on the hopper. Loads 3 and 4 are gravity loads applied to all plates increasing as you move down the hopper walls. Load 5 is the projected load from the Apron Feeder Girder. Loads 6 and 7 are x-direction pressures on all walls; Load 8 is z-direction pressure on the side walls. The values for these loads are fairly small, with the largest being 9.4 kPa. Load cases 9 through 11 model a liquefied soil condition. Load cases 12 through 17 are impact cases. The impact cases only model horizontal loads and use a pressure of 90 or 100 kPa. This is four times greater than the pressure used to calibrate the model to the data. The pressure is applied on two rows of plates along one side of the hopper, which is much smaller that the area used to calibrate the model. It is unlikely that the oil sand dumped from a truck would impact only two rows of plates. See Figure 6-23 for a comparison of the local impact cases to the load case used to calibrate the model. Krupp's local impact cases also do not have any vertical components. The oil sand does create horizontal impact, but due to gravity also has a vertical component.

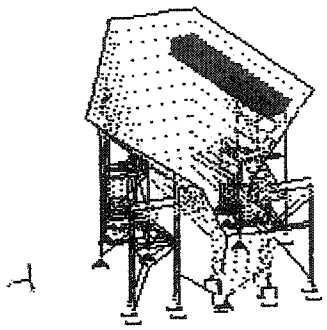

a) Load Case 13: Local Impact Case 1

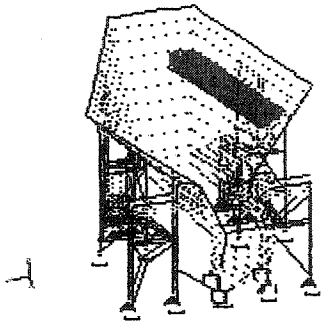

b) Load Case 14: Local Impact Case 2

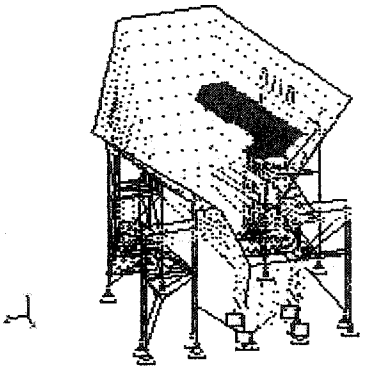

c) Load Case 16: Local Impact Case 4

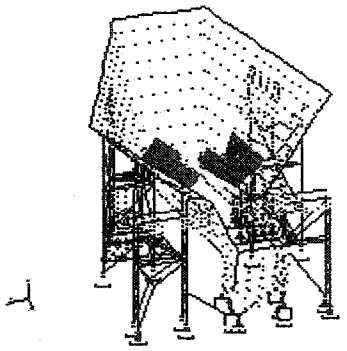

d) Right Side Dumping Model Calibration

Figure 6-23: Krupp Loads comparison with Right Side Loading

Loads 18 and 19 model the excavator load. An excavator is occasionally inserted into the hopper to clean the hopper walls. Load Cases 20 through 34 are repeat loads in STAAD. A Repeat Load is a primary load case that allows the combination of other loads but includes a P-delta analysis for the combined condition rather than only an algebraic addition of the loads. Loads 20 and 21 combine loads 3, 4, 5, 6, 7, and 8. This combination includes pressure on all walls of the hopper, which increases towards the bottom of the hopper. The combination factors used to combine these loads 18.0 or 24.3 for the vertical pressure and the apron feeder girder and 4.5 or 6.1 for the horizontal pressures. These factors result in vertical pressures in excess of 150 kPa and horizontal pressures greater than 55 kPa. Loads 22 through 26 combine the vertical pressures multiplied by a factor of 24 with the horizontal pressures multiplied by a factor of 4.5 with the impact cases 1 through 5 multiplied by a factor of 1.0. Loads 27 and 28 are Load Cases 20 and 21 without the apron feeder girder load. Loads 29 through 33 are the same as Load Cases 22 through 26 without the apron feeder girder load. Load Case 34 is the liquefied soil condition plus local impact case 1. Load 36 is the load due to a plugged

inlet chute. Load Cases 70 to 73 are two Syncrude Impact Cases. Case 1 contains a vertical pressure of 192 kPa and a horizontal pressure of 108.216 kPa. Case 2 consists of a vertical pressure of 269.5 kPa and a horizontal pressure of 157.872. The areas loaded are similar to the load case created to calibrate the model, but with pressures ten times greater. See Figure 6-24.

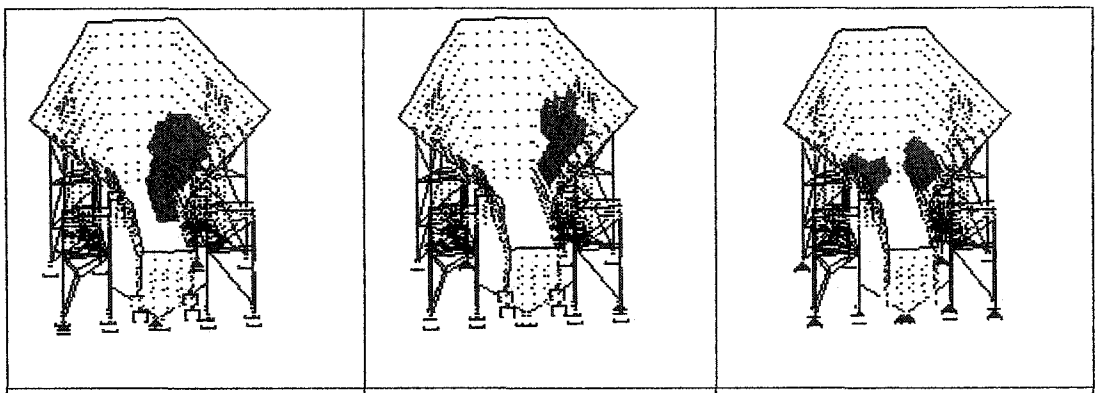

Figure 6-24: SCL Impact Case comparison with Model Calibration Load Case

The load used to calibrate with the data also has loading on both sides of the hopper. Video taken in April showed that the oil sand impacts both sides of the hopper, only more on the side of dumping. Load Cases 75 and 76 are the combination of the SCL Impact vertical and horizontal loads. Loads 80 through 100 combine the live loads described with the dead loads with factors of 1.5 for live loads and 1.25 for dead loads.

The problems with the design load cases are the values used for pressures in the impact cases, they are much too high. Only pressures of 20 kPa were needed to calibrate the data to the model. The local impact cases 1 through 5 are unlikely, because the oil sand is not likely to impact a large horizontal area without impacting an equally large vertical area. The area impacted is more square than rectangular. The combinations of the material in the hopper with the impact cases also seem to use combination factors which are too high. Krupp's model can accurately predict the behaviour of the crusher. The values used for the pressures were simply too large which resulted in stresses in the analysis being very large.

7. Summary, Conclusions and Recommendations

7.1. Summary

Syncrude's Aurora II Crusher located at Syncrude's Aurora Mine was instrumented in September of 2003. Two sets of data were collected from 58 weldable strain gauges and 9 LVDTs. The first data set collected in October of 2003, consisted of 24 hours of strain and temperature data while the crusher was not in operation and 12 hours of data during the commissioning of the crusher. A second set of data was collected on April 14 and April 15, 2004. Seven minutes of normal operation on April 14 was supplemented with video. Data collected on April 15, consisted of fifteen minutes of normal operations, fifteen minutes of controlled testing and an additional fifteen minutes of normal operations data.

Data collected while no loading was taking place was used to calculate the relationship between thermal strain and temperature. Ten minute averaged strain and temperature data was plotted and the slope of the line is the thermal coefficient for each gauge. The hopper gauges ranged from 5.08 to 6.43 $\mu\varepsilon/^{o}C$, and the pontoon gauges ranged from 2.43 to 4.26 $\mu\varepsilon/^{o}C$. Of the 37 working column gauges, 31 gauges had a linear response to temperature change with values ranging between 1.31 and 5.47 $\mu\varepsilon/^{o}C$.

By plotting strain or voltage versus time, large changes in the data were identified as events. The beginning and ending of an event were visually identified as the point where the strain is approximately level before and after the event. Static strain change was calculated as the difference in these values and static stress change was calculated by multiplying the strain change by the modulus of elasticity of steel taken from the model. Eighty-eight percent of the stress changes in the hopper were less than 5 MPa. Gauge H60 was not used for analysis because it did not show changes that were very large for an event. The largest static stress change observed in the hopper was a 13.98 MPa compressive stress. This stress was observed in gauge H62 which consistently had the largest response to events. Other than the two gauges near the end of the pontoon

directly under the loading area, 92 percent of the bottom gauges experience tensile stress changes and 85 percent of the top gauges experience compressive stress changes. The top and bottom gauges at the same horizontal location experience similar stresses to each other. These results indicate that the pontoon beam is in positive bending, as expected. The largest stresses observed in the pontoon were 9.73 MPa in tension, gauge P52, and 9.23 MPa in compression, gauge P49. Gauges P49 through P52 showed larger stress changes that the gauges at the extreme ends of the pontoon, P45 – P48, P53 and P54. Not all of the column gauges were used in analysis. The gauges on the Gridlines 5 and 6 had more noise than the other gauges; therefore were not considered. Gauges on the vertical columns on Gridline 2 and 4 were chosen for comparison because they are under the loading area. Only one of the gauges at the top of the column was used and the gauges on the bottom inclined on Gridline 5 were analyzed. Because the bottom inclined members are smaller than the vertical columns, they had the largest response to events. The maximum stress observed in these members was 33.87 MPa in compression. The largest tensile response was observed on the inner gauge of the inner columns on Gridline 4, C31 and C5. The largest stresses they experienced were 14.85 and 11.24 MPa respectively.

The maximum pontoon displacement was 2.438 mm in the x-direction. Ninety-three percent of the displacements were below 0.25 mm. The maximum column displacement was 10.321 mm in the negative vertical direction. The displacements were measured with respect to the retaining wall; therefore, they are relative displacements. The difference in the vertical displacements at the top of the columns helped to characterize the event types.

Column stress distribution and the difference between the vertical displacements at the top of the columns on either side of the hopper were used to determine signatures for five types of events. When oil sand is dumped from a truck on the right hand side of the hopper and the load stays on that side, the outer right columns have the highest stress. The difference in vertical displacements between the right and the left is negative indicating that the right side deflects more than the left side. If the oil sand is loaded

from the left side and the load stays on the left side the outer left columns has the highest stress and the difference in the vertical displacements is positive. When dumping occurs on both sides simultaneously the stresses on either side of the hopper are similar and larger than left or right dumping. For all of these events gauge H58 in the hopper experiences a tensile change. When the hopper is empty or near empty the load does not stay on the same side from which it was dumped. The oil sand slides across the empty hopper and impacts the other side. This results in the inner column on Gridline 2 on the side opposite of dumping to have the highest stress. Also, gauge H58 in the hopper experiences a compressive stress change.

Impact factors were calculated by determining the dynamic strain for each event. Dynamic strain was calculated by subtracting the maximum or minimum strain for an event from the average strain before an event. The ratio of dynamic strain to static strain is the impact factor. Impact factors were compared by stress range, location and event type. The standard deviation of the impact factor decreased as the stress range increased. Only stress changes over 5 MPa have standard deviations low enough to have confidence in the values. The impact was highest in the hopper and the gauges at the top of the column because these locations are directly impacted by the oil sand. The standard deviation in these locations was also very high because loads do not impact the same location all of the time and therefore the gauges would react differently for each event. Because the vertical stiffeners are secondary members, the impact factor was higher than the horizontal stiffeners or at the intersection of the stiffeners. The impact factor in the the vertical stiffeners was 2.26 for stress changes greater than 5 MPa, as compared to 1.18 in the horizontal stiffeners or 1.45 at the intersection of the stiffeners. Events identified as moving across have very large impact factors with large standard deviations. The average impact factor for all hopper gauges for these events was 4.26 with a standard deviation of 2.092 for stress changes greater than 2 MPa. The columns had lower impact factors than the hopper because some of the dynamic response will have been filtered out. The average impact factor for the vertical columns for left, right or both sides dumping events ranged from 1.35 to 1.46 for stress changes greater than 5 MPa. The average impact factor and the standard deviation decreased as the static stress change increased.

For moving across events, the average impact factor was higher, 2.96 with a standard deviation of 1.018. The angled members that connect to the middle of the pontoon had lower impact factors than the vertical columns. The average impact factor for these members was between 1.08 and 1.22 for stress changes greater than 5 MPa. The standard deviation was as low as 0.057 for stress changes greater than 15 MPa. The pontoon's impact factor was similar to the bottom angled members of the column because they are both the farthest away from the direct impact. The average impact factor for the pontoon for non-moving across events was between 1.25 and 1.30 for stress changes greater than 5 MPa, with standard deviation between 0.104 and 0.165. The impact factor was higher for moving across events but not as much of a difference as in the columns or the hopper. The average pontoon impact factor for stress changes greater than 5 MPa for moving across events was between 1.09 and 2.22. The impact factor was largest for moving across events, highest in the hopper and the top of the columns, decreases in the vertical columns and decreasing further in the pontoon and the bottom angled members of the columns.

Load cases were created in the STAAD model to simulate right side dumping, left side dumping and both sides dumping. These load cases were calibrated with the data by matching the column stress distribution on Gridline 4. In order to create the stress distributions seen in the model, load was applied to both sides of the hopper increasing on the side of dumping. Linear varying loads were applied perpendicular to the vertical stiffeners and pressure was applied perpendicular to the hopper plates. The largest plate pressure used was 20 kPa for both sides dumping and the largest beam load was 85 kN/m. These load cases were then used to determine the areas of largest stresses in the crusher. Consistently the area where the stresses were highest in the beams was at the top of the inner columns on Gridline 3 and 4. The highest plate stress was in a plate that connected the inner column on Gridline 2 to the hopper. The stresses from the model were much smaller than the analysis done using the loads from design. The largest stresses occurred for both sides dumping. The maximum plate stresses was 17.99 MPa and the maximum beam stresses were 66.99 MPa in tension and 68.45 MPa in compression.

7.2. Conclusions

Because STAAD's only output is stress, the thermal coefficients could not be compared to the STAAD model. However, these values can be used as the basis for a boundary condition change. Data collected during a no loading condition can be used to recalculate these values and if there is a significant change, a change in the boundary conditions has occurred.

Stresses observed were relatively low, with the largest stress being 33.87 MPa. Gauges H62, C39, C40 and P49 to P52 show the highest stress change for the hopper, columns, and pontoon and should be used when trying to identify events. Column stress distribution and the difference between vertical displacements provide a means of identifying event signatures. The impact factor is highest in the hopper and decreases as the members become farther away from the direct impact zone. The impact factor is higher than the design value of 1.4. The design value is close to the actual impact experienced in the vertical column and is higher than the impact observed in the pontoon. When the hopper is empty or near empty, events are identified as moving across and the impact factor observed is very high. Dumping oil sand on an empty hopper should be avoided to avoid such high dynamic effects.

The model used for design compared well with the data, and can be used to predict high stress areas in the crusher. The high stress zones were at the top of the inner columns on Gridlines 2, 3, and 4, and the plates that connect theses columns to the hopper. The design loads used loads greater than the loads created to calibrate the model by four to ten times. The five local impact cases were also deemed unlikely as they required the oil sand to impact a very narrow strip of the hopper that by the video taken seem very unlikely to occur. The design can be improved by using the impact factors calculated at various locations and reducing the loads for dumping events.

The information gained by this research has provided the basis for a Structural Health Monitoring Program of Syncrude's Aurora II Crusher. By understanding the structural behaviour of the crusher and providing a baseline, a monitoring program can be initiated

to create a damage detection model. The event signatures will help with data management of the data collected. This work is currently ongoing at the University of Alberta.

7.3. Recommendations

The research conducted has led to the following recommendations:

1. Instrumentation Plan
    a. Replace gauge C36 so that the average stress in the outer column on Gridline 4 can be more accurately determined
    b. Install gauges at the top of the inner columns on Gridline 2 and 4 as these were shown in the model to be the highest stresses in the crusher
    c. Do not replace LVDTs on the pontoon as the displacements were very small
    d. Use LVDTs at the top of the columns on Gridline 4 in the vertical and z-direction to help with event characterization
    e. Use smaller range LVDTs to improve accuracy as highest displacement was 10 mm.
    f. Install additional gauges on vertical stiffeners of hopper at lower locations to capture possibly higher stresses during moving across events
2. Future Testing
    a. Use additional video footage taken during normal operation to verify event signatures
    b. Additional control tests
        i. Varying hopper level – in order to determine the effect that existing oil sand in the hopper has on the loading and where the oil sand impacts the hopper walls
        ii. Extreme case – take zero readings before and after having the hopper filled with oil sand without allowing material to exit will give the maximum stress experienced by loading the hopper with oil sand, this can be compared to pressure on walls used for live load of materials used by Krupp

c. If control testing can not be done due to production constraints, record video data as well as hopper level.

3. Model

   a. Create a model of the hopper and pontoon together so that the pontoon behaviour can be verified

References

1. Carroll, M., 1997. "Mining Equipment Monitoring at Syncrude". Paper presented at the CIM 1997 District 5 Conference. 1997. 23pp.

2. Fowler, C. and Gonzalez, S., 1999. "Preliminary Investigation of DRC7 Displacement". Syncrude Canada Ltd. Research Progress Report, 28 (11) pp. 120-131.

3. Fowler, C. and Gonzalez, S., 2000. "Study of DRC7 Displacement during Frozen Ground Conditions". Syncrude Canada Ltd. Research Progress Report, 29 (5) pp. 57-66.

4. Obaia, K. and Gonzalez, S., 2001. "Investigation of support Displacement of DRC7". Syncrude Canada Ltd. Research Progress Report, 30 (9) pp. 1-18.

5. Quapp, D. and Maciejewski, W., 1991. "Crushing Technology; its current and Future Application in Oil Sand Mining". Paper presented at the Canadian Inst. Mining and Metal.

6. Research Development and Design of a Semi-Mobile Crushing Plant for a Northern Alberta Oil Sands Mine. Retrieved May 29, 2003, from http://www.krupp.ca%20crusher.htm